ARCHIVES

OF CIVIL AND MECHANICAL

ENGINEERING

WROCŁAW 2007

ARCHIVES
OF CIVIL AND MECHANICAL
ENGINEERING

Contents

Spis treści

Experimental investigation into behaviour of CFRP composite-strengthened RC beam under cyclic loading

ANDRZEJ KMITA

Wrocław University of Technology , Wybrzeże Wyspiańskiego 27, 50-370 Wrocław

This paper presents selected results of research on the behaviour of an RC beam strengthened with composite materials (CFRPs). The designed tests were to provide data for an assessment of such reinforcement system's performance under cyclically variable loads.

The test plan included the effect of the CFRP reinforcement on: beam rigidity, cracking morphology and the interaction of the reinforcement components with regard to bond uniformity in the whole structure and the durability of the bond under cyclic loads.

The tests were carried out on two RC beams with the same dimensions, reinforcement and material quality. Only one of the beams was strengthened with CFRP, but both were subjected to the same loading and the same quantities were measured. This facilitated a quantitative and qualitative assessment of the performance of the CFRP reinforcement system.

The research was carried out as part of project "Theoretical and experimental investigations of load-bearing capacity and service limit states of reinforced concrete and prestressed concrete structures" (also to be used for educational purposes) in the Accredited Laboratory of the Institute of Building Engineering at Wrocław University of Technology.

Keywords: *CFRP composite material, cyclic loads, RC beam*

1. Introduction and background

This paper presents experimental results relating to the static-strength performance of RC beams strengthened with composites. Such reinforcement is used particularly in cases when:

• in building structures in service there is a need to change their service conditions, including to increase their load;

• in newly built structures whose function changes together with the loads acting on their structural components;

• in existing structures which have been in service for many years and whose structural components show a reduction in load-bearing capacity as a result of the service and the associated aggressive impact of the environment.

Such reinforcement systems are made from various composite materials, among which composites based on CFRP (carbon fibre reinforced plastic) are widely used [1, 2, 3, 4].

Experimental tests carried out on RC beams strengthened with CFRPs are presented here.

The choice of this type of reinforcement is mostly dictated by the small size of the space available for reinforcement and also by the CFRP reinforcement's excellent strength parameters. Of major importance is also the high resistance of such reinforcement to the action of aggressive factors.

Tables 1–4 show the main parameters of the materials used in the tests [4, 8].

Table 1. Sika CorboDur System

Type of strip	Density g/cm^3	Average tensile strength MPa	Characteristic tensile strength MPa	Modulus of elasticity GPa	Strain at rupture %	Width mm	Thickness mm
S512	1.5	3050	> 2800	> 165	> 1.7	50	1.2
Mat SikaWrap	1.76	4100		231	> 1.7		0.131

Table 2. Adhesive Sikadur 30/SikaDur-30 for strip.

Density, kg/m^3 (after components A+B have been mixed)	1700
Shrinkage, %	0.04
Glass transition temperature, ℃ / ℃K	+62 / 0355
Elasticity modulus, GPa	1.28
Adherence to moist concrete, MPa	4
Adherence to dry concrete, MPa	5
Compressive strength, MPa	>95
Shear strength, MPa	15
Coefficient of expansion, 1 / ℃K	9×10^{-3} (–10 – +40 ℃K)

Table 3. Strength characteristics of adhesive Sikadur 30

Specimen No.	Tensile strength f_{cl}, f_g [MPa]		Compressive strength f_{cs} [MPa]		Age of adhesive days
	results	averages	results	averages	
1	42.2		89.8		
2	65.6		104.6		
3	50.2	53.5	103.3	103.7	15
4	58.8		106.0		
5	51.6		107.9		
6	52.7		96.0		

Table 4. Adhesive for Sikadur 330 mats (wraps)

Compressive strength, [MPa]	> 65
Shear strength, [MPa]	> 6
Adherence to concrete, [MPa]	> 4
Elasticity modulus, [GPa]	3.8

As the comparison of the materials' parameters shows they have much better strength and permissible deformability than concrete and steel.

This paper presents tests of RC beams strengthened with CFRP strips and mats, taking into account beam bending and shear strain and load cyclicity.

The following elements distinguish the proposed research from the research described in references [1, 2, 3, 4, 7]:

– application for reinforcement both strips and mats [1, 4],
– research on *T* girders [1, 4, 7],
– research on natural scale elements [1, 2, 3, 4, 7],
– method and range of loading, type and range of measured values.

The range of planned loading was based on the serviceability limit state of deflection and cracking set in a code provisions. So the research will include loadings which are characteristic for exploitation stage which distinguish them from most of the research presented in the references.

2. Object and aim of tests

The tests were carried out on two RC beams having the same geometry and reinforcement, whose concrete grade was as shown in Figure 1a. Since a comparative analysis was to be made only one of the beams (beam no. 2) was strengthened with CFRP. The reinforcement had the form of two Sika Carbodur S512 strips stuck on in the beam's tensioned zone and a Sika Wrap 230 mat in the support zone.
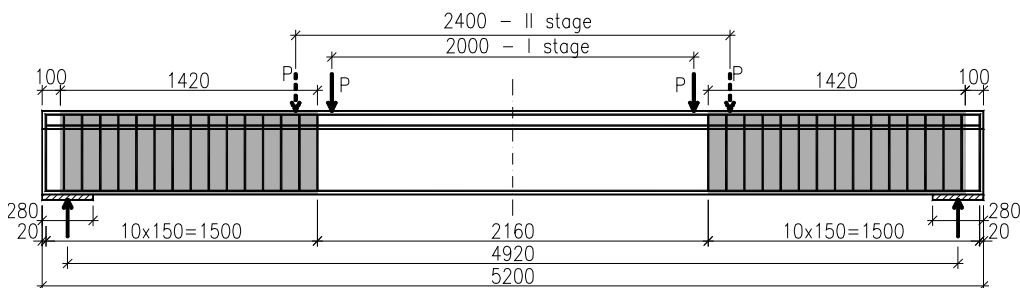
Fig. 1a. Tested element loading configuration longitudinal section with CFRP mats arranged in support zone

Figures 1b and 1c show the CFRP reinforcement system along the tested element's length.

The main aim of the tests was to compare the static-strength performance of the two elements, particularly their behaviour in the support zone at different strain levels under cyclic loading [6].

The support zone, subject mainly to shear loading, is highly sensitive to overloads and difficult to reinforce effectively. For this reason it was given special attention.

When the elements were being prepared for the tests, several electric resistance strain gauges were mounted on the beams' reinforcement (still before concreting) so

that during loading one could evaluate the level of strain in the reinforcing steel of the stirrups and in the bearing reinforcement (Figure 1b).
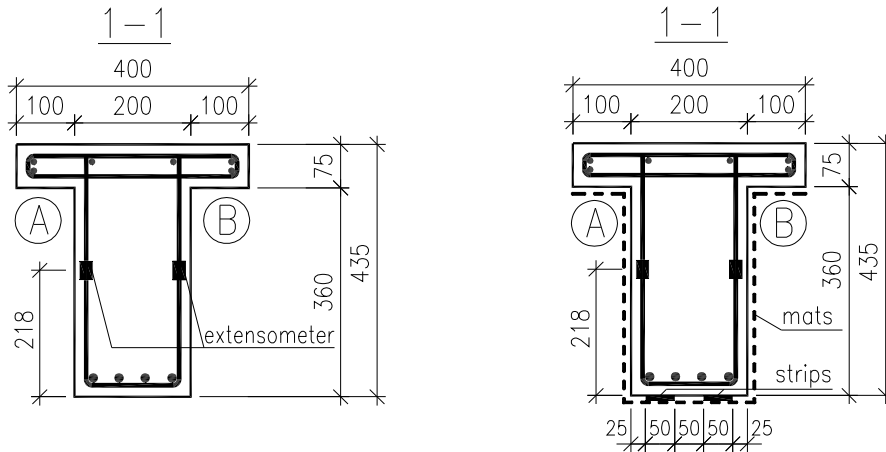
Fig. 1b,c. Tested element loading configuration cross section of element without CFRP reinforcement (beam no.1) (b), cross section of strengthened element with marked strips and mats (beam no.2) (c)

An exemplary arrangement of strain gauges on the concrete and on the mats in the support zone is shown in Figure 1d. In the case of the beam strengthened with mats (beam no. 2) strain rosettes were located on the concrete and on the mat on the beam's two sides and in the two support zones.
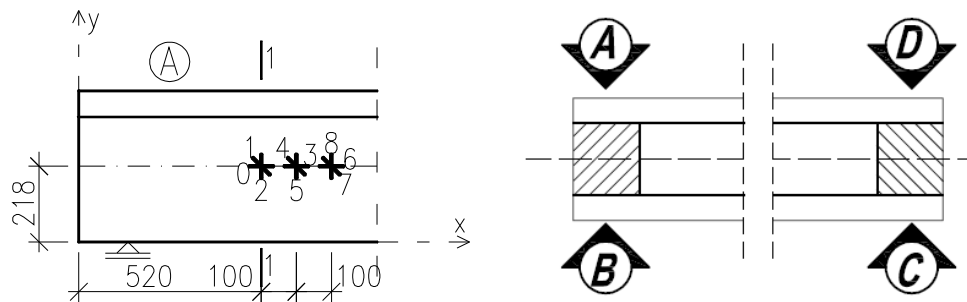
Fig. 1d,e. Tested element loading configuration exemplary arrangement of strain rosettes (side A) (d), description of sides in beam support zones (top view) (e)

In order to investigate the effect of CFRP reinforcement on bending, the beam was strengthened with two strips (Figures 1c and 3). Changes in the deflection of the tested beams versus the number of cycles for different load levels are presented further below.

The strain gauges arranged in the form of rosettes in the support zone (whereby it became possible to determine the main strain components in the concrete and in the mat) were considered to be the primary ones.

3. Test stand

The two beams were tested on the same test stand. A static scheme of the system is shown in Figure 1. A general view of the test stand is shown in Figures 4 and 5. An Instron loading device (two 500 kN servomotors) was mounted on two steel frames anchored in special foundation channels. The beams were loaded with two concentrated forces via metal plates glued to the top surface of the beams. The force was applied statically, with the load increased every 5 kN. Once the target value was reached, the amplitude of load values for cyclic loading was determined. The maximum frequency of applied load was: 1 Hz and 1.5 Hz in respectively the initial stage – stage 1 and stage 2. Once 20000 cycles were reached, the loading configuration was changed by shifting loading forces P by 200 mm towards the supports in order to reduce the bending moment and increase the transverse force in the support zone. The loading histogram is shown in Figure 6.

Fig. 2. Support zone of strengthened beam no. 2

Fig. 3. Reinforcement with CFRP strips along span of beam no. 2

Fig. 4. View of test stand

Fig. 5. Loading effected by two hydraulic servomotors
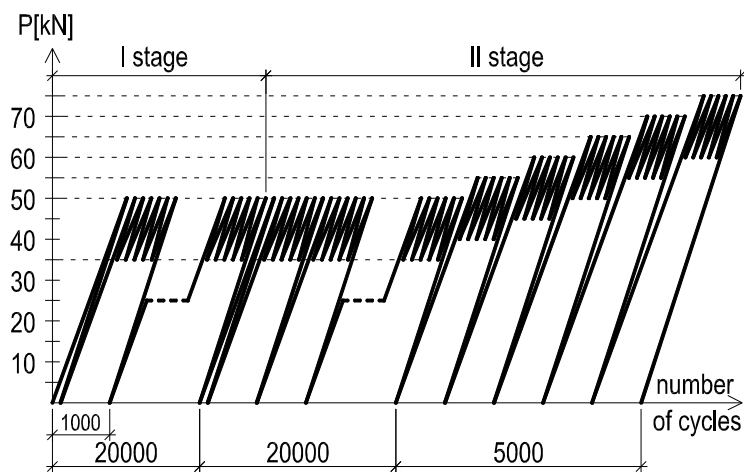
Fig. 6. Loading histogram for tested elements

During the loading (as shown in the histogram) strains, displacements and crack opening widths in the element were measured as follows. At the first static loading

and relief all the above quantities were measured for load change $\Delta P = 10\text{kN}$ (to P_{max}). The first loading and relief is understood here as the first loading cycle. Then loading to P_{max} was executed followed by 1000 cycles with a given frequency, relief to $P = 0$ and another cycle. This means that at every 1000 loading cycles with an amplitude of 15kN and a given frequency static loading and relief were executed at which all the quantities were measured.

4. Measured quantities

As the beams were subjected to loading, the following quantities were measured:
– The vertical displacements of the element by means of induction gauges with an accuracy of ± 0.01 mm.
– Unit strains in the concrete and in the steel by means of electric resistance strain gauges with an accuracy of 1×10^{-6} (μm/m).
– Unit strains in the CFRP mats and strips by means of electric resistance gauges with an accuracy of μm/m.
– Crack opening width and length along the height of the element. Crack morphology was examined using a spyglass (adapted for crack opening measuring) with an accuracy of ± 0.01 mm. For six selected cracks dial gauges with an accuracy of ± 0.01 mm for measuring crack opening width for different number of loading cycles were mounted on a 15 mm base.

All the electronic gauges were serviced by a Hottinger UPM-100 universal bridge and the data were acquired using the Catman software.

5. Test results

5.1. Presentation of results

The paper presents results which characterize behaviour of the tested elements in the range of vertical displacements, cracks morphology and state of strains in support zone. The results are presented on graphs with its analysis.

5.2. Vertical displacement (deflection)

The diagram in Figure 7 shows deflection versus load for the RC beam and the beam with the CFRP reinforcement during the first test stage. The increment in permanent deflection at midspan versus the number of loading cycles is shown in Figure 8.

In the case of the strengthened beam at loading stage 2, after 40 000 cycles the load was gradually increased. For each successive 1000 cycles (according to the histogram in Figure 6) force P was increased by $\Delta P = 5.0$ kN until $P_{\text{max}} = 75$ kN was reached, i.e. until cracks with opening width as in the nonstrengthened beam (see section 5.3.) appeared.
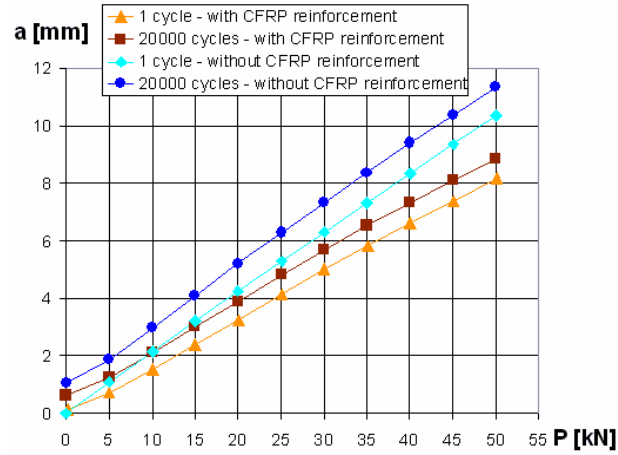
Fig. 7. Midspan deflection versus load *P*
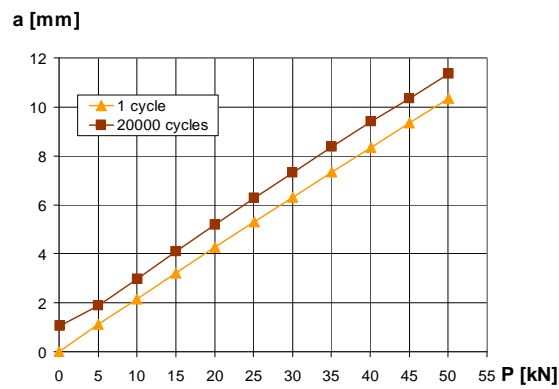
Fig. 7a. Midspan deflection a versus load *P*, *a* = f(*P*) beam no. 1
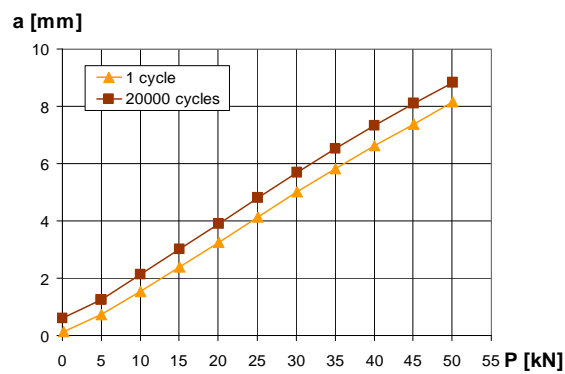
Fig. 7b. Midspan deflection a versus load *P*, *a* = f(*P*) beam no. 2

a [mm]
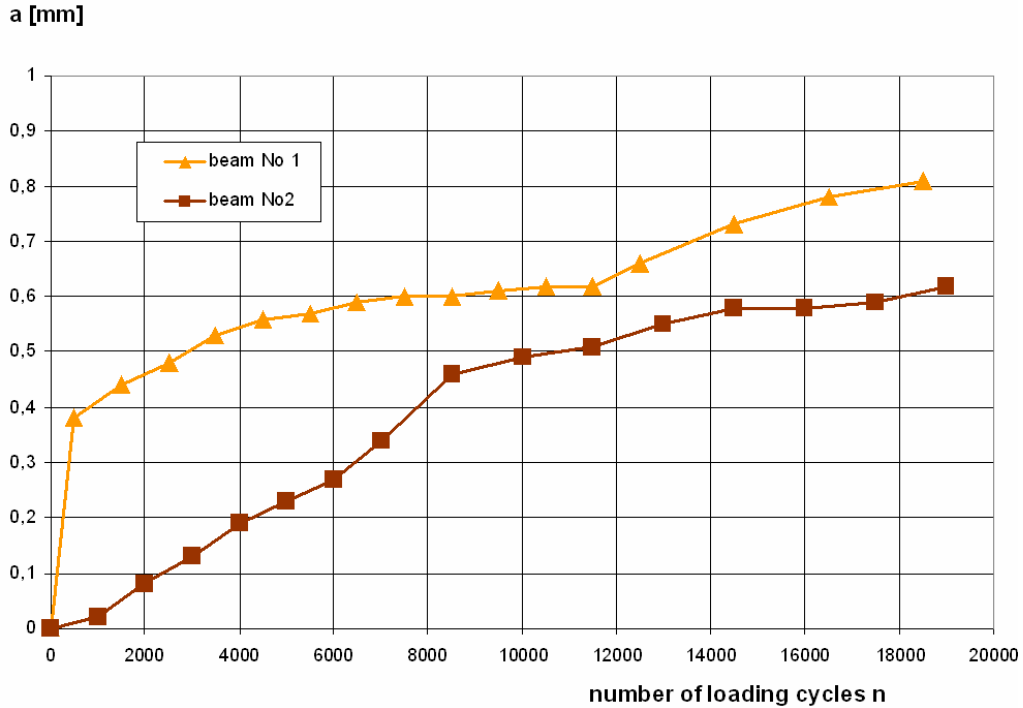
Fig. 8. Midspan permanent deflection increment a versus
number of loading cycles n, $a = \mathrm{f}(n)$

One should note here the much smaller deflection of the strengthened beam in comparison with the ordinary beam at the same level of loading.

Considering that the two elements have the same geometry and the same amount of reinforcement distributed in the same way, the difference can be explained by a change in gidity caused by the CFRP reinforcement in the form of strips along the span and mats in the support zone.

Using the basic relation for maximum deflection a [9]:

$$a = \alpha_k \cdot \frac{M_{\max}}{B} \cdot l_{eff}^2 , \qquad (1)$$

where:

α_k – a coefficient dependent on bending moment distribution, having the same value in both cases;

$M_{\max}$ – the maximum bending moment along the span;

B – cross-sectional rigidity at the moment when $M_{\max}$ occurs;

a – the maximum deflection;

l_{eff} – the design span, l_{eff} = 4920 mm.

The measured strengthened beam deflections a_w and nonstrengthened beam deflections a_b (the rigidities are correspondingly denoted as B_w, B_b) can be written as follows:

$$a_w = \alpha_k \cdot \frac{M_{max}}{B_w} \cdot l_{eff}^2 , \qquad (2a)$$

$$a_b = \alpha_k \ \frac{M_{max}}{B_w} \cdot l_{eff}^2 , \qquad (2b)$$

hence

$$a_w/a_b = B_b/B_w, \qquad (3)$$

and since for the considered case the deflection ratio is $a_w/a_b \approx 0.75$, then $B_w = 1.25\ B_b$.

One should bear in mind that this is simplified estimation in which the total rigidity is reduced to flexural rigidity. Therefore one cannot neglect the effect of the mat glued on in the support area, which reduces some of the span deflection caused by the transverse force [7, 10].

As concerns the deformations of the steel in the beam without CFRP reinforcement (beam no. 1), the relationship after the two stages (45 000 cycles) has a linear character and at a crack opening width ≤ 0.30mm the deformations reach ~1450 μm/m, which corresponds to a stress of ~290 MPa. One should note that for beam no. 2 (with the CFRP reinforcement) this value is reached at a ~20% higher load.

5.3. Crack morphology

In both elements crack morphology was examined using a spyglass with an accuracy of ± 0.01 mm during the first loading while in the next loading cycles besides crack opening width measurement also gauges with a measurement base of 15 mm and an accuracy of ± 0.01 mm were employed.

The loading level was set at P = 50 kN (stage 1) so that crack opening width in the beam without CFRP reinforcement did not exceed condition w ≤ 0.25 mm. Cracks were measured at the level of the beam bearing reinforcement. Exemplary graphs of crack opening width at midspan versus load for the two beams are shown in Figure 10.

The graph of crack opening width along beam height for the beam with the CFRP reinforcement is different that the one for the beam without such reinforcement (Figure 11).

a) ε_s [µm/m]

b) ε_s [µm/m]
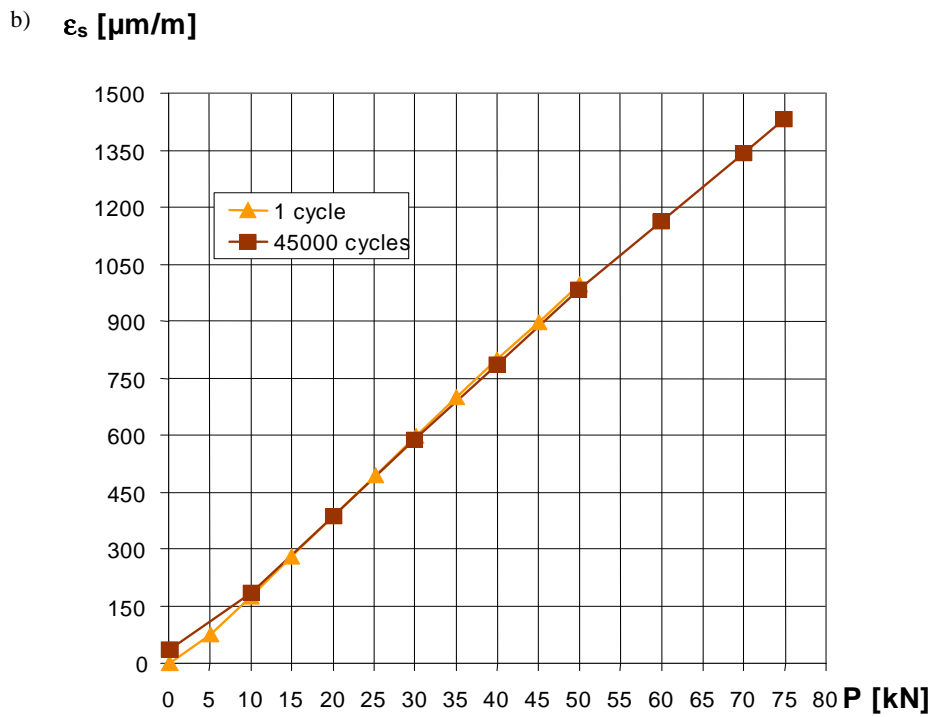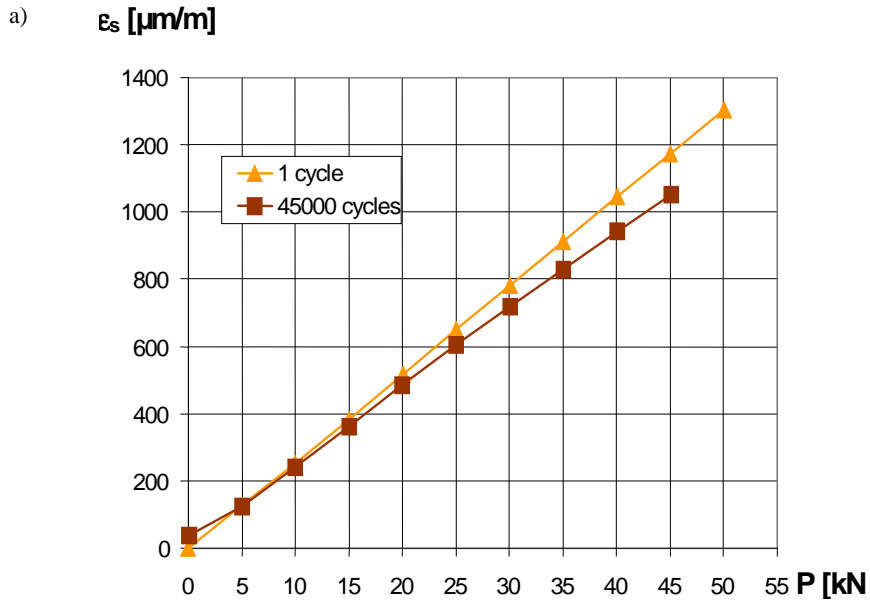
Fig. 9. Strains ε_s in steel at midspan versus load P after 45000 cycles,
$\varepsilon_s = \mathrm{f}(P)$; a) beam no 1 ,b) beam no 2
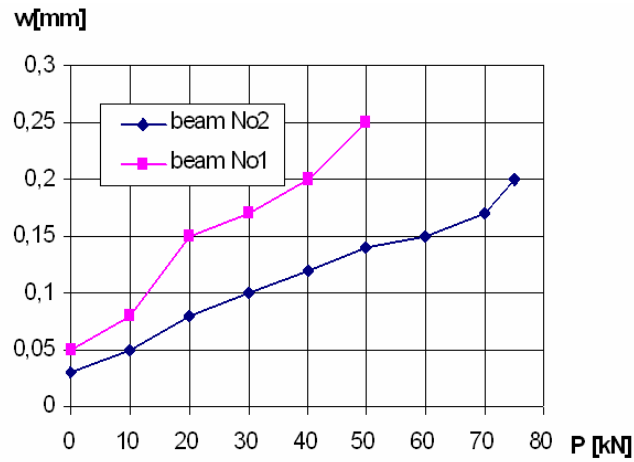
Fig. 10. Crack opening width w versus beam load *P*, *w* = f(*P*)
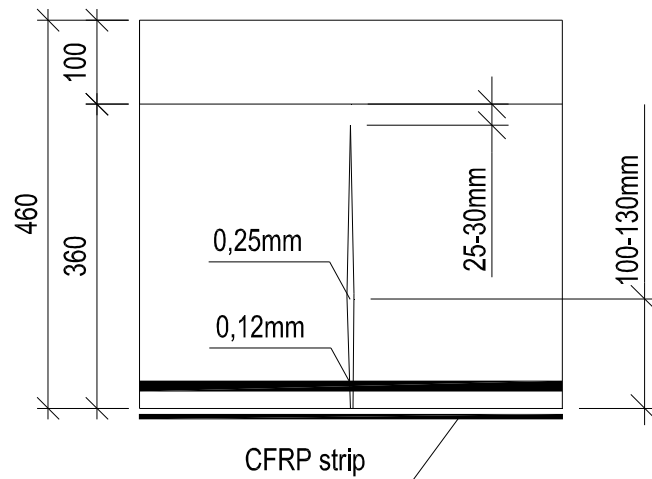
Fig. 11. Beam no. 2 crack opening width at height h of tested element

The distribution is favourable for the strengthened beam since the bearing rein-forcement is protected from the impact of the environment.

5.4. Strains in beam support zone

As Figures 1d and 2 shows, strains in the support zone were measured by strain rosettes. The rosettes were installed in three cross sections on the left and right side of the beam at the two support zones.

The main aim of the tests was to determine the degree of mat-concrete interaction for different degrees of strain in the support zone and different numbers of loading cycles [5, 6].

The condition that in a given point the state of strain on both the concrete's surface and the mat's surface is the same (of course, provided that no crack propagates through the point), i.e. $\varepsilon_{1m} \approx \varepsilon_{1b}$, $\varepsilon_{2m} \approx \varepsilon_{2b}$, where ε_{1m}, ε_{1b} – the principal (tensile) strain in respectively the mat and the concrete, ε_{2m}, ε_{2b} – the principal (compressive) strain in respectively the mat and the concrete, was adopted as the criterion of proper interaction.

Figure 12 shows relationships between principal strains ε_1, ε_2 for the concrete and the mat. One can see that in the area where the concrete is uncracked the interaction is harmonious. For a point located closer to the cracked area at a load greater than $P = 50$ kN differences between the deformations of the concrete and those of the mat are clearly visible, mainly due to local discontinuities in the concrete (Figure 12).

The angle of inclination of principal strains ε_2 relative to axis *x* changes in a range of 35° – 42°, depending mainly on the stage of loading.
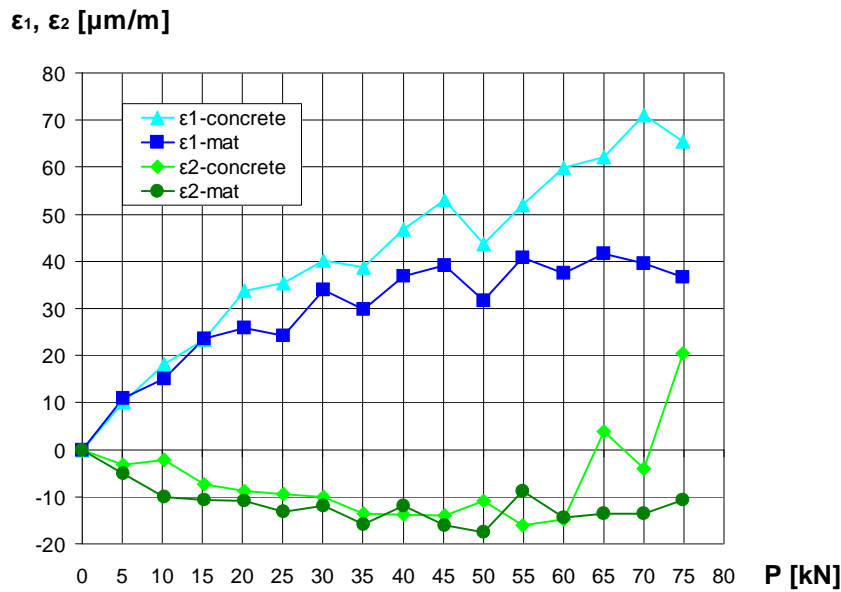
Fig. 12. Principal strains ε_1, ε_2 for concrete and mat (beam no.2) after 45000 cycles

As strains ε_1, ε_2 were being measured in the support zone also strains ε_s in the stirrups located in the places of the rosettes were being measured. The strains are plotted in Figure 13. A sharp increase in ε_s occurred once load $P = 70$ kN was exceeded, which is associated with cracking in this area.

ε_s **[μm/m]**
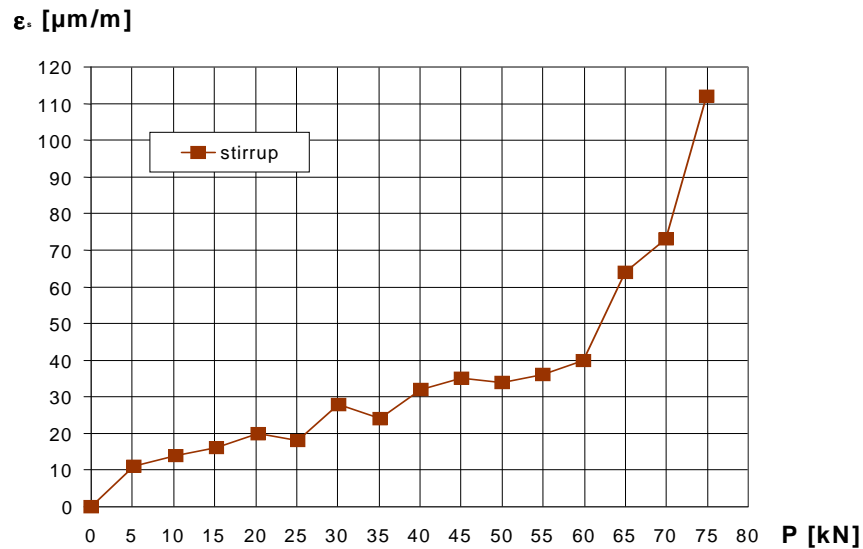
Fig. 13. Strains in steel in stirrup located in place of gage rosette (Figure 12)

6. Conclusions

From the results of the tests one can draw the following conclusions.

1. The CFRP reinforcement significantly increased the rigidity of the tested structure, which means that such reinforcement can be considered to be a special kind of composite construction.

2. The interaction between the reinforcement in the form of strips and mats and the concrete proved to be reliable throughout the whole period of cyclically variable loading effected at the limit of usability set by the permissible crack opening width.

3. Both the strips and the mats significantly contributed to a reduction in the width of opening of the cracks and their dispersion along the span and in the zone of greatest shear near the supports.

References

[1] Khalifa A., Nanni A.: *Rehabilitation of rectangular simply supported RC beams with shear deficiencies using CFRP composites*, Constructions and Building Materials, 16, 2002, pp. 135–146.
[2] Triantafillou T.C.: *Composites: A new possibility for the shear strengthening of concrete, masonry and wood*, Composites Science and Technology, 58, 1998, pp. 1285–1295.
[3] Chen J.F., Teng J.G.: *Shear capacity of FRP-strengthened RC beams: FRP debonding*, Constructions and Building Materials, 17, 2003, pp. 27–41.

[4] Kamińska M.E., Kotynia R.: *Experimental tests of RC beams strengthened with CFRP strips* (in Polish), No. 9, Experimental Tests of Structural Components and Structures, Concrete Construction Department of Łódź Polytechnic, 2000.

[5] Kwiecień A.*: Tests of adhesion layer in composite CFRP reinforcements* (in Polish), The 4th all-Poland Conference of Bridge Engineers: Bridge Construction and Accessories, Wisła, 2005.

[6] Derkowski W.: *Studies of the influence of polymer and carbon fibre strip reinforcement on the fatigue strength of RC beams under bending* (in Polish), 2nd Scientific-Technical Conference on Composite Materials in Bridge Building, Łódź, 2006.

[7] Pellergrino C., Modena C.: *Fibre-Reinforced Polymer Shear Strengthening of Reinforced Concrete Beams: Experimental Study and Analytical Modelling*, ACI Structural Journal September-October, 2006, pp. 720–728.

[8] Sika CarboDur system Sika catalogue.

[9] Polish Standard PN-B-03264:2002, *Reinforced Concrete and Prestressed Concrete Structures*, *Static Calculations and Design* (in Polish).

[10] *Reinforced Concrete and Prestressed Concrete Structures. Scientific Commentary to Polish Standard PN-B-03264:2002* (in Polish), Vol. 2, ITB, Warsaw, 2005.

Zachowanie się belki żelbetowej wzmocnionej materiałami kompozytowymi CFRP pod obciążeniem cyklicznym w badaniach eksperymentalnych

W pracy przedstawiono wybrane wyniki badań nad zachowaniem się belki żelbetowej wzmocnionej materiałami kompozytowymi CFRP. Badania te zaprojektowano jako badania rozpoznawcze dla oceny skuteczności tego systemu wzmocnienia przy obciążeniach o charakterze cyklicznie zmiennym.

W zrealizowanym programie badań ujęto takie zagadnienia jak: wpływ wzmocnienia na sztywność belek, na morfologię zarysowania i współpracę elementów wzmocnienia w aspekcie równomierności zespolenia w całym obszarze obiektu i trwałości tego zespolenia w czasie pod cyklicznymi obciążeniami.

Badania przeprowadzono na dwóch belkach żelbetowych o takich samych wymiarach, zbrojeniu i jakości materiału. Jedna z tych belek została wzmocniona, ale obie zostały poddane jednakowemu procesowi obciążenia i pomiarowi tych samych wielkości. Ułatwiło to ocenę jakościową i ilościową skuteczności zastosowanego systemu wzmocnienia belek.

Badania przeprowadzono w ramach zadania „Badania teoretyczne i doświadczalne stanów granicznych nośności i użytkowalności konstrukcji żelbetowych i sprężonych" (z wykorzystaniem do celów dydaktycznych) w Akredytowanym Laboratorium Instytutu Budownictwa Politechniki Wrocławskiej.

Hot forming parameters research of bearing steel

P. GEMBALOVA, J. BORUTA,

VÍTKOVICE – Research&Development., Pohranicni 693/31, 706 02 Ostrava-Vitkovice

E. GRYCZ, K. M. CMIEL

TRINECKE ZELEZARNY, a. s., Prumyslova 1000, 739-70, Trinec-Stare Mesto

The paper deals with an analysis of the hot forming parameters of the bearing steel 100Cr6 according to ČSN EN ISO 683-17, performed by means of the plastometer. Bearing steels belong to high carbon steels, generally alloyed by chromium, i.e. precipitation of carbides of type $(FeCr)_3C$ takes place. Uneven distribution of carbide phases, together with inclusions, deteriorates the resulting steel quality. Thus service properties, especially lifetime of bearings, are limited. Degradation of structure in the production process results mainly in carbide banding, carbide segregations and carbide network. By a suitable cooling rate it is possible to remove completely the carbide network after rolling; in addition, an appropriate structure for subsequent heat treatment may be prepared. Metallurgical process parameters, constitution and cleanliness of steel have significant influence on grain size and banding of the formed steel. Mainly correctly performed control of finishing rolling conditions and final cooling have considerable influence on quality of rolled products. Sufficiently fast cooling after forming decreases occurrence of carbide network, of course with danger of arising micro- and macro-cracks especially on weakened gamma-grains boundaries. This contribution illustrates selected results of the plastometric and metallographic investigation of deformation behaviour of high carbon steels alloyed with chromium, including bearing steel.

Keywords: *deformation behaviour, bearing steel, plastometric torsion test, plastometric simulation, carbide network*

1. Introduction

In association with permanent development and updating in production of bars and wire rod, conditions are gradually created for implementation of process of normalized and thermo-mechanical rolling on a scientific basis by means of physical/metallurgical research. Through its thorough analysis it is possible to gain effective mathematical models for control of technological processes of structure controlled forming, not only in low carbon, micro- and low-alloyed, but also in high carbon alloyed steels.

For the physical modelling of metal forming and experimental study of structure forming processes, for research of laws of plastic deformation and for development of the new or optimized processes of forming of various materials and products, chances that offer special machines – plastometers may effectively be used.

On the universal plastometer SETARAM-VÍTKOVICE in VÍTKOVICE – Research & Development we carried out physical simulation of the entire forming process – heating to forming temperature, rolling and subsequent cooling. We started from possibilities of TŘINECKÉ ŽELEZÁRNY, a. s., a renowned producer of hot rolled products from alloyed steels [1].

2. Characteristics of 14109 steel

It must be admitted that bearing steels belong with regard to their use to a group of structural steels but as far as their chemical composition, deformation behaviour in hot forming, heat treatment and methodology of testing is concerned they belong rather to tool steels. In these steels carbides occur, contents of Fe and Cr in which may be considered to some extent as variables dependent on temperature of arising of the carbide. Bearing steels belong to hypereutectoid steels, for which a broad temperature interval between start and end of solidification is typical. In this range enrichment of interdendritic areas with carbon and segregation elements occurs. This phenomenon occurs similarly in tool steels. Cleanliness of steel and distribution of carbide phases, and homogeneity and fine grain structure in general, have a great influence on lifetime of antifriction bearings. Cleanliness of steel is influenced by not only a content of nonmetallic inclusions, sulphides, oxides and aluminosilicate globular inclusions, but also their morphology [2].

As high carbon steels are apt to coarsening of grains, temperatures of heating should be in the range of 1150–1200 °C. Heating to this temperature should also compensate heterogeneity of chemical composition that arises during solidification of ingots and results mainly in carbide banding. Removal of carbide segregations in cast ingots can be carried out only by diffusion, which depends on temperature and dwell time at the temperature. The heating temperature can't be increased very much due to quality of products; that is why the dwell time at temperature has been raised. This may be done by homogenization as a separate operation or by extension of heating before subsequent forming.

Unlike homogenization of rolled bars, which are annealed only when inconvenient carbide banding is found out, the homogenization annealing of ingots has been carried out with a preventive aim. Decarburization and scaling of surface due to prolongation of heating are not so harmful in this case. A layer of scale prevents from diffusion of carbon towards the surface and thus decreases decarburization; scale falls off during forming.

Another important factor having impact on microstructural cleanliness of steel is the reduction ratio. The total inclusions content in steel is constant but shape and distribution of inclusions change, due to stretching of plastic inclusions and crumbling of non-plastic ones. Occurrence of carbide segregations decreases when the reduction ratio rises.

Not only carbide banding but also carbide network can cause decrease in the lifetime of bearings. An appropriate cooling after forming can lead to elimination of this defect and, besides, it can prepare a suitable initial structure for subsequent annealing.

Production of bearing steels via continuous casting belongs to the most exacting processes, particularly from the point of view of maintaining segregation of carbon and other elements in the core as low as possible. There are principally two kinds of

solution of this issue: installation of a final stirrer (F-EMS) or soft-reduction (SR). F-EMS has disadvantage in high investment cost and the fact that when the stirrer is used then shrinkage porosity in the core of the conticast product will arise. Most bearing steels are produced via ingot route, utilization of the SR method made it possible to use continuous casting with improved quality of conticast products in their central parts and so achievement of products with better quality in general [1].

In industrial practice the greatest emphasis is put on cleanliness of bearing steels. The current technology enables to produce dimensionally accurate small bearings. Load of such bearings is very high and they are also apt to an initial rolling contact fatigue. That is another reason why steel for bearings has to be very clean. By means of ultrasound it is possible to determine quantity of inclusions in steel. An intensive research was carried out, in accordance with requirements of the bearing industry. Steel plants produce successfully both hardened and case-hardened steels which are able to match demands of foremost producers of bearings.

Antifriction bearings belong to the most important machine parts, used in a wide product mix. Dimensions of bearings determine their carrying capacity. Size of bearings is decisive for size of other components, such as shafts and bushings. In close past demands on increase of nominal load for a given size of the bearing had been raised, with the aim to make it possible to assemble smaller parts with higher energy efficiency and cheaper as well. Nowadays bearings have been stressed more and more and they are more inclined to crumbling if the initial rolling contact fatigue occurs. It is known that the rolling contact fatigue begins in hard non-metallic inclusions. That is the reason why large emphasis has currently been put on a high level of cleanliness of steel, from viewpoint of not only oxide inclusions but also other non-metallic inclusions, such as e.g. nitrides and carbides of titanium [3].

In the field of bearing steels permanent development of new steel grades can be visible. For example authors [4] proposed a new steel grade that is based on the conventional steel 100Cr6, modified by addition of Si and Mn, and has better resistance to high loading and high temperature. Conditions of steel production and forming processes remained the same.

Use of bearings in industrial conditions has become more and more demanding. These more exacting applications include automobile components and systems, mainly gearboxes and wheels. In these cases and on the current level of cleanliness of bearing steels, crumbling of races can be caused by splinters (chips), evolving due to damage of the surface, and by local loss of the matrix strength in loading and temperatures that are higher than usual.

Bearings used in gearboxes can be damaged by notches or wear of surface, according to size of chips and their hardness. In these conditions stress and temperatures surpass locally levels that are currently acceptable for steels of type 100Cr6 [4].

It results from the performed analysis that for increase of lifetime and service properties of bearings, homogeneity and fine-grained structure are extraordinarily important, of course besides of steel constitution and its cleanliness. Forming carried out

with control of structure can have a considerable impact on these parameters already in the course of production of hot formed semifinished products.

3. Deformation behaviour of high carbon steels

The universal plastometer SETARAM-VITKOVICE [5] and forming tests of metallic materials in hot state are used for experimental investigation of deformation behaviour in the plastometric laboratory at VÍTKOVICE – Research & Development. This testing equipment is in the current configuration universal one, with the ability to perform tensile tests, compression tests, torsion tests or combined torsion tests with additional tension. Wide upgrade of this experimental equipment has taken place in last time. Tests could be carried out without interruption up to complete loss of plasticity with a subsequent fracture, or with interrupted deformation and exactly defined breaks (pauses) for a possibility of recovery of the tested material [6, 7].

Table. Chemical composition of investigated steels (in wt. %, according to the standard)

ČSN	W. Nr.	C	Si	Mn	Cr	Mo	V
14109	1.3505	0.90 1.05	0.15 0.35	0.25 0.45	1.35 1.65	–	–
19569	1.2362	0.60 0.65	1.00 1.20	0.30 0.50	5.0 5.5	1.00 1.30	0.25 0.35
19573	1.2379	1.50 1.60	0.10 0.40	0.15 0.45	11.0 12.0	0.60 0.80	0.90 1.10

The basic research of deformation behaviour of 14109 bearing steel was carried out. For a basic description of deformation behaviour the continuous test without interruption has normally been used. This test can be performed in steels at temperatures above 650 °C (the upper testing temperature is limited only by melting of material) and strain rates ca between 10^{-4}–$10\,s^{-1}$. An example of results from the program for determination of maximum deformation resistance under various temperatures and strain rates for three high-carbon steel types alloyed with Cr: 14109 – 1.5 % Cr, 19569 – 5 % Cr a 19573 – 11 % Cr, is shown in Figure 1. Chemical composition of steels is given in Table.

Figure 2 shows comparison of formability limit Se_f in dependence on temperature for three steels with different Cr contents. The Cr influence has been confirmed again. Higher Cr content leads to lower formability.

Knowledge of limiting criteria and their implementation in technological processes of the production of hot formed semifinished and final products from formable materials is a prerequisite for successful control of hot forming. Formability and deformation resistance belong to the most important characteristics of hot deformation behaviour of steel. The bearing steel is alloyed by chromium, which retards recrystallization; hence knowledge of deformation behaviour in conditions of not only continuous but also interrupted (intermittent) deformation is very important for successful forming.
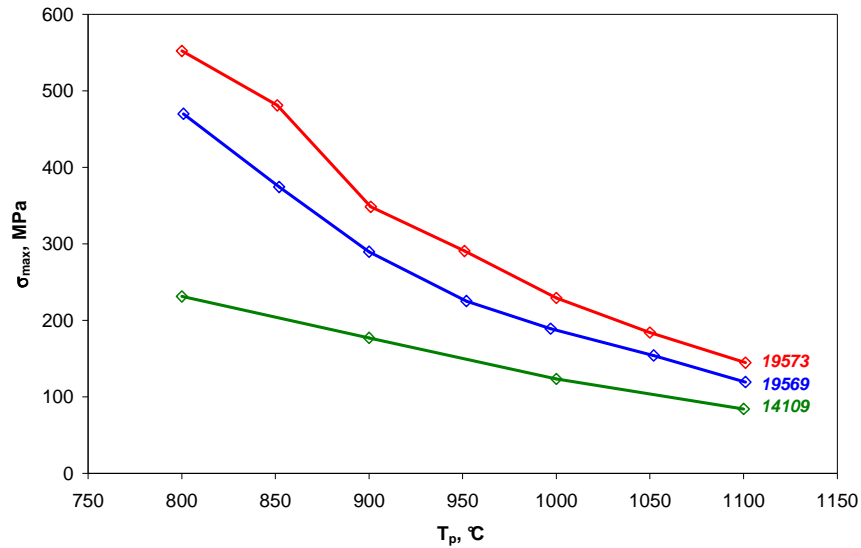
Fig. 1 Dependences of the maximal value of deformation resistance on temperature
for 3 Cr steels types, for strain rate 3.63 s^{-1}

It is evident from the figure that higher Cr content in steel markedly increases the deformation resistances mainly at lower temperatures.
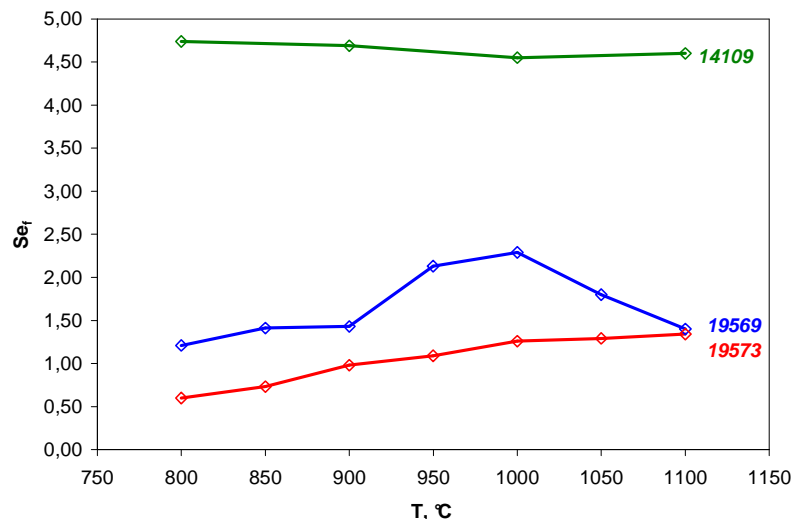
Fig. 2 Formability comparison of three given steels

For evaluation of chances of thermomechanical rolling of the bearing steel an influence of intermittent forming with pauses of 10 seconds in the austenite region was in-

vestigated. Nevertheless, finishing rolling was realized in a two-phase region at variable temperature and constant strain and strain rate.

Figure 3 presents the regime of anisothermic intermittent test (APZ) with preheating to 1180 °C/10´, followed by further 12 deformations with "inter-pauses" of 10 seconds from temperature of 1150 °C. This regime takes into account terms of thermomechanical rolling in final passes. It means that the region of thermomechanical rolling occurs in temperature range of 815–780 °C.
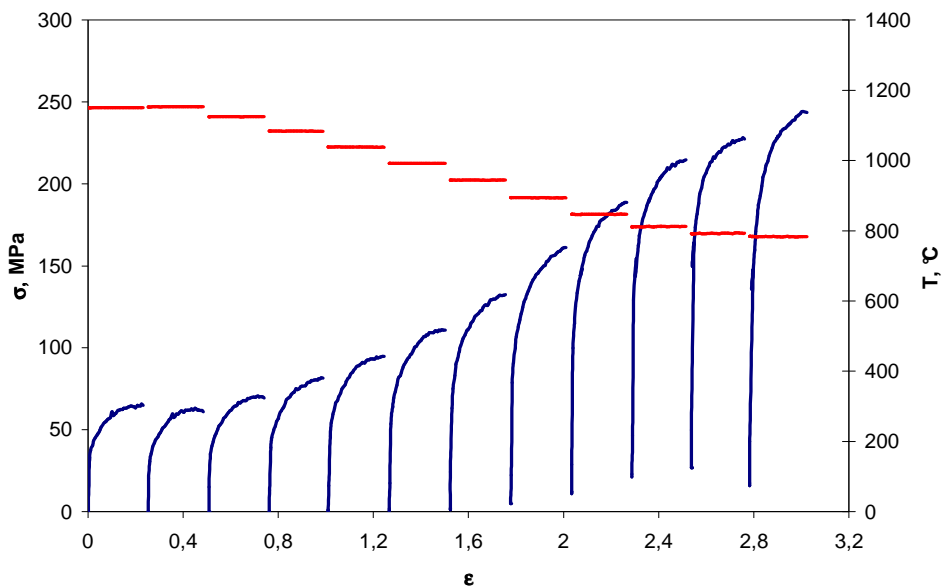
Fig. 3 14109 steel. APZ followed after heating to 1180°C/10´
and after 12 deformations, then water quenching
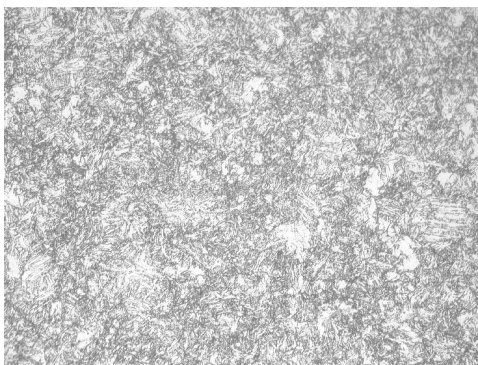
Fig. 4a The microstructure after APZ – surface of sample (×500)

Fig. 4b The microstructure after APZ – centre of sample (×500)

The results of following metallographic analysis show the final structure after 12 passes deformation regime as we can see in Figures 4a and 4b. There are presented microstructures from surface and centre areas of test sample.

4. Conclusions

The experimental research of deformation behaviour and hot formability of 14109 bearing steel was carried out with the plastometric tests. The performed experiments and their evaluation by means of the proved methodology made possible to obtain supporting materials on deformation behaviour of the investigated steel. The results gained in such a way, as well as developed methodology of plastometric and metallographic testing, create a good basis for gradual optimization of the process technology in production of bars and wire rod made of this steel. The way leads through plastometric simulations of thermomechanical (controlled) rolling.

Temperature-deformation conditions of the previous forming influences the conditions for suppression of carbide networks. Suppression of carbide network can be reached under conditions that enable a sufficiently fast transition by the critical range of temperatures during cooling after forming, or after heat treatment. On the other side, excessively fast cooling can cause development of micro- and/or macrocracks, mainly in weakened places of gamma grain boundaries.

References

[1] Klimek, K., Musalek, J., Grycz, E.: *Improvement of centre quality of continuous cast round bloom with soft reduction in Trinecke zelezarny*, Conference METAL 2004, Hradec nad Moravici, 2004.

[2] Gembalova, P., Grycz, E., Boruta, J., Turonova, P.: *Investigation of possibilities of structure optimization of bearing steels*, In. FORMING 2005, Lednice, September 2005, p. 57–62, ISBN. 80-248-0888-9.

[3] Ganguly, S., Chakrabarti, I., Maheshwari, M.D., Mukherjee, T.: *Ultra Clean Steel For Anti-Friction Bearing Applications*, Bearing Steel Technology, ASTM STP 1419, J.M. Beswick, Ed. Americian Society for testing and Materials International, West Conshohocken, PA, 2002. p. 47–68.

[4] Daguier, P., Baudry, G., Bellus, J.: *Improved Bearing Steel For Applications Involving Debris*, Higher Loads and Temperatures, Bearing Steel Technology, ASTM STP 1419, J.M. Beswick, Ed. Americian Society for testing and Materials International, West Conshohocken, PA, 2002. p. 320–329.

[5] Boruta, J., Gembalova, P., Jilek, L., Kubina, T., Rusz, S.: *History and present days of Materials Forming Research in VITKOVICE*, In HADASIK, E.; SCHINDLER, I. (eds). Plasticity of Metallic Materials, Gliwice, Wydawnictwo Politechniki Śląskiej, 2004, p. 95–142. ISBN 83-7335-197-3.

[6] Schindler, I., Boruta, J.: *Utilization Potentialities of the Torsion Plastometer*, Poland, Katowice, Silesian University, 1998, p. 106, ISBN 83-910722-0-7.

[7] Pernis, R.: *Ciągnienie rur na trzpieniu swobodnym*, Rudy i Metale Nieżelazne, R 46, 2001, 7, p. 305–311, ISSN 0035-9696.

Ocena parametrów kształtowania na gorąco stali łożyskowej

W artykule przedstawiono ocenę parametrów odkształcania na gorąco stali łożyskowej 100Cr6 przy zastosowaniu plastometru skrętnego. Stale łożyskowe charakteryzują się wysoką zawartością węgla z dodatkiem chromu. Nierównomierne rozłożenie węglików i wtrąceń niemetalicznych pogarsza jakość stali, co limituje właściwości użytkowe, głównie żywotność łożysk. Obniżenie jakości struktury w procesie produkcji jest efektem występowania pasm węglików, segregacje oraz siatkę węglików na granicach ziaren. Przy zastosowaniu odpowiedniej prędkości chłodzenia można siatkę węglików zupełnie usunąć, a także uzyskać odpowiednią strukturę do dalszej obróbki cieplnej. Największy wpływ na wielkość ziarna austenitu oraz pasma węglików mają parametry metalurgiczno-technologiczne, skład chemiczny oraz czystość stali. Odpowiednie dotrzymywanie warunków końcowych etapów kształtowania plastycznego oraz chłodzenia jest zasadnicze dla uzyskania odpowiedniej jakości wyrobów. Odpowiednio duża szybkość chłodzenia zmniejsza ilość węglików na granicach ziaren, jednak może powodować powstanie mikro i makro szczelin, głównie na granicach austenitu.

Microstructure and mechanical properties of cold rolled, annealed HSLA strip steels

M. JANOŠEC, I. SCHINDLER, V. VODÁREK, J. PALÁT, S. RUSZ, P. SUCHÁNEK
VŠB – Technical University of Ostrava, 708-33, Ostrava, Czech Republic

M. RŮŽIČKA, E. MÍSTECKÝ
NOVÁ HUŤ – Válcovna za studena, spol. s r.o., Štramberská ulice, 706-02, Ostrava, Czech Republic

A large testing programme of a strip steel grade, microalloyed by vanadium, titanium and niobium, was conducted. The experiment was based on combination of cold rolling, recrystallization annealing, mechanical testing, metallographic examinations, SEM and TEM analyses. Samples in the form of stripes with dimensions of 3.9×25×500 mm were rolled in several passes with the total height reduction of 5 to 75 %. Particular partial strains were realized at room temperature in the housingless, hydraulically prestressed laboratory mill. Afterwards the laboratory mill products were annealed in the vacuum furnace with the protective gas atmosphere consisting of N_2+H_2. The annealed samples underwent the tensile test at the room temperature and the Brinell hardness test. The gained results – hardness, yield stress, tensile strength and their ratio, as well as elongation A80, were summarized in dependence on cold deformation before annealing.

1. Introduction

A significant part of hot rolled sheets and strips is subjected to process of cold rolling; in this process recrystallization cannot be realized due to low forming temperatures. Hence, during rolling structural changes have to come into existence, in which grains forming the basic matrix of the material are gradually stretched in the direction of the principal deformation and at the same time the directional arrangement of the crystallographic lattice is developed. So due to the deformation, structural and crystallographic texture is formed. Besides changes in the grain character also a "banding" arrangement of other structural phases, such as inclusions, carbides or pearlitic blocks, is formed [1].

A typical feature of such deformed structure is anisotropy of mechanical properties. The directional arrangement mentioned above is mostly undesirable with regard to demands that are put on the cold rolled strip or sheet. Therefore heat treatment in the form of annealing is integrated in the process for removal of this phenomenon. The chosen parameters of annealing, mainly temperature and time, have (together with other factors to which belong total cold reduction, the initial structural state of the material, etc.) the decisive influence on the character of microstructure and hence mechanical properties after annealing. Strength properties of the material decrease with

increasing of annealing temperature whereas, on the contrary, plastic properties increase. Values of strength or hardness decrease significantly at temperatures close to 600 °C; the larger is the previous cold reduction the more pronounced is the mentioned decrease [2, 3]. Influence of cold reduction of the material before annealing on transition of the recrystallization temperature is remarkable as well. The higher cold reduction of the material before annealing the lower recrystallization temperature. However, the time needed for accomplishment of recrystallization becomes very long at low temperatures [2].

Properties of the material reflect in principle its microstructure. The recrystallized grains should have an optimum size after annealing, which ensures favourable strength and plastic characteristics of the material.

It is good to remind that the principle of annealing consists not only in formation of the optimum microstructure after rolling but also in obtaining an appropriate structure before rolling [4] because the proper process of cold rolling is mostly difficult to realize without integration of intermediate annealing, by which restoration of plastic properties will occur.

2. Experiment

The initial material was in the form of pickled cuts of the hot rolled strip with thickness of 3.9 mm. Chemical composition of the studied HSLA steel is presented in Table 1.

Table 1. Chemical composition of steel (wt. %)

C	Mn	Si	P	S	Al	V	Ti	Nb	N
0.081	1.36	0.185	0.018	0.008	0.022	0.033	0.0297	0.067	0.0053

Samples in the form of stripes with dimensions 3.9×25×500 mm were rolled in several passes with the total height reduction of 5 to 75 %. Particular partial strains were realized at room temperature in the housingless, hydraulically prestressed laboratory mill stand Q110 [5]. Annealing with one of three modes mentioned below followed. The process was carried out in a laboratory vacuum resistance furnace in the protective atmosphere consisting of 90 % of nitrogen and 10 % of hydrogen. Parameters of particular annealing modes are shown in Table 2.

Table 2. Description of applied annealing modes

mode 1	120 °C/h // 530 °C // 2 h // 15 °C/h // 580 °C // 12 h // ----------- // ---------
mode 2	120 °C/h // 600 °C // 2 h // 15 °C/h // 650 °C // 6 h // ----------- // ---------
mode 3	120 °C/h // 650 °C // 2 h // 15 °C/h // 700 °C // 14 h // – 10 °C/h // 640 °C

They may be described in a following system: heating rate to an intermediate dwell // temperature of the intermediate dwell // time of the intermediate dwell // heat-

ing rate up to the dwell // temperature of the dwell // time of the dwell // rate of controlled cooling // temperature for finishing of controlled cooling.

The annealed samples underwent the tensile test at the room temperature and the Brinell hardness test (a ball of diameter 2.5 mm). The gained results – hardness HB, yield stress YS [MPa], tensile strength TS [MPa] and their ratio, as well as elongation A80 in %, were summarized in graphs in Figures 8–10 in dependence on cold deformation (i.e. relative height reduction) before annealing – ε [%]. The found out points were plotted in a coordinate system and the corresponding curves were constructed „in a manual way", without any exact mathematical rules.

3. Metallographic analysis

The samples for evaluation of structure by optical microscopy were taken from central parts of rolled out products (in the perpendicular section, parallel with the direction of rolling). The structure was evaluated from selected samples after annealing, but for comparison also from the initial – non-cold deformed sample. It may be seen in Figure 1 that structure after hot rolling was consist of very fine grains of ferrite (ferritic grain size G = 12–13) with occurrence of pearlite. Nevertheless, not all ferritic grains were equiaxed.

Microstructures of cold deformed samples after annealing may are shown in Figures 2–4. The selection of samples was based on the known fact that mechanical properties are essentially influenced by a character of microstructure. The structure in the case of all annealed modes was therefore evaluated for the reduction values in which significant changes of values of mechanical properties occur. In all annealing modes the structure consists of ferrite with a low fraction of pearlite, whose character and occurrence region (like the ferritic grain) depends on deformation and selected annealing mode.
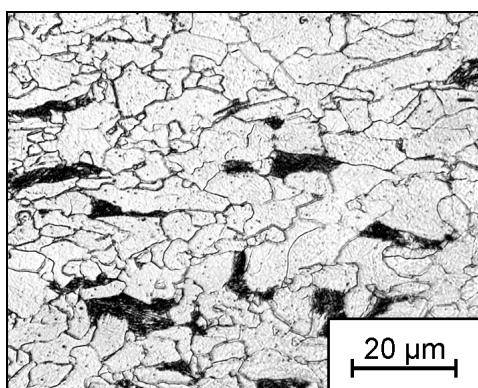
a) $\varepsilon = 5$ %

Fig. 1. Microstructure after hot rolling
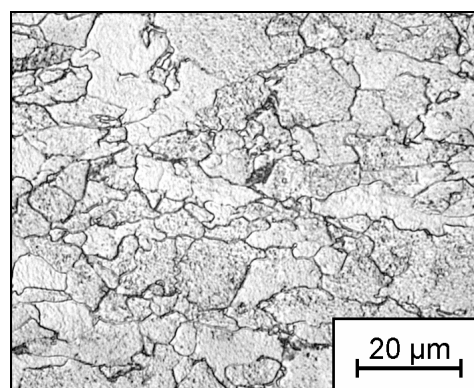
Fig. 2. Microstructure of samples annealed by mode 1 depending on previous cold deformation

M. JANOSEC et al.

b) $\varepsilon = 30$ %

c) $\varepsilon = 75$ %

Fig. 2. Microstructure of samples annealed by mode 1 depending on previous cold deformation

a) $\varepsilon = 5$ %

b) $\varepsilon = 15$ %

Fig. 3. Microstructure of samples annealed by mode 2 depending on previous cold deformation

c) $\varepsilon = 30$ %

a) $\varepsilon = 5$%
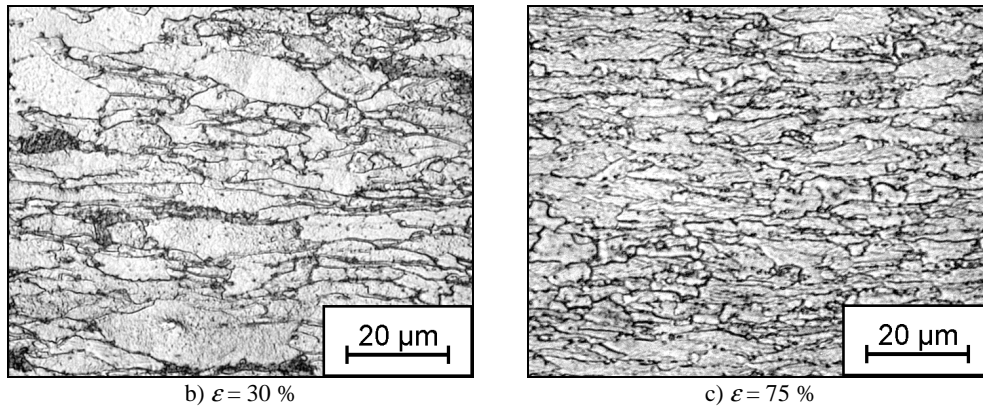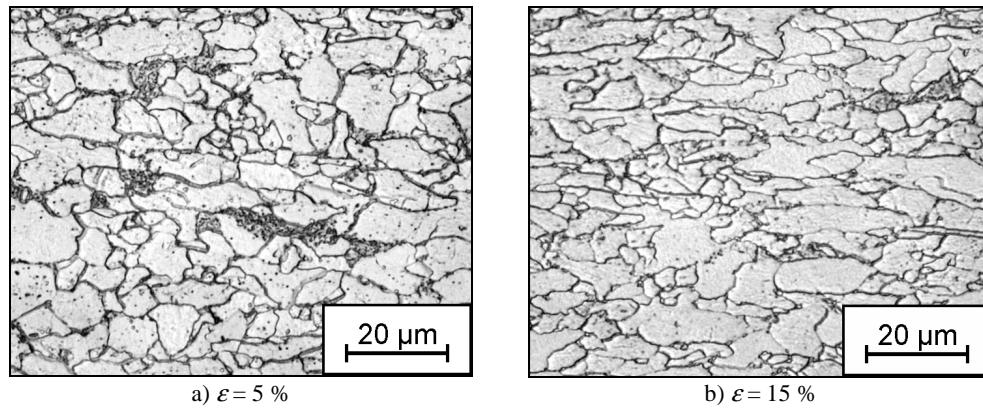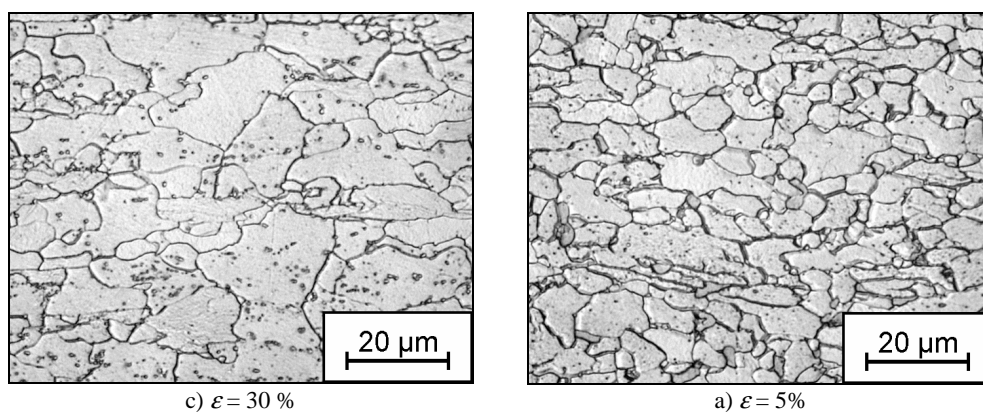
Fig. 3. Microstructure of samples annealed by mode 2 depending on previous cold deformation

Fig. 4. Microstructure of samples annealed by mode 3 depending on previous cold deformation

| b) $\varepsilon = 15$ % | c) $\varepsilon = 75$ % |
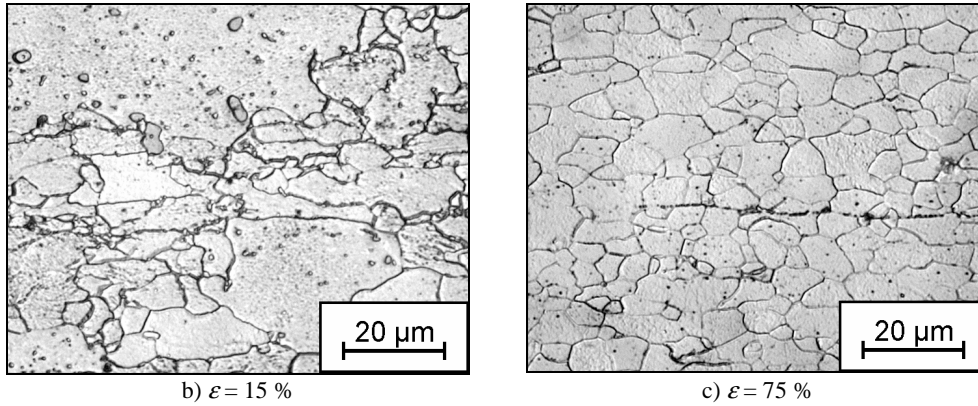
Fig. 4. Microstructure of samples annealed by mode 3 depending on previous cold deformation

4. SEM and TEM analysis of samples

The scanning electron microscopy (SEM) and transmission electron microscopy (TEM) was used for more detailed microstructure analysis and evaluation of minority phases in the investigated steel (compare with [6, 7]). The primary information was gained, the evaluating size, quantity and distribution of precipitates for the chosen samples annealed by mode 2. Moreover, also the initial microstructure after hot rolling was evaluated, because occurrence of particles mentioned above was anticipated also in this case.

Presence of complex particles of carbonitride or carbide of niobium and titanium was found out in the structure of the sample after hot rolling (Figure 5.).

| a) SEM | b) TEM |
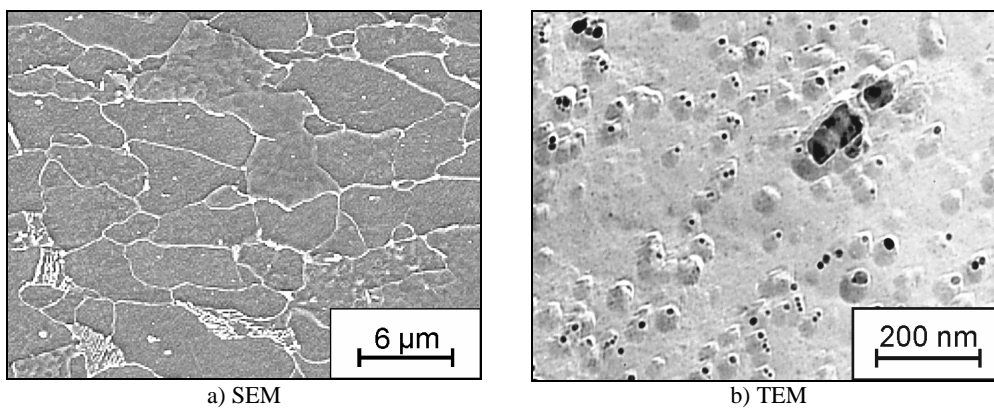
Fig. 5. Analysis of sample with microstructure after hot rolling

These complex precipitates were observed on boundaries, and also inside of slightly elongated ferritic grains bordered with cementite. Very fine MX particles,

relatively uniformly precipitated, which arose during hot deformation or during cooling of the rolled strip, were found out inside grains. With regard to solubility products of particular carbides and nitrides of microalloying elements in austenite and ferrite it may be assumed that fine particles are created by carbide of vanadium, in which a smaller amount of niobium can be dissolved. Size of these particles reached several tens of nanometers, at the maximum. Due to solubility of particles of carbide of vanadium in ferrite and austenite, precipitation of particles of this phase can be expected only at temperatures below ca 900 ºC, i.e. at normal hot rolling temperatures there is vanadium in the solid solution [8].

In Figure 6 microstructure of the sample annealed by mode 2 after cold deformation of 20 % is shown. Size or shape of ferritic grains is not significantly different as compared to the initial state. However, globularization of cementite particles, which occur both on grain boundaries and inside ferritic grains, came into being. The relatively uniform distribution of these particles in ferrite is due to cold deformation that crumbled pearlitic colonies, present in the initial microstructure. The subsequent annealing resulted in globularization of cementite particles.

a) SEM   b) TEM
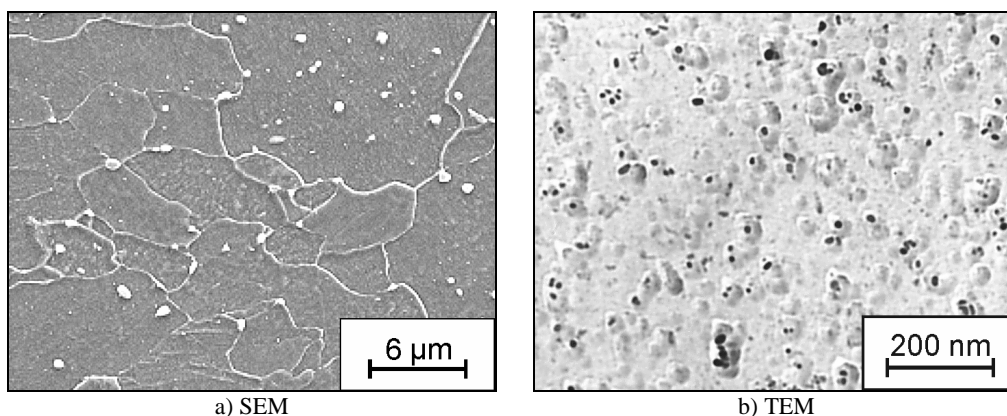
Fig. 6. Analysis of sample with microstructure after cold
deformation of 20 % and annealing in the mode 2

A large amount of fine, to a certain extent unspecified and relatively uniformly distributed MX particles occurs inside ferritic grains. It can be presumed that these particles are carbides of vanadium, in which niobium used to be dissolved to a lesser extent. A mean size of these particles was slightly larger in comparison with the hot rolled sample. Fine MX particles were precipitated locally in lines as a result of possible precipitation on grain boundaries. However, this hypothesis would have to be added with investigation of thin foils. The origin of these fine, to a certain extent unspecified particles can essentially be double. The overwhelming majority of precipitates was already present in the initil material before deformation and annealing. Speed of growing or coarsening of these particles during annealing was subsequently

accelerated by the previous cold deformation. On the contrary, only a small share of these precipitates could be evolved during annealing in the case that vanadium and/or niobium content surpassed a value of solubility of the given elements at the used annealing temperatures (600 or 650 °C).

In Figure 7 microstructure of the sample after annealing with the preceding total height reduction of 50 % is presented. Insignificant differences regarding to features of ferritic grains as well as distribution of cementite particles in comparison with the sample with deformation of 20 % are not necessary to comment. Nonetheless, more significant differences occur in size, shape (see the sticks in Figure 7b) or distribution of fine MX particles (it is probable that carbides of vanadium contain niobium to a lesser extent). A mean size of these precipitates was significantly higher and occurrence rate in the matrix lower in comparison with the sample that underwent cold deformation of 20 %. Thus it is clear that the cold deformation has a key importance – it represents constraining force of growing and coarsening of precipitates.

a) SEM   b) TEM
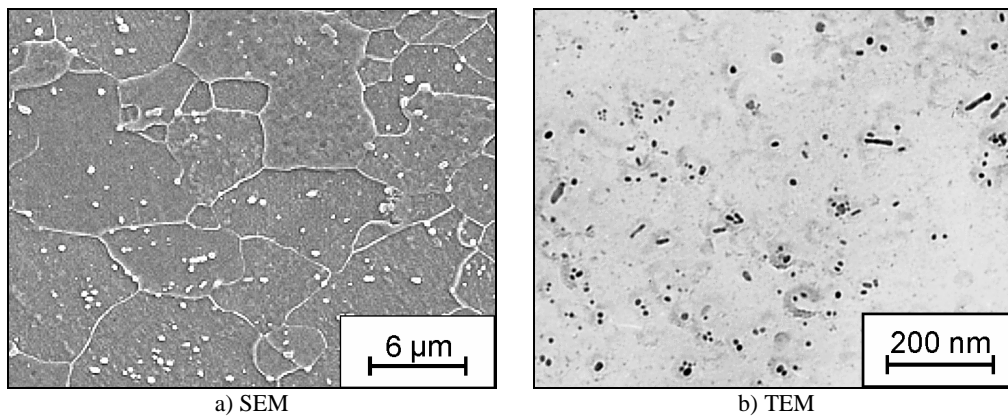
Fig. 7. Analysis of sample with structure after cold
deformation of 50 % and annealing in the mode 2

5. Discussion of results

Annealing mode 1 (Figure 8) is featured by a slow increase of strength properties with rising strain up to the value of $\varepsilon = 30$ %, after reaching this value a relative steep drop follows, which is caused by the course of recrystallization. The plastic properties (elongation and YS/TS ratio) were relatively less influenced by the previous deformation and they are worse than in case of other annealing modes.

The trend of strength properties in case of the second annealing mode (Figure 9) is a little bit more complicated in comparison to the first one because a steep fall of the strength properties follows after a mild raise of yield stress and tensile strength. In the first annealing mode the maximum strength properties correspond to deformation of 30 %. On the other side, in the second annealing mode the lowest strength properties

correspond to reduction of 30 %. Development of the plastic properties is not so complicated, but the trend of elongation A80 corresponds to development of the strength properties.

The third annealing mode (Figure 10) exhibits the trend of the strength properties similar to the second annealing mode, with a difference that decrease in yield stress (YS) or tensile strength (TS) is shifted towards lower strains and it is not so steep. The strength properties achieved by this mode of annealing are the lowest ones and, on the contrary, the plastic properties the best ones, what is not surprising with regard to a high annealing temperature.
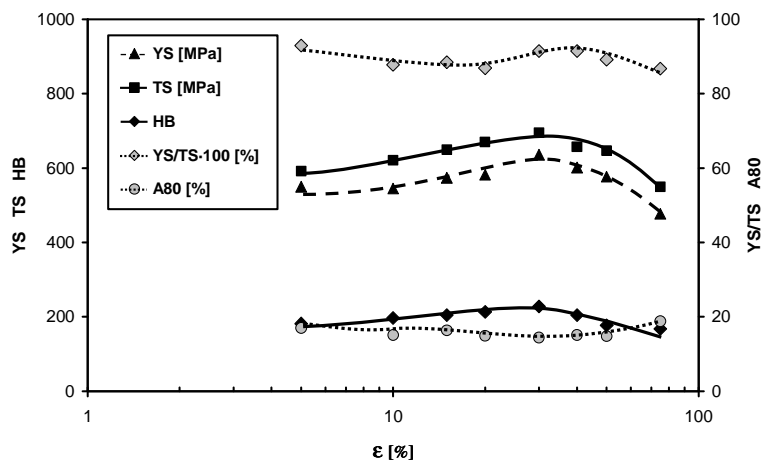
Fig. 8. Mechanical properties of samples annealed by mode 1
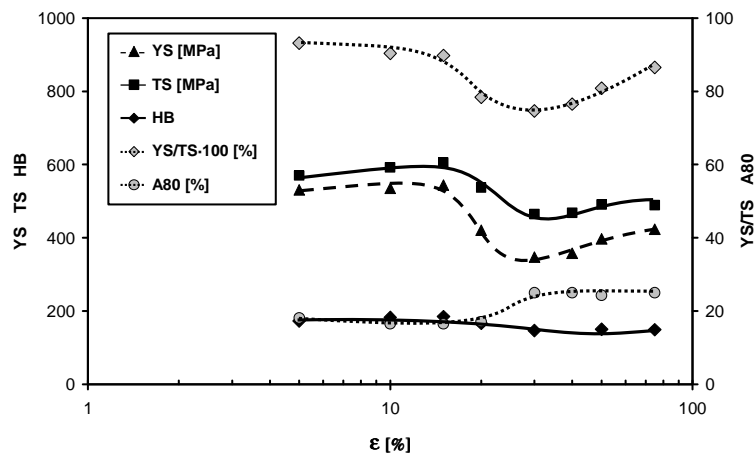
Fig. 9. Mechanical properties of samples annealed by mode 2
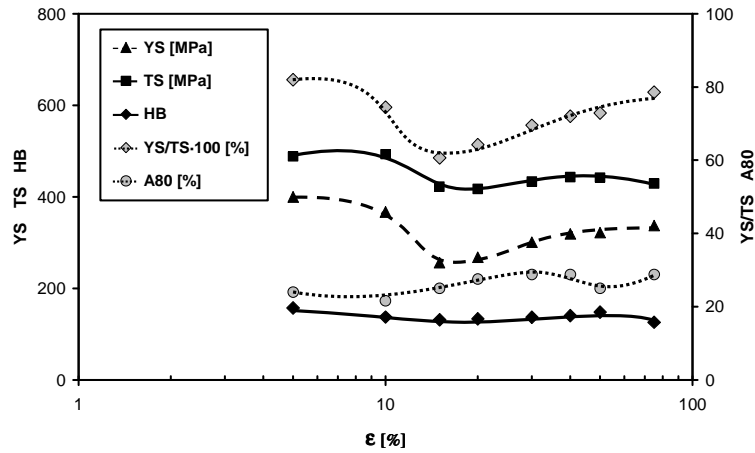
Fig. 10. Mechanical properties of samples annealed by mode 3

Trends of particular curves in all graphs reflect well the known relation between strength and plastic properties. Formability rises and vice, the versa strength properties fall with an increasing temperature of recrystallization annealing.

6. Conclusions

The obtained information on precipitates is compatible with character of grains of ferrite – see micrographs in Figure 3. A complicated course of the curves in Figure 9, which reflects effect of previous cold deformation on mechanical properties of the annealed strips, can be thus explained more acceptably.

By the described way it is possible to homogenize microstructure of strip and gain a major share of equiaxed grains of ferrite, but an average size of resulting grains is by no means significantly smaller than that one after hot rolling. It was confirmed that by a suitable combination of size of previous cold deformation and parameters of the following recrystallization annealing it is possible to influence (with a certain intention) a complex of the mechanical properties of particular strips. The strength properties of material were more or less decreasing with the rising annealing temperature, whereas plastic properties were increasing.

With regard to the fact that demands of the client on the resulting mechanical properties can vary a lot, it is of course not possible to establish a general-purpose annealing mode that would be the most suitable. Particular trends of the strength and plastic properties correspond to each other and they may be utilized for optimization of heat treatment terms of the investigated HLSA steel in a cold rolling mill, exactly in accordance with specific requirements for the relation between plastic and strength properties of the given material.

References

[1] Kollerová M. et al.: *Valcovanie*, ALFA, Bratislava, 1991.
[2] Dědek V.: *Tepelné zpracování ocelových pásů válcovaných za studena*, SNTL, Praha 1964.
[3] Prasat N. et al.: *Mechanical properties of cold-rolled annealed HSLA steel*, Journal of Material Science, Vol. 26, No. 19, 1991, 5158.
[4] Wiesner F.: *Válcování ocelových pásů za studena*, SNTL, Praha/Bratislava, 1961.
[5] http://www.fmmi.vsb.cz/model/
[6] Mishra (Pathak) S.K. et al.: *Investigations on precipitation characteristics in a high strength low alloy (HSLA) steel*, Scripta Materialia, Vol. 39, No. 2, 1998, 253.
[7] Pereloma E. V. at al.: *Strain-induced precipitation behaviour in hot rolled strip steel*, Materials Science and Engineering, Vol. 299, No. 1–2, 2001, 27.
[8] Pandit A. et al.: *Strain induced precipitation of complex carbonitrides in Nb-V and Ti-V microalloyed steels*, Scripta Materialia, Vol. 53, No. 11, 2005, 1309.

Mikrostrukura i właściwości mechaniczne wyżarzanych taśm stalowych HSLA walcowanych na zimno

Przedstawiono wyniki badań właściwości taśm ze stali mikrostopowych z dodatkami V, Ti oraz Nb. Przeprowadzony eksperyment obejmował walcowanie na zimno, wyżarzanie rekrystalizujące, badania mechaniczne oraz badania metalograficzne metodami SEM i TEM. Próbki w postaci pasów blachy o wymiarach 3,9×25×500 mm walcowano w temperaturze pokojowej, w kilku przepustach z całkowitym gniotem wynoszącym od 5 do 75% na laboratoryjnej bezstojakowej walcarce konstrukcji sprężonej. Odwalcowane pasma następnie wyżarzano w próżniowym piecu w atmosferze gazu ochronnego N_2+H_2. Wyżarzone próbki poddano próbie rozciągania w temperaturze pokojowej oraz pomiarowi twardości Brinella. Uzyskane wyniki – twardość, granica plastyczności, wytrzymałość na rozciąganie oraz wydłużenie A80 zestawiono na wykresach w zależności od odkształcenia względnego. Wyniki badań metalograficznych metodami SEM i TEM były podstawą do analizy zależności pomiędzy właściwościami mechanicznymi a mikrostrukturą. Wykazano, że zwiększanie odkształcenia plastycznego na zimno ogranicza skłonność do rozrostu wydzieleń podczas wyżarzania.

The impact of compression with oscillatory torsion on the structure change in copper

ANDRZEJ WROŻYNA, GRZEGORZ NIEWIELSKI, KINGA RODAK, DARIUSZ KUC,
FRANCISZEK GROSMAN, JACEK PAWLICKI
Silesian University of Technology, ul. Krasińskiego 8, 40-019 Katowice

The influence of compression with oscillatory torsion on the copper structure and force parameters are presented. The compression with oscillatory torsion method, developed in the Faculty of Materials Science and Metallurgy at the Silesian University of Technology, is used to achieve severe plastic deformation resulting in homogeneous ultrafine-grained structure of metals.

The deformation resistance of copper for various torsion frequency and compression rate is presented. The results of microstructural observations by using LM (light microscope) and TEM (Transmission Electron Microscope) technique are displayed as well. The geometrical parameters of structure elements and their misorientation angles were characterized by using TEM method.

Application of compression with oscillatory torsion was found to cause a remarkable decrease of deformation resistance as compared to compression without torsion. Plastic flow localized in shear bands was observed. Structures with large misorientation occur in microbands areas. The banded structure formed during compression with oscillatory torsion consists of well-formed, elongated subgrains.

Keywords: *copper, compression with oscillatory torsion, ultrafine-grained structure*

1. Introduction

Ultrafine-grained materials (both nano- and submicrometric) possess favourable physical and mechanical properties in comparison with conventional alloys. Ultrafine-grained metallic materials are mainly obtained by the following severe plastic deformation methods: high pressure torsion (HPT) [1], equal-channel angular pressing (ECAP) [2], cyclic extrusion/compression (CEC) [3]. The nanometric structures obtained by means of these deformation methods differ in many aspects such as structure refinement, homogeneity as well as mechanical and physical properties [4, 5].

Compression with oscillatory torsion is one of forming methods characterized by controlled strain path [6]. The discovered effects, such as force parameters modification and structure change, imply feasibility of much higher effective strain than the ones acquired by traditional forming methods [7, 8]. Moreover, there is a total lack of information concerning the impact of the presented method of deformation on structural phenomena co-occurring with grain size refinement. In this article, the the investigation results of the influence of compression with oscillatory torsion on submicrometric and nanometric structure have been presented, as observed in copper of 1ME grade.

2. Material for the study

In the study, the cylindrical samples of electrolytic copper M1E, of initial diameter $d_o = 10$ mm and initial height $h_o = 15$ mm ($h_o/d_o = 1.5$), have been used. Prior to the deformation, the copper had been annealed for two hours at the temperature of 550 °C and air-cooled. The mean grain diameter in copper initial state equaled 35 µm. The samples were deformed to the half of its initial height ($\Delta h = 7.5$ mm), applying the process parameters displayed in Table 1.

Table 1. The deformation process parameters

Pos.	Torsion frequency, f [Hz]	Torsion angle, $\pm \alpha$ [°]	Compression rate, v_t [mm/s]
1	0	0	0.6
2	0.4	6	0.15
3	0.4	6	0.6
4	1.6	6	0.15
5	1.6	6	0.6

3. The study

3.1. Deformation resistance

On the basis of the measurements taken during the deformation process, the relationship between the level of deformation resistances p_m and true strain ε_h was determined (Figure 1).
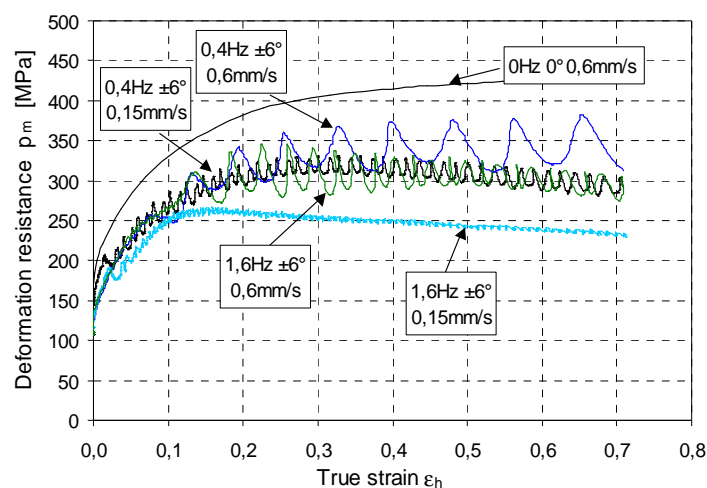
Fig. 1. The influence of strain parameters on deformation resistance value

The simultaneous increase of torsion frequency f (from 0.4 Hz to 1.6 Hz) and compression rate v_t (from 0.15 mm/s to 0.6 mm/s) does not seem to have any significant impact on the deformation resistance level. However, both the decrease of the compression rate v_t while maintaining the constant torsion frequency f, and the increase of the torsion frequency f while maintaining the constant compression rate v_t result in the reduction of the deformation resistance. This suggests that the force characteristics during the compression with oscillatory torsion are determined by the proportion of torsion cycles to the increase in the true strain $\Delta\varepsilon_h$ in a given time interval Δt.

The torsion strain – compression strain ratio (1) is a parameter determining the strain path (d_ε), which controls structural and force effects of the deformation. The torsion strain value is determined by the following: torsion amplitude (α_s) and torsion frequency (f). The compression strain contribution is determined by the compression rate (v_t). For a given time interval Δt, the relation of the strain is directly proportional to the increase in the torsion angle ($\Delta\alpha_s$) and inversely proportional to the increase in the reduction in height (Δh):

$$d_\varepsilon = \frac{\Delta\alpha_s}{\Delta h} = \frac{\alpha_s \cdot f \cdot \Delta t}{v_t \cdot \Delta t} = \frac{\alpha_s \cdot f}{v_t} \ . \tag{1}$$

For the constant torsion angle amplitude, this relationship is directly proportional to the torsion frequency and inversely proportional to the compression rate.

3.2 Structure assessment

The investigation was performed on the longitudinal section in the area representative for the compression process [9], which is to be found at the half-height of the sample at a distance 0.8 of the sample radius. The substructure has been tested with JEOL 100B transmission electron microscope (TEM) with an accelerating voltage 100 kV. The quantitative tests have been performed with MOP-AMO 3 semi-automatic image analyser.

The light microscope microstructure analysis has revealed that in the samples compressed without and with oscillatory torsion deformation bands are visible, grouped in macrobands (Figures 2 and 3). The modification in the deformation technique apparently has not affected the microscopic image of the deformation or shear bands (Figure 3).

Thin foil analysis provides more information about the structure change occurring during compression with or without oscillatory torsion.

Apart from the forming cellular dislocation microstructure (Figure 4a) and dislocation bands (Figure 4b), the compression is followed by the creation of a system of intersecting dislocation bands (Figure 4c), which proves that deformation has commenced in two slip systems.
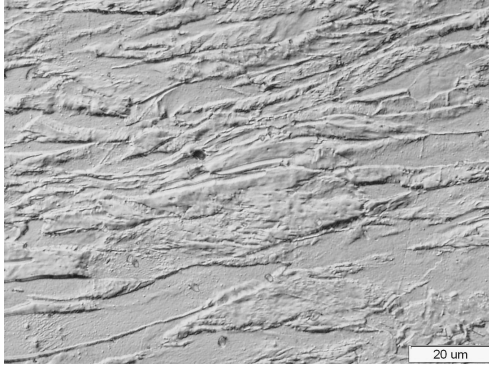
Fig. 2. The microstructure of copper following
the compression without oscillatory torsion
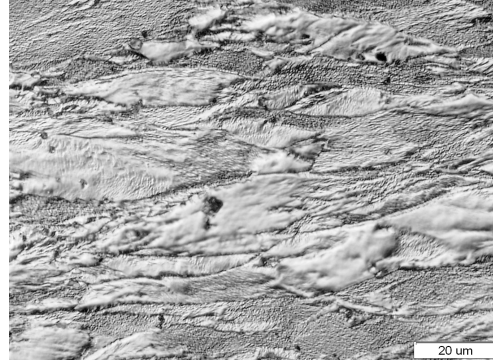
Fig. 3. The microstructure of copper following
the compression with oscillatory torsion
($f = 0.4$ Hz, $\alpha = 6°$, $v_t = 0.6$ mm/s)
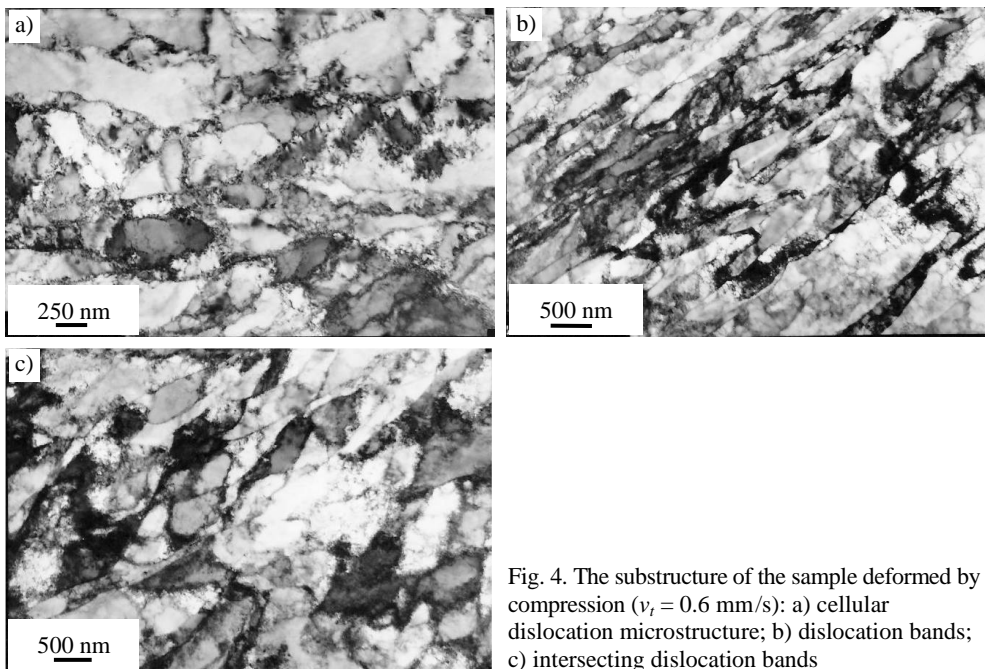
Fig. 4. The substructure of the sample deformed by
compression ($v_t = 0.6$ mm/s): a) cellular
dislocation microstructure; b) dislocation bands;
c) intersecting dislocation bands

The cellular dislocation microstructure prevails in the copper compressed at $f = 0.4$ Hz, $\alpha = 6°$, $v_t = 0.15$ mm/s (Figure 5a). In other areas, banded structure is formed, in which dislocation cells are frequently visible among the elongated dislocation boundary systems (Figure 5b). Occasionally, the intersection of dislocation bands can be observed (Figure 5c). In addition to this, narrow, largely disoriented bands appear, mainly in the cellular dislocation microstructure zones (Figure 5d).
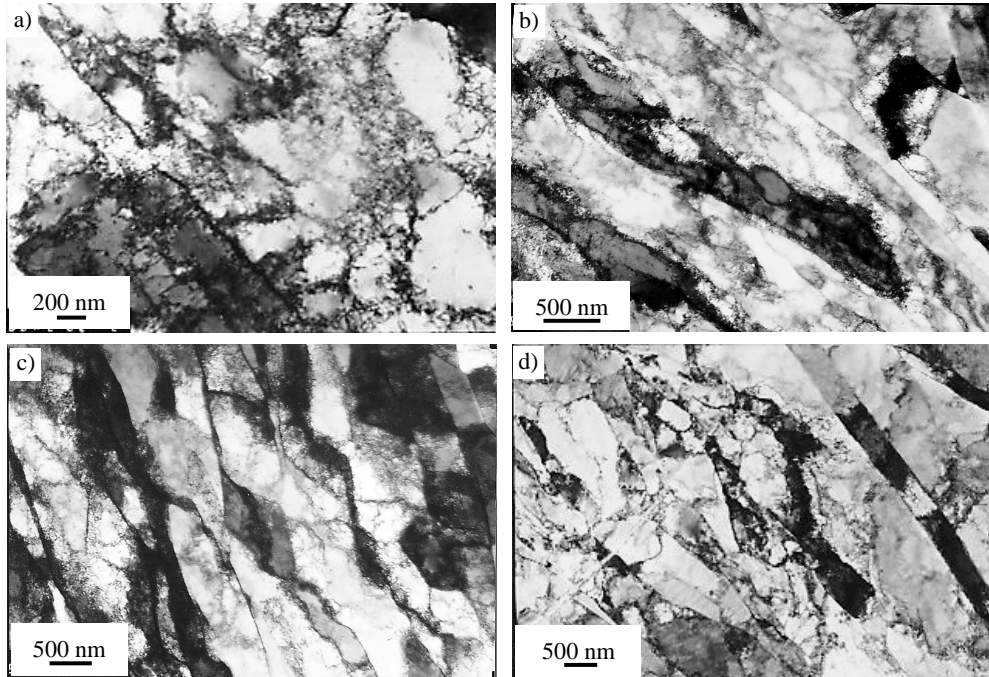
Fig. 5. The substructure of the sample compressed with oscillatory torsion ($f = 0.4$ Hz, $\alpha = 6°$, $v_t = 0.15$ mm/s): a) the cellular dislocation structure; b) the banded structure; c) the intersecting dislocation bands; d) the microband in the cellular dislocation microstructure zone

The qualitative assessment of the dislocation density indicates its reduction in the cellular zone following the compression with oscillatory torsion. This suggests that the density of the defects affects partial recovery phenomenon.
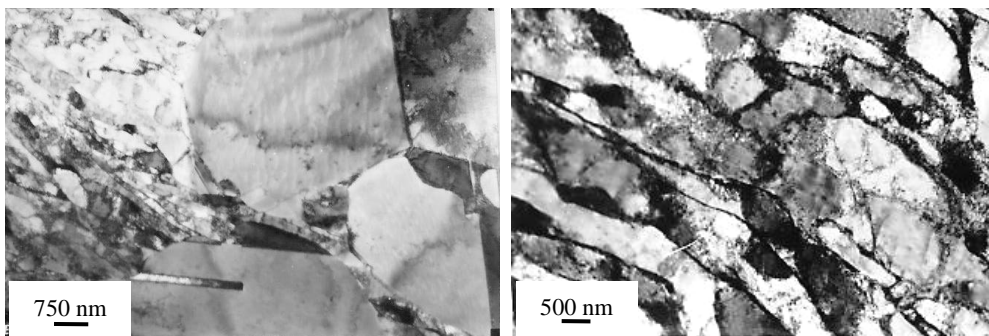
Fig. 6. The recovery and recrystallization in the sample deformed at $f = 0.4$ Hz, $\alpha = 6°$, $v_t = 0.6$ mm/s

Fig. 7. Banded structure containing elongated, well-formed subgrains ($f = 1.6$ Hz, $\alpha = 6°$, $v_t = 0.15$ mm/s)

As the compression rate increases to $v_t = 0.6$ mm/s, the creation of cellular and band microstructure or intersecting dislocation bands is accompanied by recovery and recrystallization processes (Figure 6).

The torsion frequency rise up to $f = 1.6$ Hz without changing other parameters ($\alpha = 6°$, $v_t = 0.15$ mm/s) intensifies largely disoriented microband formation processes. The dislocation banded structure differs from the typical long bands characteristic of compression: well-formed, elongated subgrains are visible (Figure 7), which confirms the presence of continuous strengthening and reconstruction processes.

In the samples compressed with oscillatory torsion at $f = 1.6$ Hz, $\alpha = 6°$, $v_t = 0.6$ mm/s, fine elongated grain structure is present inside shear bands (Figure 8a, b). Diffraction analysis has proved the crystallites to be divided by wide-angular boundaries (Figures 8a, b).

The quantitative analysis indicates that their average width equals 227 nm, and crystallites ranging from 100 to 250 nm in width are the most frequent (Figure 8d).
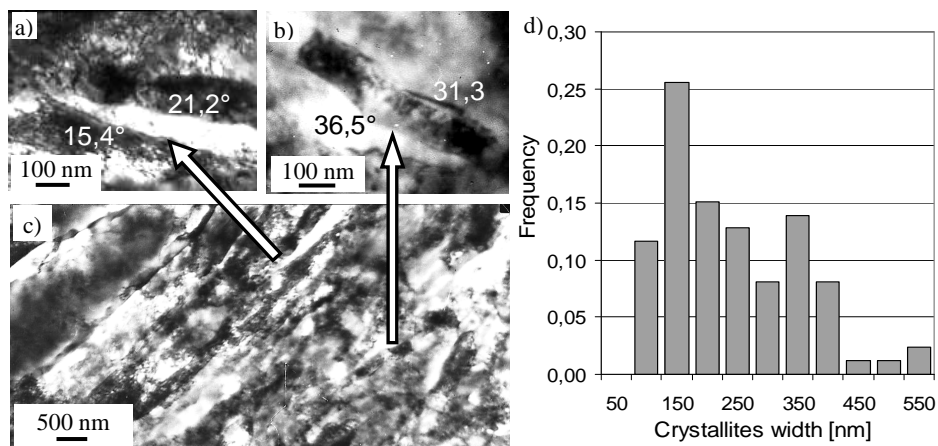
Fig. 8. The substructure of copper following the deformation at $f = 1.6$ Hz, $\alpha = 6°$, $v_t = 0.6$ mm/s : a, b, c) the shear bands containing fine, elongated crystallites; d) the histogram of crystallite width

4. The result analysis

There are notable differences between the structures of copper deformed by the compression with and without oscillatory torsion. It is a result of the change in the plastic flow mechanism from multi-system one, typical for the compression (Figure 4c) to shear band-located one, distinctive for compression with oscillatory torsion (Figure 8). The application of compression with oscillatory torsion results in the dominance of dislocation bands converting into elongated grain systems without the width change (Figure 8) instead of lamellar structure formation, typical for the compression.

The formation of shear bands, resulting from the strain localization, is also distinctive for the compression with oscillatory torsion, which were formed at $f = 1.6$ Hz, $\alpha = 6°$, $v_t = 0.6$ mm/s (Figure 8). In the sample deformed at $f = 0.4$ Hz, $\alpha = 6°$, $v_t = 0.6$ mm/s, intensive recovery and recrystallization processes have been detected. The shear bands, transferring numerous strains, exhibit strengthening gradient, and therefore they may constitute new grains nucleation places. This suggests that shear bands, with consecutive nucleation and recrystallization front migration, determine the strain mechanism in the compression with oscillatory torsion method and restrain the process of new grain refinement below 150 nm.

5. Conclusions

The following conclusions have been drawn on the basis of the conducted study:
- the strain path course has a decisive impact on the deformation resistance,
- the method of forming determines the properties of the newly-formed structure,
- banded structure and cellular dislocation systems are typical for the compression,
- in the compression with oscillatory torsion, a structure containing cellular dislocation systems as well as well-formed, elongated subgrains and grains is created,
- the application of compression with oscillatory torsion initiates the strain localization processes as well as recovery and recrystallization processes.

References

[1] Hyoung Seop K., Sun Ig H., Young Shin L., Dubravina A., Alexander I.: *Deformation behaviour of copper during a high pressure torsion process*, Journal of Materials Processing Technology, 2003, 2, p. 334.

[2] Hyoung Seop K., Min Hong S., Sun Ig H.: *Plastic deformation analysis of metals during equal channel angular pressing*, Journal of Materials Processing Technology, 2001, 113, p. 622.

[3] Richert M., Liu Q., Hansen N.: *Microstructural evolution over a large strain range in aluminum by cyclic-extrusion-compression*, Materials Science and Engineering, 1999, A260, p. 275.

[4] Ferguson D., Chen W., Kuziak R., Zając S.: *New developments in the field of physical simulation of thermomechanical processing*, Proceedings of the 5th Scientific Internation Conference on Materials Forming, ESAFORM, (ed. by Pietrzyk M.), AGH, Kraków, 2002, p. 599.

[5] Richert M., Korbel A.: *The effect of strain localization on mechanical properties of A199,992 in the range of large deformation*, Journal of Materials Processing Technology, 1995, 53, p. 331.

[6] Pawlicki J., Grosman F.: *Charakterystyki materiałowe dla oscylacyjnego skręcania*, FiMM 2003 – Fizyczne i matematyczne modelowanie procesów obróbki plastycznej, Prace Naukowe Politechniki Warszawskiej, z. Mechanika, 2003, 201, p. 139.

[7] Valiev R.Z., Islamgaliev R.K.: *Bulk nanostructured materials from severe plastic deformation*, Progress in Materials Science, 2000, 45, p. 106.

[8] Salishchev G., Zaripova R., Galeev R., Valiakhmetov O.: *Nanocrystalline structure formation during severe plastic deformation in metals and their deformation behaviour*, Nanostructured Materials, 1995, 6, p. 913.

[9] Grosman F. i wsp.: *Określenie dla próby ściskania reprezentatywnego obszaru badań twardości i struktury*, Forming 2001 International Conference, Stara Lesna, 30 August – 2 September, 2001, p. 63.

Wpływ odkształcania metodą ściskania z oscylacyjnym skręcaniem na zmianę struktury miedzi

W pracy przedstawiono wpływ ściskania z oscylacyjnym skręcaniem na mikrostrukturę miedzi i zmiany parametrów siłowych procesu odkształcania. Metodą ściskania z oscylacyjnym skręcaniem, nad którą trwają prace na Wydziale Inżynierii Materiałowej i Metalurgii Politechniki Śląskiej, realizuje się duże odkształcenia plastyczne w celu uzyskania jednorodnej struktury ultradrobnoziarnistej.

W pracy opisano wpływ parametrów procesu na przebieg średnich nacisków jednostkowych oraz strukturę miedzi obserwowanej metodami mikroskopii świetlnej i transmisyjnej mikroskopii elektronowej. Określono cechy geometryczne elementów substruktury oraz ich wzajemną dezorientację.

Stwierdzono, że zastosowanie metody niekonwencjonalnego odkształcania spowodowało spadek średnich nacisków jednostkowych w porównaniu z parametrami odkształcenia konwencjonalnego. Obserwowano lokalizację płynięcia plastycznego w pasmach ścinania. W obszarach mikropasm ścinania powstała struktura o dużym stopniu wzajemnej dezorientacji. Ponadto stwierdzono, że struktura pasmowa tworząca się w procesie niekonwencjonalnego odkształcenia złożona jest z dobrze ukształtowanych i wydłużonych podziarn.

Measurements of geometrical parameters of clad wires

W. KAZANA, L. CIURA
The Institute of Non-Ferrous Metals, Gliwice

J. SZALA, E. HADASIK
The Silesian University of Technology, Katowice

The measurements of geometrical parameters of the FeNi42Mn1/Cu clad wires obtained by various deformation schemes have been presented. Analysis of geometrical parameters of a wire cross-section was made by means of a computer program for digital image analysis. The measurements of geometrical parameters of several sets of clad wires 0.30 mm in diameter obtained by different drawing schemes show that thickness non-uniformity of an outer layer was small, within a range specified by the ASTM F29 standard.

Keywords: *clad wire, geometrical parameters*

1. Introduction

The bimetallic materials exhibit specific physical and mechanical properties, which are combination of the properties of the constituent metals and which can hardly be obtained for monometallic materials. The research works have been conducted at The Institute of Non-Ferrous Metals in Gliwice on the technology for fabrication of clad wires [1, 2] by longitudinal welding of a strip onto a base metal so as to obtain a product 5 mm in diameter, which is then subjected to further drawing and heat treatment. Forming of the welded bimetallic composite is conducted using drum-type and slip multiple drawing machines.

The clad wires composed of a core from FeNi42Mn1 alloy coated with a copper layer have been widely applied in electronic and electrical subassemblies, particularly as lead-in wires in light bulbs. Besides meeting specific requirements concerning mechanical and electrical properties and quality of a joint between base metal and a coating, it is important to ensure that the outer copper layer is distributed uniformly over the whole surface of a base metal thus making the vacuum-proof joint with glass sufficiently stable to withstand any thermal stresses that might occur within the joint. As a measure of this uniformity the ratio between maximum and minimum thickness of the coating (S_{max}/S_{min}) can be assumed, which according to the ASTM F29 standard [4] should be kept below 2.5.

In this work, examination results of geometrical properties of the FeNi42Mn1/Cu clad wires obtained using various deformation schemes have been presented. Analysis of geometrical parameters of a wire cross-section has been made by means of a digital

image analysis software developed in cooperation with the Silesian University of Technology in Katowice [3].

2. Experimental

Tests were made with the FeNi42Mn1/Cu bimetallic wires 0.30 mm in diameter, obtained from a welded charge subjected to forming by various schemes differing in a reduction per pass and in overall reduction. The charge material for welding process was copper strip 0.34 mm thick and 15 mm wide, and base metal wire of FeNi42Mn1 alloy, 4.1 mm in diameter. Welding was conducted by the TIG method with the rate 3 m/min at the welding current of 40 A. The processing schemes of welded bimetallic material are given in Tables 1–3.

Table 1. Drawing scheme No. 1

No	Operation	Parameters
1.	Drawing – $\phi5$–$\phi4.1$ mm	$\varphi_s = 0.377$
2.	Annealing – $\phi4.1$ mm	650°C/3h, 5%H_2 + 95%N_2
3.	Drawing – $\phi4.1$–…–$\phi0.3$ mm	$\varphi_s = 5.23$

where: φ_s – overall true strain.

Table 2. Drawing scheme No. 2

No.	Operation	Parameters
1.	Drawing – $\phi5$–$\phi4.1$ mm	$\varphi_s = 0.377$
2.	Annealing – $\phi4.1$ mm	650°C/3h, 5%H_2 + 95%N_2
3.	Drawing – $\phi4.1$–…–$\phi1.8$ mm	$\varphi_s = 1.65$
4.	Annealing – $\phi1.8$ mm	650°C/3h, 5%H_2 + 95%N_2
5.	Drawing – $\phi1.8$–…–$\phi0.3$ mm	$\varphi_s = 3.58$

Table 3. Drawing scheme No. 3

No.	Operation	Parameters
1.	Drawing – $\phi5$–$\phi4.1$ mm	$\varphi_s = 0.377$
2.	Annealing – $\phi4.1$ mm	650°C/3h, 5%H_2 + 95%N_2
3.	Drawing – $\phi4.1$–…–$\phi2.3$ mm	$\varphi_s = 1.16$
4.	Annealing – $\phi2.3$mm	650°C/3h, 5%H_2 + 95%N_2
5.	Drawing – $\phi2.3$–…–$\phi1$ mm	$\varphi_s = 1.67$
6.	Annealing – $\phi1$ mm	650°C/3h, 5%H_2 + 95%N_2
7.	Drawing – $\phi1$–…–$\phi0.3$ mm	$\varphi_s = 2.47$

3. Results

Exemplary microstructure images of bimetallic wires's cross-section of 0.30 mm in diameter obtained after drawing conducted in according to the schemes specified above are shown in Figures 1a–1f.
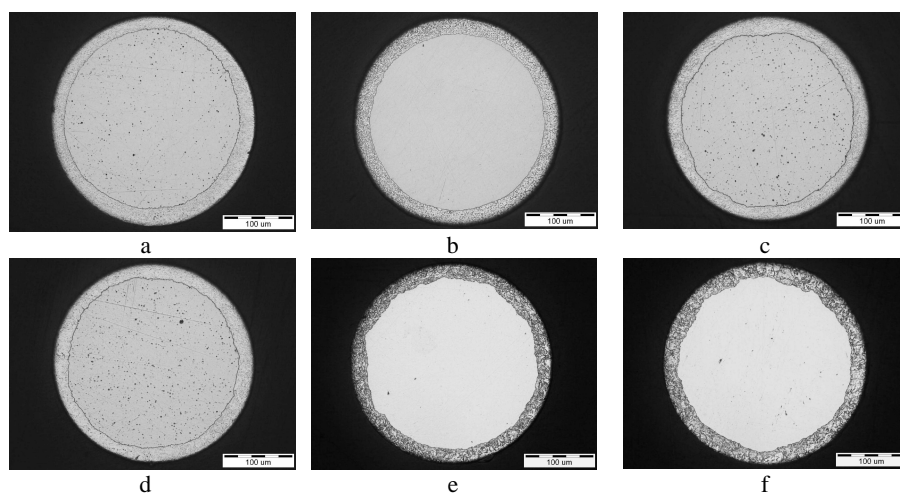
Fig. 1. Exemplary microstructure images of a cross-section of bimetallic wires 0.30 mm in diameter:
a) drawing scheme No. 1, $\varphi_p = 0.1625$, (set 1A), b) drawing scheme No. 1, $\varphi_p = 0.2744$, (set 1B),
c) drawing scheme No. 2, $\varphi_p = 0.1625$, (set 2A), d) drawing scheme No. 2, $\varphi_p = 0.2744$, (set 2B),
e) drawing scheme No. 3, $\varphi_p = 0.1625$, (set 3A), f) drawing scheme No. 3, $\varphi_p = 0.2744$, (set 3B),
(φ_p – true strain per pass)

The cross-section images have been subjected to digital analysis using GEODRUT software. The sheme of the clad wire's analysed cross-section is schematically shown in Figure 2. The developed software enables:
- measurement of clad wire diameter,
- measurement of base metal wire diameter,
- measurement of coating thickness; S_{max}, S_{min},
- wire/core eccentricity measurement.
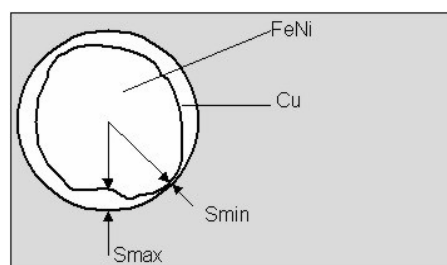
Fig. 2. Diagram of the clad wire analysed cross-section

A sequence of images illustrating multi-stage procedure of processing of the initial wire cross-section image, leading to the determination of an outer wire contour and the core contour, has been shown in Figure 3.
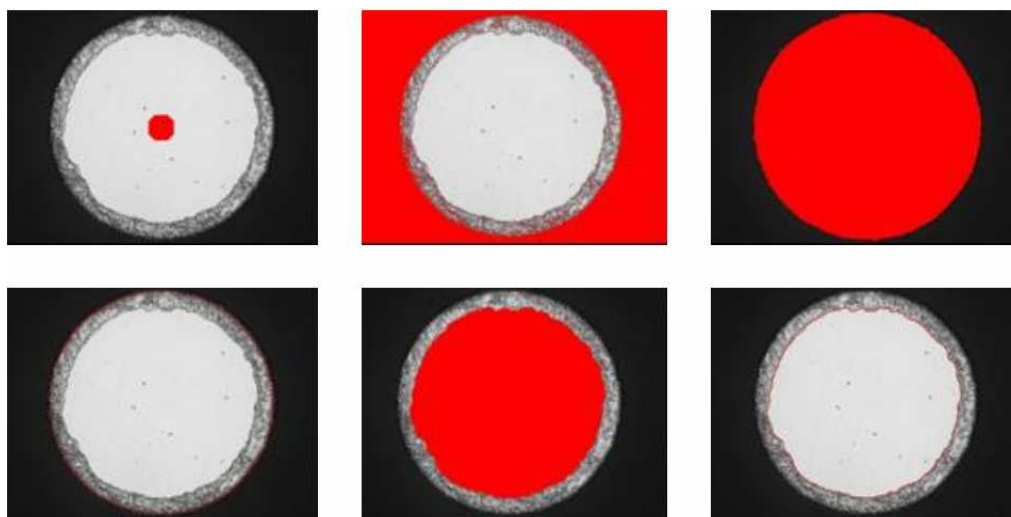
Fig. 3. Selected images obtained during multi-stage procedure
of processing initial image of a wire cross-section

The values of geometrical parameters of a cross-section of bimetallic wire produced by drawing according to the scheme no. 3 at $\varphi_p = 0.2744$, obtained from digital image analysis, are given in Table 4.

Table 4. Geometrical parameters of a cross-section of bimetallic wire produced
by drawing according to the scheme No. 3 at $\varphi_p = 0.2744$ (set 3B)

Parameter	Unit	Minimum	Maximum	Average	Change [%]
Wire diameter (average)	µm	293	297	296	0.346
Wire diameter (min)	µm	286	293	291	0.506
Wire diameter (max)	µm	297	303	300	0.44
Non-uniformity of wire diameter	%	0.512	0.641	0.565	7.06
Core diameter (average)	µm	250	252	252	0.192
Core diameter (min)	µm	238	243	241	0.643
Core diameter (max)	µm	260	267	262	0.689
Non-uniformity of core diameter	%	1.23	1.82	1.53	10.9
Layer thickness (average)	µm	21.2	23.3	22.4	2.62
Layer thickness (min)	µm	13.6	18.4	17	6.82
Layer thickness (max)	µm	25.8	29.4	27.7	3.91
Non-uniformity of a coating (S_{max}/S_{min})		1.48	1.96	1.63	7.34
Eccentricity wire-core	µm	0	1.46	0.82	42.97

Table 5. Geometrical parameters of bimetallic wire cross-sections at different drawing schemes applied

Set No.	Average wire diameter	Wire diameter variability index	Average core diameter	Core diameter variability index	Cu layer thickness (average)	Cu layer thickness (max.)	Cu layer thickness (min.)	Cu layer thickness variability index
	μm	%	μm	%	μm	μm	μm	%
1A	297	0.419	256	0.416	20.6	21.3	19.1	2.57
1B	296	0.331	255	0.489	21.2	21.9	20.5	1.53
2A	296	0.318	255	0.189	21.2	21.9	20.2	1.88
2B	294	0.350	253	0.177	21.0	21.5	20.0	1.80
3A	297	0.118	256	0.185	21.0	21.4	20.5	1.23
3B	296	0.346	252	0.193	22.4	23.3	21.2	2.58

Measurements of geometrical parameters of the FeNi42Mn1/Cu bimetallic wires 0.30 mm in diameter have shown that an average thickness of the copper layer was ranging from 20.6 to 22.4 μm, whereas an average non-uniformity of the copper layer expressed by the S_{max}/S_{min} ratio was ranging from 1.39 to 1.76, so it was below the maximum value specified in the ASTM F29 standard.

4. Conclusions

Computer program for digital image analysis, which can be used for quantitative description of layer morphology on a cross-section of single wire or a set of clad wires, has been developed. It enables to determine of a maximum and minimum thickness of an external layer bonded onto the base wire, what is important in the qualitative assessment of the clad wires. Under this work, measurements of geometric parameters of several sets of clad wires 0.30 mm in diameter, obtained by different drawing schemes, show that thickness non-uniformity of an outer layer was small, within a range specified by the ASTM F29 standard.

References

[1] Kazana W. Ciura L. Księżarek S.: Report from the targeted project No. 6T08 0097 2002 C/05766, (unpublished).
[2] Kazana W., Księżarek S., Ciura L., Besztak B.: *Selected scientific and technological aspects of fabrication of clad wires designed for specific applications*, Hutnik-Wiadomości Hutnicze, 2005, 2, p. 74–76.
[3] "Geodrut" computer program, Silesian University of Technology – IMN Gliwice, ASTM F29 standard.

Pomiar parametrów geometrycznych drutów płaszczowych

Przedstawiono wyniki pomiarów geometrycznych parametrów drutów bimetalowych FeNi42Mn1/Cu otrzymanych w procesie ciągnienia przy zmiennych warunkach odkształcania. Analiza parametrów geometrycznych na przekroju porzecznym drutów była wykonana przy pomocy opracowanego programu komputerowego do cyfrowej analizy obrazu. Wykonane pomiary dla drutów o średnicy 0.30 mm wykazały niewielką nierównomierność grubości zewnętrznej warstwy miedzi, poniżej wartości określonej w normie ASTM F29.

Bearing materials obtained by diffusion bonding of aluminium and aluminium bronze chips

W. CHMURA, Z. GRONOSTAJSKI

Wrocław University of Technology, Institute of Engineering and Automation, ul. Łukasiewicz 3/5, 50-371, Wrocław, Poland

An original concept of production a bearing composite by the mixing and bonding of aluminium and aluminium bronze chips through press molding, extrusion and heat treatment has been developed. Diffusion bonding process of aluminium and aluminium bronze chips leads to creation of phases typical for Cu-Al. alloys. The phases are created in small amount during extrusion of cold compacted mixture of aluminium and aluminium bronze chips and mainly during heat treatment applied after extrusion. This way, without participation of metallurgical processes good bearing materials can be manufactured

Keywords: *aluminium, bonding, phases, chips, sintering criterion*

1. Introduction

Among the different production possibilities of composites with predetermined properties, one of them is manufacturing composites from waste products. During the recycling of the waste by remelting a lot of the metal is lost as a result of oxidation, especially in the case of aluminium and its alloys, and the costs of labour and energy as well as the expenditures on environment protection raise the general cost of the manufacturing processes. Thus the great interest has been shown in chips recycling processes other then remelting [1].

The different ways of waste products recycling, consisting in the direct conversion of waste into compact metal by granulation, remoulding and hot extrusion or hot forging, where melting is eliminated, was elaborated. This kind of recycling can be applied not only to aluminium [2–5] and its alloys but also to iron, copper and, to some extent, to cast iron [6–9].

In the metallurgical process less than 54% of the aluminium and aluminium-alloy chips is recovered. In the case of the direct conversion of the same metals chips into compact metal by extrusion ultimately 95% of the metal is recovered [10–12].

The direct conversion of aluminium and aluminium-alloy scrap into compact metal include also a possible reduction in the funds spend on the labour, energy and environment protection as a result of the reduced consumption of ores and energy carriers, and less degradation of the natural environment because of reduced air-pollution emission.

Factors that contribute significantly the bonding of aluminium and aluminium-alloy chips contain: granulation degree of the aluminium and aluminium-alloy chips,

remoulding parameters, stress and strain states in consolidation pocesses, temperature and rate of consolidation processes, lubrication method and the used lubricants. In the case of composites with additional introduced reinforcing phases the amount, form and size of these phases are also very important. For the good bonding of granulated chips the large plastic deformation is needed. Such a deformation can be obtained in extrusion process with extrusion ratio, at least 4. The good lubrication improves the uniform deformation but it cannot hinder the bonding of the chips alone and with the consolidating phase.

The direct conversion recycling process was applied to aluminium and its alloy chips without reinforcing phases [2–4] and with the following reinforcing phases: tungsten, carbon, silicon carbide, ferro-chromium and aluminium oxide [5, 13, 14]. On the one hand reinforced phases decrease free movement of dislocations and increase the yield and the tensile strength but also increase the porosity and reduce these properties as well.

In recent years, researches have been aimed at producing composite materials based on aluminium for the manufacturing of bearings [15–17]. Such composites are conventionally produced from aluminium powders with silicon, silicon-carbide and graphite additions [18].

The new concept of producing composite by mixing and bonding of aluminium chips with aluminium bronze chips through press moulding and extrusion has been developed [19]. The particle dispersion has distinct effect on the kinetic of processes [20, 21] and conditions of sintering and extrusion can be analysed using deformation processing map [22, 23].

The main aim of the paper is to investigate the possibility of manufacturing of bearing materials obtained by diffusion bonding of aluminium and aluminium bronze chips, the phases created in the process and the composite properties and usefulness of elaborated sintering criterion.

2. Sintering criterion

The elaboration of the best method of chips recycling was based on sintering criterion. The sintering criterion is based on the assumptions that on the bonding of particles two factors have fundamental effect that are:

• the contribution of clear surface of particles, which are exposed during working processes as a results of the brittle surface layer fracture, to whole particle surface.

• the values of normal stresses acting on the clear surface of particles to bring them together on the atomic distance.

So the sintering criterion can be effected by these both factors in the following form:

$$dW_s = f\left(\sigma_n, d\varepsilon_1\right), \tag{1}$$

where:

dW_s – sintering indicator characterising the local quality of particles junction,

$d\varepsilon_1$ – increment of largest tensile strain,

σ_n – compression stress normal to the direction of largest tensile strain.

For isotropic materials there is consistence of principal stress and strain directions and the normal compression stress σ_n is equal to the largest principal compression stress σ_3.

Taking into account that the greater outspread of native surface the lower value of stresses is needed for good sintering, the indicator characterizing the local quality of sintering of particles can be described by the product of both factors as follows

$$dW_s = \sigma_3 d\varepsilon_1, \tag{2}$$

The good junction of the particles in the whole considered volume take place when sintering indicator W_s obtain the some critical value C_{cr}:

$$W_s = \int_0^{\varepsilon_1} \sigma_3 d\varepsilon_1 = C_{cr}, \tag{3}$$

For axisymetrical metal forming processes of incompressible materials component of principal strain state ε_1 can be expresses by other component of strain state ε_3

$$d\varepsilon_1 = -2d\varepsilon_2 = -2d\varepsilon_3, \tag{4}$$

Taking into account that sintered materials, especially during manufacturing, do not keep incompressible condition, that fact was expressed by introducing into relation (4) the compressible coefficient α:

$$d\varepsilon_1 = -2\alpha d\varepsilon_3, \tag{5}$$

where α is compressible coefficient.

Combining equations (3) with (5) the following relation is obtain:

$$W_s = \int_0^{\varepsilon_3} 2\alpha\sigma_3 d\varepsilon_3 = C_{cr}, \tag{6}$$

That means that for sintering of particles the defined unit work of largest principal compression stress on the largest suitable displacement is needed. For application of

such criterion the critical value of C_{cr}, which secures good junction of particles has to be known.

The parameter C_{cr} can be determined experimentally or analytically. Experimentally determination of the parameter can be obtained by measuring the forces of compacting by plastic deformation of particles in some kind of processes with different degree of deformation at different temperatures and strain rates. Then by using finite element method (FEM) the components of strain state ε_{ij} and stress state σ_{ij} are determined and plastic work of largest compression stress on the proper displacement according to relation (6) was calculated. The critical value of plastic work C_{cr} is the values on the flow stress – plastic work relation at the point of outset of plateau (Figure 1). This experimental method is very labour-consuming and strenuous. Much easier is to apply into analysis of sintering in metal working processes the theoretically calculated values of C_{cr} parameter.
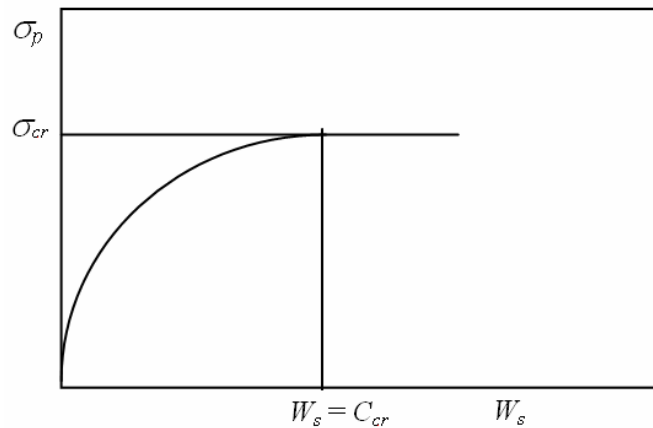
Fig. 1. Relation between flow stress and unit plastic work needed to manufacturing of composite

The theoretical calculation of the parameter C_r is based on the assumption that a n-fold increase of the particle surface area is enough to fracture the brittle surface layer and to exposure the native structure for joining of particles. As a measure of the deformation degree of the particle, the change of its surface area is taken. Assuming the cylindrical shape of the individual particle, the degree of the deformation can be given by the relation

$$S_p = \frac{2P_f + O_f H_f}{2P_o + O_o H_o}, \tag{7}$$

where:

P_o, P_f – the surface areas of the initial and final cross sections of the particle, respectively,

O_o, O_f – the peripheral lengths of the initial and final particle cross sections, respectively,

H_o, H_f – the initial and final heights of the particle, respectively.

In the former criterion [26] only side surface without the surface of cross sections perpendicular to cylindrical axis was taken into account. Since the volume V of the particle does not change, the following relations hold.

$$H_o = \frac{V}{P_o}, \quad H_f = \frac{V}{P_f},$$

which allows to rewrite (7) as follows

$$S_p = \frac{P_o}{P_f} \frac{2P_f^2 + O_f V}{2P^2_o + O_o V} = \frac{P_o}{P_f} \frac{2P_o^2 \left(\frac{P_f}{P_o}\right)^2 + O_o V \left(\frac{O_f}{O_o}\right)}{2P^2_o + O_o V} = A\sqrt{R_p} + (1 - A)\frac{1}{R_p}, \qquad (8)$$

where

$$R_p = \frac{d_o^2}{d_f^2} = \frac{P_o}{P_f} = \frac{O_o^2}{O_f^2} \quad \text{and} \quad A = \frac{VO_o}{2P_o^2 + VO_o}, \qquad (9)$$

where d_o, d_f are the initial and final substituted diameters of the particles.

Unfortunately, the values of A depends on the initial shape of the particle. To avoid this inconvenience, the following averaged values of S_p will be used

$$S_p = \beta\left(\sqrt{R_p} + \frac{1}{R_p}\right), \qquad (10)$$

where β is the coefficient equal to 0.5.

To apply the above given analysis to the whole volume of extruded ingot the α – compressible coefficient have to be introduced into equation (10), so it takes following form

$$S = \alpha\beta\left(\sqrt{R} + \frac{1}{R}\right), \qquad (11)$$

where R is the reduction of the cross section of the ingot, S is the ratio of the initial surface area to the final one of the. From that relation of the surface expansion $S/\alpha\beta$ as a function of the cross section reduction R (Figure 2) it can be stated that the lower compressibility of the composites the smaller deformation is needed for obtaining a good junction of the particles. For investigated aluminium composite containing 15% mass fraction of reinforcing CuAl8 phase and the aluminium particle size below 2 mm, the compressible coefficient α should be equal to 0.7.
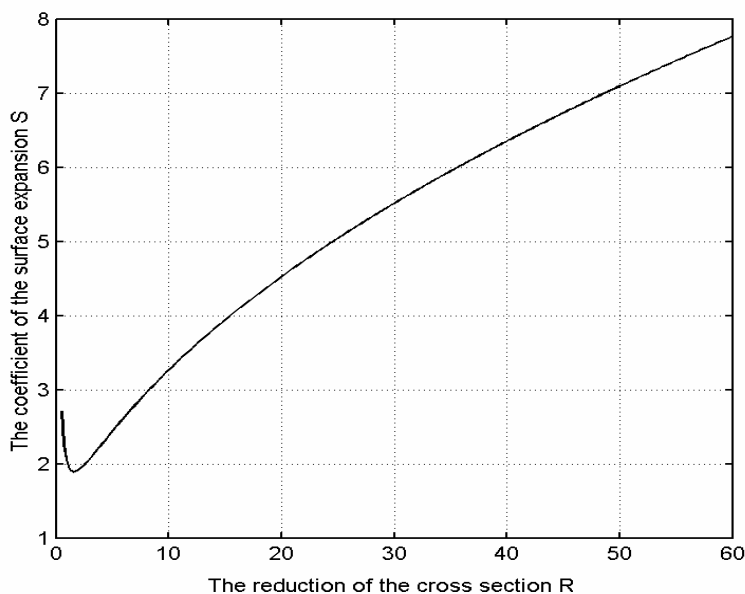
Fig. 2. The surface expansion $S/\alpha\beta$ as a function of the cross section reduction R

For a given surface expansion S, the limit strain needed for a good junction of particles in axisymetrical processes like extrusion can be obtained from the relation

$$\varepsilon_l = \ln \frac{d_0}{d_f} = \ln \sqrt{R} \tag{12}$$

The value of R appearing here can be determined from the Equation (11). To do this, the equation is transformed to the cubic algebraic equation

$$aR^3 + bR^2 + cR + d = 0 \tag{13}$$

with the coefficients $a = 1$, $b = -(S/\alpha\beta)^2$, $c = 2S/\alpha\beta$ and $d = -1$.

It is solved in the standard way. First auxiliary quantities

$$p = \frac{3ac - b^2}{9a^2} \text{ and } q = \frac{b^3}{27a^3} - \frac{bc}{6a^2} + \frac{d}{2a} \tag{14}$$

are introduced and the discriminate of Equation (13) is calculated

$$D = p^3 + q^2. \tag{15}$$

It should be noted that p, q and D depend on $z = S / \alpha\beta$.

The Relation (11) is not a one-to-one correspondence between S and R in general but from the practical point of view the values of $z = S / \alpha\beta > S_{min} / \alpha\beta \approx 2$ and $R > 2$ are interesting only. In this case, a one value of S corresponds to an exactly one value of R. Further, only such values of S and R will be considered.

Since then $p = p(z) < 0$, $q = q(z) < 0$ and $D = D(z) < 0$, the roots of Equation (13) are given by formulas:

$$R_1(z) = 2r(z)\cos(\varphi(z) / 3) - b / 3a,$$

$$R_2(z) = -2r(z)\cos(\pi / 3 - \varphi(z) / 3) - b / 3a,$$

$$R_3(z) = -2r(z)\cos(\pi / 3 + \varphi(z) / 3) - b / 3a,$$

where

$$r(z) = \sqrt{|p(z)|} \text{ and } \varphi(z) = \arccos\left|\frac{q(z)}{r(z)^3}\right|.$$

As the sought value of R, the greatest root of Equation (13) is chosen, which gives

$$R = 2r(z)\cos\varphi(z) / 3 - b / 3a .$$

Since $\left|\dfrac{q(z)}{r(z)^3}\right| \to 1$ or equivalently $\varphi(z) \to 0$, as $z \to \infty$ rapidly enough, the following approximate formula is proposed

$$R \approx Rap = 2r(z) - b / 3a = \left(2\sqrt{z(z^3 - 6)} + z^2\right) / 3 =$$
$$\left(2\sqrt{(S / \alpha\beta)((S / \alpha\beta)^3 - 6)} + (S / \alpha\beta)^2\right) / 3 \tag{16}$$

The R and R_{ap} values as a function of surface expansion are illustrated on the Figure 3.

For known stress–strain curves of aluminium composite containing 15 % of reinforcing CuAl8 phase (Figure 4) of the composite materials the calculation of critical values of the plastic work by using relation shown in Figure 2 can be performed.

$$C_{cr} = \int_0^{\varepsilon_l} \sigma_p d\varepsilon_{\text{int}} = W_s \,. \tag{17}$$
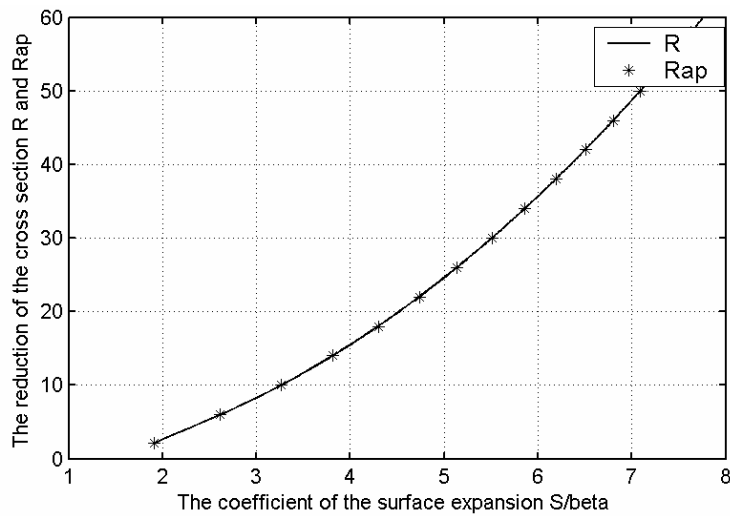
Fig. 3. The cross section reduction R and R_{ap} as a function of the surface expansion $S/\alpha\beta$
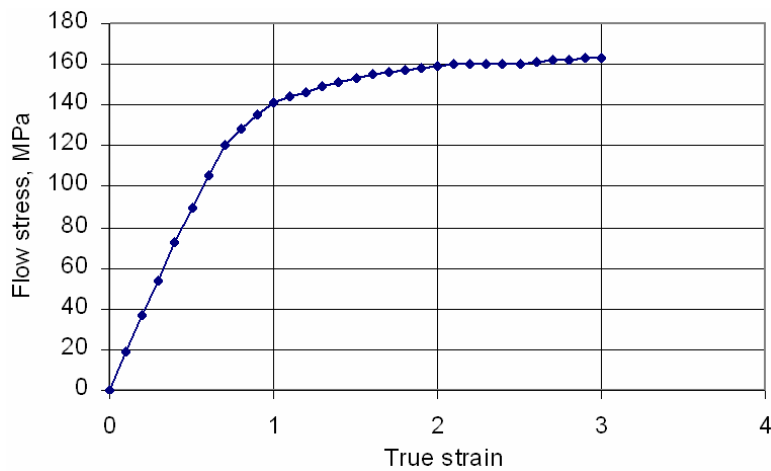
Fig. 4. True stress-true strain relation of aluminium composite
containing 15 % of reinforcing CuAl8 phase

The expansion of surface equal to 2 usually is enough to obtain good bonding of paticles that means from Figure 2 reduction about 6.25 and according to Equation (11) such reduction in area meet elongation equal to 0.916. By integration of Equation (17) the critical value of unit plastic work needed for good particles bonding determined from Figure 5 is equal to about 14×10^{-3} J.
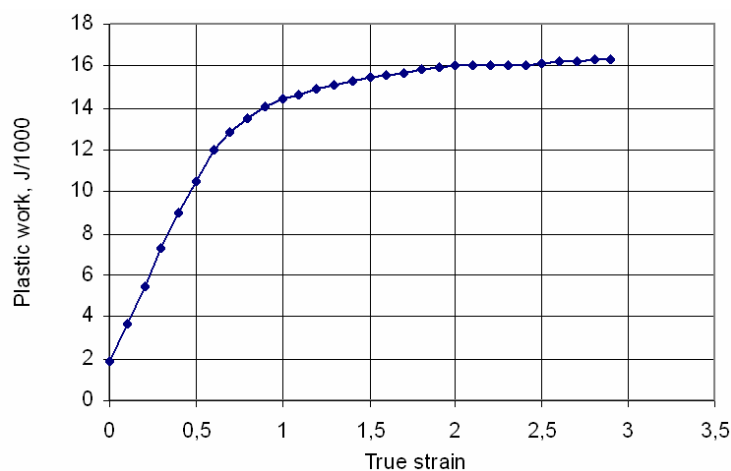
Fig. 5. The relation between unit plastic work and true strain

That is in good agreement with experimental results, where two values of reduction in area during extrusion was applied: 6.25 and 16. It was stated that even lower values of reduction was enough for good bonding of investigated composite particles. It means that sintering conditions of bearing aluminium matrix composites manufactured by recycling of communited aluminium and CuAl8 aluminium bronze chips determined experimentally were proper chosen.

3. Results and discussion

From Figure 6 it can be seen that diffusion in hot extruded composites is very small.

The heat treatment increases distinctly reciprocal diffusion of elements. The typical structures at the primary boundary between matrix and reinforcing phase are shown on the Figure 7.

The phase's identification performed by diffraction method in Ferrous Institute in Gliwice shows, that during heat treatment following new phases were created: γ_1, δ, ξ_2, η_2 and θ. All the phases are typical for phases in Cu-Al equilibrium diagram [25]. As a result of diffusion, the aluminium matrix of composites was slightly enriched in copper and CuAl8 reinforcing phase in aluminium also. In this way the typical structure of bearing materials was obtained.
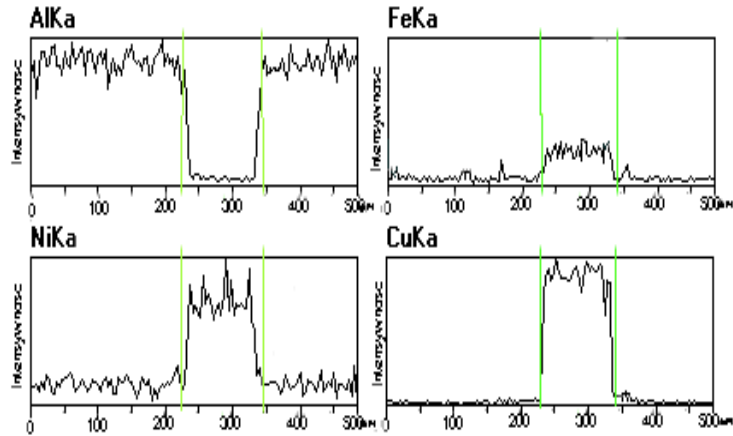
Fig. 6. Linear distribution of elements at grain boundary before heat treatment
of composite containing 22 % of aluminium bronze
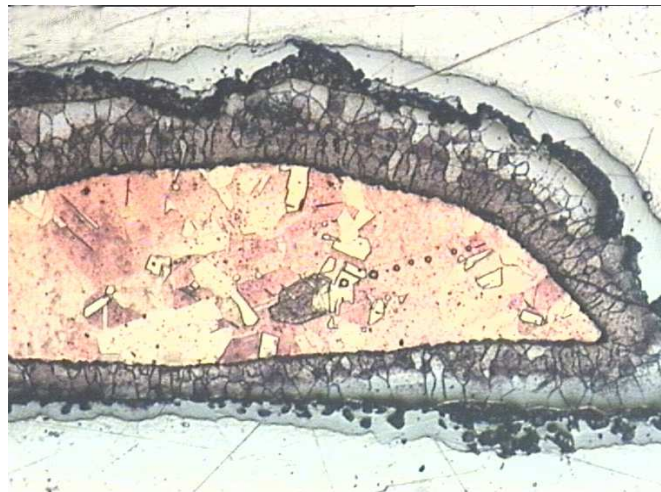
Fig. 7. Structure of composite containing 22% of aluminium bronze
after annealing in 545 ºC during 7 hours

The distribution of element concentrations at the aluminium matrix-reinforcing particle boundary after heat treatment is shown in Figure 8.

Composites before heat treatment are characterized by the weak bonding between particles of matrix and matrix and reinforcing phase. The weak bonding could deteriorate the wear of composites, because small particles could be pull out from the surface by collaborating sliding element. To improve the bonding the heat treatment of composites after extrusion was applied.
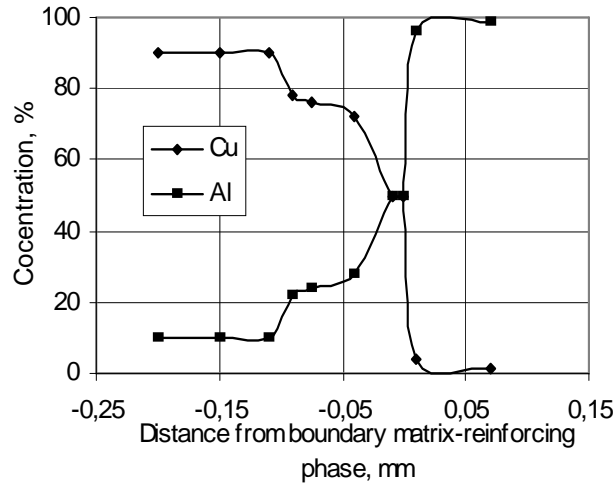
Fig. 8. Linear distribution of elements at grain boundary after 7 hours annealing
in 545 ºC of composite containing 22 % of aluminium bronze

The effect of annealing time on the mass wear, friction coefficient and temperature of composites is shown on Figure 9.
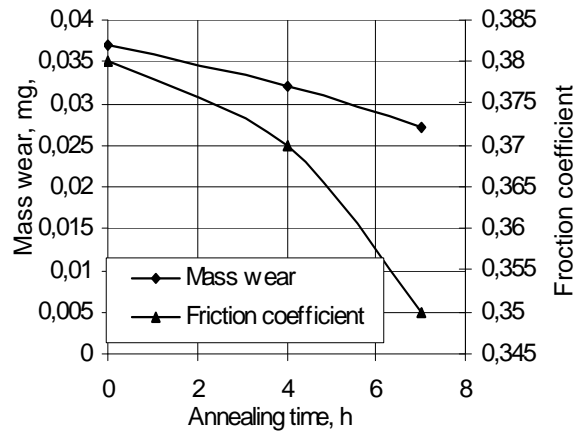
Fig. 9. The mass wear and friction coefficient of composites with coarse reinforcing particles
extruded with 16 fractional reduction as a function of annealing time

From the figures it can be seen that the mass wear of composites and friction coefficient decreases with time of annealing. The distinct decrease of friction coefficient is

observed with increase of annealing time over 4 hours, but the decrease of mass wear in the whole applied time is nearly constant. Increase of fractional reduction has very small effect on the wear of composites. Heat treatment has positive effect on mechanical properties of composites determined in tensile as well as in compression tests.

Hard phases obtained in elaborated process means that without participation of metallurgical processes good bearing materials can be manufactured.

4. Conclusions

On the base of presented investigation of manufacturing composites from granulated aluminium and CuAl8 aluminium bronze chips it has been conclude that:

• new method of manufacturing bearing composites from aluminium and aluminium bronze chips without metallurgical process was elaborated,

• the method contains hot extrusion of cold compacted mixture of aluminium and aluminium bronze chips and heat treatment applied after extrusion,

• the diffusion bonding during extrusion of cold compacted mixture of aluminium and aluminium bronze chips is low,

• the intensive diffusion bonding takes place during heat treatment applied after extrusion and the hard phases are created,

• hard phases have positive effect on the tribological properties of composites,

• to obtain the highly strengthened and compacted product the layer of aluminium oxide on the surface of particles must be destroyed by large shear plastic deformation.

References

[1] Sharma C.S., Nakagawa T.: *Recent development in the recycling of machining shafts by sintering and powder forging*, Ann. of CIRP, 25/1, 1977.

[2] Gronostajski J., Kaczmar J., Marciniak H., Matuszak A.: *Recycling of aluminium alloys by diffusion bonding process*, Proc. of Int. Conf. „The Recycling of Metals", Amsterdam, 1994, p. 287–294.

[3] Gronostajski J., Marciniak H., Matuszak A.: *Production of composites on the base alloy chips*, J. Mat. Proc. Technol., 60, 1996, p. 719–728.

[4] Gronostajski J., Kaczmar J., Marciniak H., Matuszak A.: *Direct recycling of aluminium chips into extruded products*, Proc. of 14th Int. Conf. Advanced Materials and Technologies, AMT'95, Zakopane, 1995, p. 133–140.

[5] Gronostajski J., Kaczmar J., Marciniak H., Matuszak A.: *Production of composites on the base of Al and AlMg$_2$ alloy chips*, J. Mat. Proc. Technol., 77, 1998, p. 37–41.

[6] Grodecki J.: *Możliwości wykonywania odkuwek matrycowych i wyprasek wyciskanych z odpadów metalowych*, Mechanik, 53, 1980, p. 31–33.

[7] Stępień M., Włosiński W.S.: *Doświadczalna produkcja części maszyn technologią zgrzewania objętościowego*, Przegląd Mechaniczny, 50, 1991, p. 33–37.

[8] Stępień M., Włosiński W.S.: *Zgrzewanie objętościowe wiórów*, Przegląd Mechaniczny, 50, 1991, p. 21–24.

[9] Stępień M., Włosiński W.S.: *Problemy badawcze w technologii zgrzewania objętościowego*, Przegląd Mechaniczny, 50, 1991, p. 12–14.

[10] Lazzaro G., Vittori S.: *Metal and energy saving by direct and continuous extrusion of aluminium scraps*, 121th TMS Annual Meeting, San Diego, California, 1992.

[11] Pardoe J.A.: *CONFORM continuous extrusion process - its contribution to energy conservation*, Metals Technology, 1, 1984, p. 358–365.

[12] Lazzaro G., Atzori C.: *Recycling of aluminium trimmings by conform process*, Light Metals, 1992, p. 1379–1384.

[13] Gronostajski J., Marciniak H., Matuszak A., Samuel M.: *Aluminium-ferro-chromium composites produced by recycling of chips*, Proc. of Int. Conf. Advances Mater. Process. Technol. AMPT, Dublin, 1999, p. 1327–1334.

[14] Gronostajski J., Matuszak A.: *The recycling of metals by plastic deformation: an example of recycling of aluminium and its alloy chips*, J. Mat. Proc. Technol., 92, 1999, p. 35–41.

[15] Jang J.: *The wear properties of an alumina-aluminosilicate fibre hybrid reinforced Al-Si alloy in a lubricated condition*, Wear, 171, 1994, p. 163–168.

[16] Pathak J.P., Karimi D., Tiwari S.N.: *Room temperature wear characteristics of Al-Si-Cd bearing alloys*, Wear, 170, 1993, p. 109–117.

[17] Torabian H., Pathak J.P., Tiwari S.N.: *Wear characteristics of Al-Si alloys*, Wear, 172, 1994, p. 49–58.

[18] Samuel M., Gronostajski J., Matuszak A.: *Mechanical properties and industrial application of aluminium base composites*, Proc of II Int. Sem. Zagadnienia Transferu Nowoczesnych Technologii Obróbki Plastycznej Wrocław, 1996, p. 107–124.

[19] Chmura W., Gronostajski J.: *Bearing materials produced by recycling of aluminium and aluminium bronze chips*, Proc. of Int. Conf. Challanges to Civil and Mechanical Engineering in 2000 and Beyond, CCME'97, Wrocław, 2, 1997, p. 205–214.

[20] Gronostajski Z.: *Correlation between stress-strain relation and phase transformation in copper alloys*, J. Mat. Proc. Technol., 119, 2001, p. 244–250.

[21] Gronostajski Z.: *Grain size evolution of selected copper alloys bases on new methods of softening kinetics determination*, J. Mat. Proc. Techn., 106, 2000, p. 243–249.

[22] Gronostajski Z.: *The deformation processing map for control of microstructure in CuAl9.2Fe3 aluminium bronze*, J. Mat. Proc. Technol., 125/126, 2002, p. 119–124.

[23] Gronostajski Z.: *Deformation processing map for control of in CuSi3.9 bronze microstructure*, J. Mat. Proc. Technol, 159, 2005, p. 377–382.

[24] Gronostajski Z., Mydlarczyk W.: *Application of sintering criterion in production of Al-base composites*, Arch. of Metals., 48, 2003, p. 75–85.

[25] Hansen M., Anderko K.: *Constitution of binary alloys*, McGraw-Hill Book Co, New York, 1958.

Materiały łożyskowe otrzymane poprzez dyfuzyjne łączenie wiórów aluminium i brązu aluminiowego

Opracowano oryginalny sposób wytwarzania kompozytowych materiałów łożyskowych poprzez mieszanie i dyfuzyjne łączenie wiórów aluminium i brązu aluminiowego CuAl8 obej-

mujące prasowanie na zimno, wyciskanie na gorąco i wyżarzanie. W wyniku dyfuzyjnego łączenia wiórów aluminium i brązu aluminiowego powstają fazy międzymetaliczne typowe dla układu równowagi Cu-Al. Fazy takie powstają w stosunkowo małym stopniu podczas procesu wyciskania na gorąco, natomiast głównie tworzą się podczas obróbki cieplnej na gorąco, zastosowanej po procesie wyciskania. Twarde fazy odgrywają istotna rolę w nadaniu właściwości łożyskowych wytwarzanym kompozytom. Dyfuzyjne łączenie zachodzi dopiero po rozkruszeniu warstewki powierzchniowej tlenków, co uzyskuje się poprzez zastosowanie dużych odkształceń postaciowych w procesie wyciskania i następującej po nim obróbce cieplnej.

Investigations of underwater FHPP for welding steel overlap joints

ANDRZEJ AMBROZIAK, BARTŁOMIEJ GUL

Institute of Production Engineering and Automation, Wrocław University of Technology,
Łukasiewicza 5, 50-371, Wroclaw

Friction Hydro Pillar Processing (FHPP) is one of the most innovative friction welding processes. FHPP can be used under water whereby it can be employed to repair marine structures or undersea oil pipelines. Every new technique requires testing and further development and in the present case this was made possible by the PIPETAP research project sponsored by the European Community. The main idea of PIPETAP is to develop an advanced hot tapping system for operations on undersea deep-water oil and gas pipelines [1]. The system will also improve the safety and reduce the cost of onshore hot tapping operations. This report presents experimental work on a FHPP welding system, focusing on sleeve welds.

Key words: *friction welding, FHPP, welding parameters*

1. Introduction

Friction Hydro Pillar Processing (FHPP) is a very young welding process. It was invented and patented by The Welding Institute which describes FHPP as a recently developed technique for joining and repairing thick section materials. Conventional thick section repair involves expensive consumables and lengthy processing, while FHPP is a low cost rapid process offering significant savings in terms of operating costs and logistics and resulting in high joint quality [2].
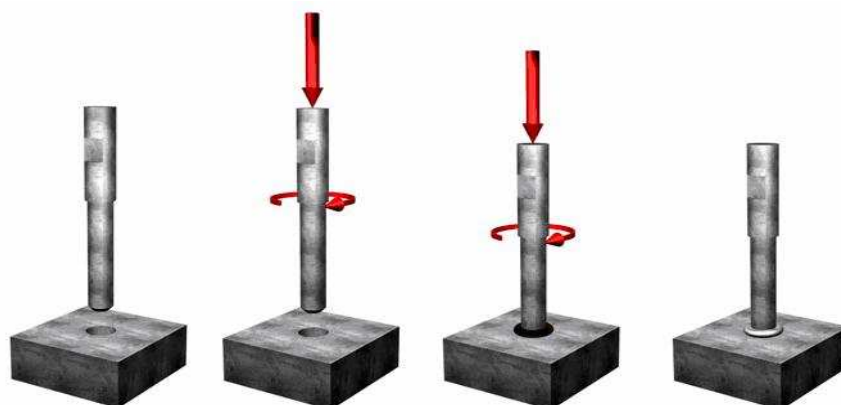
Fig. 1. Schematic illustration of FHPP

2. Process Parameters

The key friction welding process parameters are [3, 4, 5]:
- rotational speed,
- axial pressure,
- burn-off,
- the forging force,
- heating time and welding time.

Although all the parameters are important the first three will be considered here in more detail. The description of the welding parameters is based on [3, 6, 7, 9].

Rotational Speed. The general function of rotation is to produce a relative velocity at the faying surfaces, which is necessary to weld the pieces. Its maximum value (6500 rpm) is limited by the system. The minimum speed for FHPP welding depends on the material, the geometry or the axial pressure. Rotational speed affects the mechanical properties of friction welded joints. The higher the rotational speed, the longer the heating time and the lower the cooling rate. This can result in lower tensile strength and lower hardness. Low velocity reduces the heating time and increases the cooling rate, resulting in greater hardness.

Axial Pressure. Axial pressure needs to be high enough to hold the faying surfaces in intimate contact. Another function of axial pressure is to control the temperature gradient and the drive power. Axial pressure depends on the materials and the joint geometry. A higher pressure reduces the heat input and increases the cooling rate. Mechanical properties such as ultimate tensile strength and hardness increase with axial pressure.

Burn-Off. The general function of burn-off is to fill the hole with plasticised stud material. The magnitude of burn-off depends mainly on the sample's geometry. Burn-off governs both rotational speed and axial pressure since a proper speed and pressure are chosen in order to achieve the desired burn-off. The proper magnitude of this parameter can be determined from mathematical calculations (especially for a simple geometry) or from experiments (various configurations, including sleeve geometry).

Forging Force. At the end of the friction welding process (when rotation stops) a forging force is applied. The force has three beneficial effects on the weld. Forging is required to break up the coarse inclusions which were reoriented during the friction process and to refine coarse austenite grains by hot-working as well as to reduce the tendency to form a Widmanstätten structure which may affect the cooling rate. The forging force also increases ultimate tensile strength and hardness, which means that it should be properly applied.

3. Advantages and Limitations of FHPP

The most important advantages and limitations of FHPP are presented below.
Advantages:

- FHPP is suitable for welding many dissimilar metal combinations that are difficult or even impossible to weld by other welding processes.
- No filler metal, flux or shielding gas is needed in the friction process.
- The process is safe for divers – there is no radiation, fumes, arcs, sparks or high-voltage electric hazard.
- In the solid state process melting-solidification defects do not occur.
- The process is easily automated for mass production and the costs are lower.
- Welds are made faster than in other welding processes.
Limitations:
- Generally, one workpiece must have an axis of symmetry and be capable of being rotated about this axis.
- Dry bearing and nonforgeable materials cannot be welded.
- The cost of equipment and tools is very high.
- FHPP welding has also geometry limitations concerning, for example, the stud diameter or length.

4. Experimental investigation

4.1. Material

The material used for all the welding experiments was low-alloy construction steel S355 (according to German standard DIN EN 10025). This steel is widely used for offshore construction, pipelines and in the marine industry. Tables 1 and 2 present its chemical composition and mechanical properties while Figure 2a,b shows its structure.

Table 1. Chemical composition of base material – S355 (All values in weight percentage)

	C	Si	Mn	P	S	Al	Cu	Mo	Ni	Cr	V	B	Sn	C_{eq}
Manufacturer's Certificate	0.150	0.250	1.360	0.010	0.007	0.034	0.260	0.009	0.060	0.070			0.020	0.412
Chemical Analysis	0.175	0.300	1.370	0.015	0.007	0.030	0.290	0.017	0.094	0.084	0.005	0.001		0.451

Table 2. Mechanical properties of base material – S355

	Tensile Strength[1]	Yield Strength[1]	Elongation[1]	Charpy Impact Values[2] [J]			
	[MPa]	[MPa]	[%]	+20 °C	0°C	–20°C	–40°C
Manufacturer's Certificate	542	363	27	–	–	39	–
Own Test Results	565	335	23	–	67	57	–

[1] Mean values for at least three specimens
[2] Mean values for at least five specimens

a)

b)
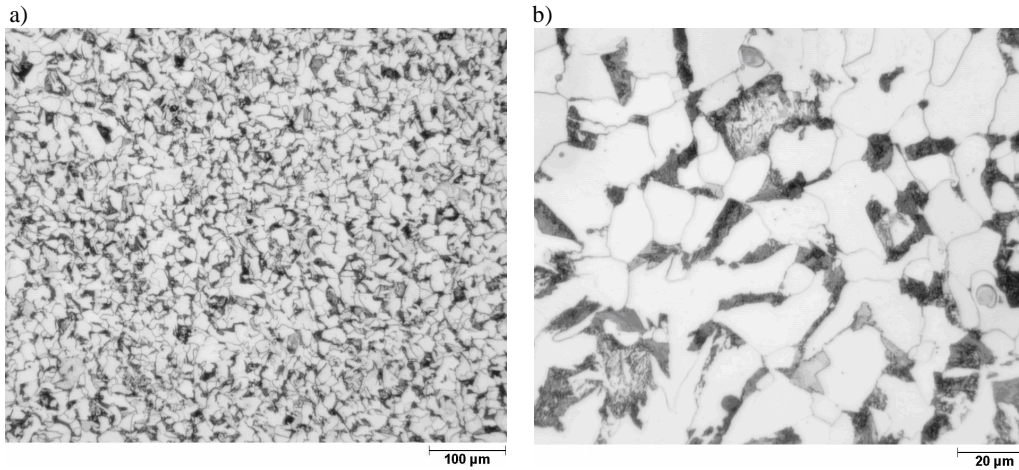
Fig. 2. Microstructure of base material – S355

4.2. Welding System

The machine used for the welding experiments was an HMS 3000 manufactured by Circle Technical Services. Figure 3 shows the welding head which is fixed in a special tank simulating sea conditions. The HMS 3000 is a hydraulically powered friction welding machine, fully programmable (rotational speed and weld pressure) during the process. The machine is also under full control of a computer system and all the data are saved in real time in the computer during welding. The system consists of four major components: a hydraulic power unit, a valve block, a control system and a welding head.

Fig. 3. System for underwater friction welding

In the configuration used, the HPU's pump is driven by a 50 kW electric motor supplying up to 115 dm^3/mm at 315 bar. The maximum oil pressure is continuously adjusted while the pump automatically adjusts the flow. Depending on the required weld head power the oil pressure may be lower than the set maximum. During idle running the pressure drops to a value just enough to overcome the flow resistance in the system.

5. Results and Discussion

The general aim of the experiments was to determine the maximum diameter of a stud to be used in FHPP welding and to optimize the welding parameters for the current system. The first task was to be carried out for four different geometries. The second task depended mainly on the result of the first task because if some configurations are not weldable (system limits), the process parameters cannot be optimized.

Experimental Procedures

Four geometries were tested. The material used in FHPP welding had been machined from steel S355. A parameter matrix was created for every geometry on the basis of A. Meyer's work [8]. The basic welding parameter matrix shown in Figure 4 was helpful in this.
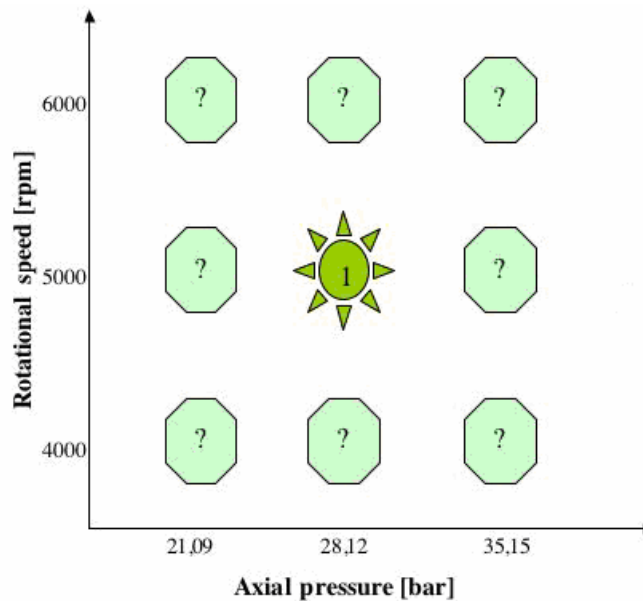
Fig. 4. Basic welding parameter matrix

The general idea of the matrix was to find the best relations between rotational speed and axial pressure. Welds were produced on the basis of the parameter matrix to

determine proper welding parameters. In order to create a welding parameter matrix one must select a point on the diagram, corresponding to an axial pressure and a rotational speed. Such a point was selected on the basis of experiments carried out on different base materials in GKSS-Forschungszentrum [8]. Additional points were selected near the first point in every direction as shown in Figure 4. All the combinations were tested in experiments.

The friction hydro pillar process depends on the stud and plate geometry. In this study only a cylindrical stud and cylindrical holes were tested for four diameters.
An important parameter for FHPP welding is burn-off. It depends on the geometry and can be estimated from the following equation:

$$B = 1,15 \cdot \left(\frac{d_s^{\,2}}{d_h^{\,2}} \right) \cdot H_h$$

where:

B – burn-off [mm],
d_S – the diameter of the stud [mm],
d_h – the diameter of the hole [mm],
H_h – the depth of the hole [mm],

The welding data monitored during the friction process were helpful in this regard. All the data were saved in DRS (Data Recording System). Before each test the specimens were named and cleaned in acetone to remove any undesirable effects. Finally the specimens were prepared for visual and hardness examinations in accordance with the relevant preparation standards.

Parameter Optimization for Single FHPP Welds

This paper presents only some results from single FHPP experiments. The full list of the investigated welding parameters can be found in Table 6-1 in [10]. The table includes more than 30 different welds. Significant results are presented in more detail below:

PT4-B10. A cylindrical geometry with a 12 mm stud diameter. This weld was produced underwater at water temperature $t = 20$ °C. The results are in the form of: a macrograph, hardness graphs and a welding diagram. On this basis the parameters were optimized for the geometry variants shown in the table below.

Figure 5a,b,c shows the cross section of a welded specimen and two hardness diagrams. The weld was produced in water conditions according to the above table of optimised welding parameters. The macrostructure shows the different areas in the welded sample:

• The base material – a normal pearlite-ferrite structure for low-alloy steel (S355). According to the hardness graphs, hardness in this region is around 180 HV10.

• The heat affected zone – the size of HAZ depends mainly on the heat input and the cooling rate. The macrostrcture shows that the size of HAZ is increasing towards

the top of the plate, which is normal for FHPP welding. The hardness survey diagrams show the different dimensions of HAZ, i.e. 2.5 mm for the weld's lower part and 1.0 mm larger for its upper part.

• The weld metal – this area has a hardness of about 430 HV10, which means that probably a martensitic or Widmanstätten structure occurs here.

a)

Axial pressure [bar]	Burn-off [mm]	Rotational speed [rpm]
14.06	20	5000
14.06	Hold	for 3 s

b)

c)
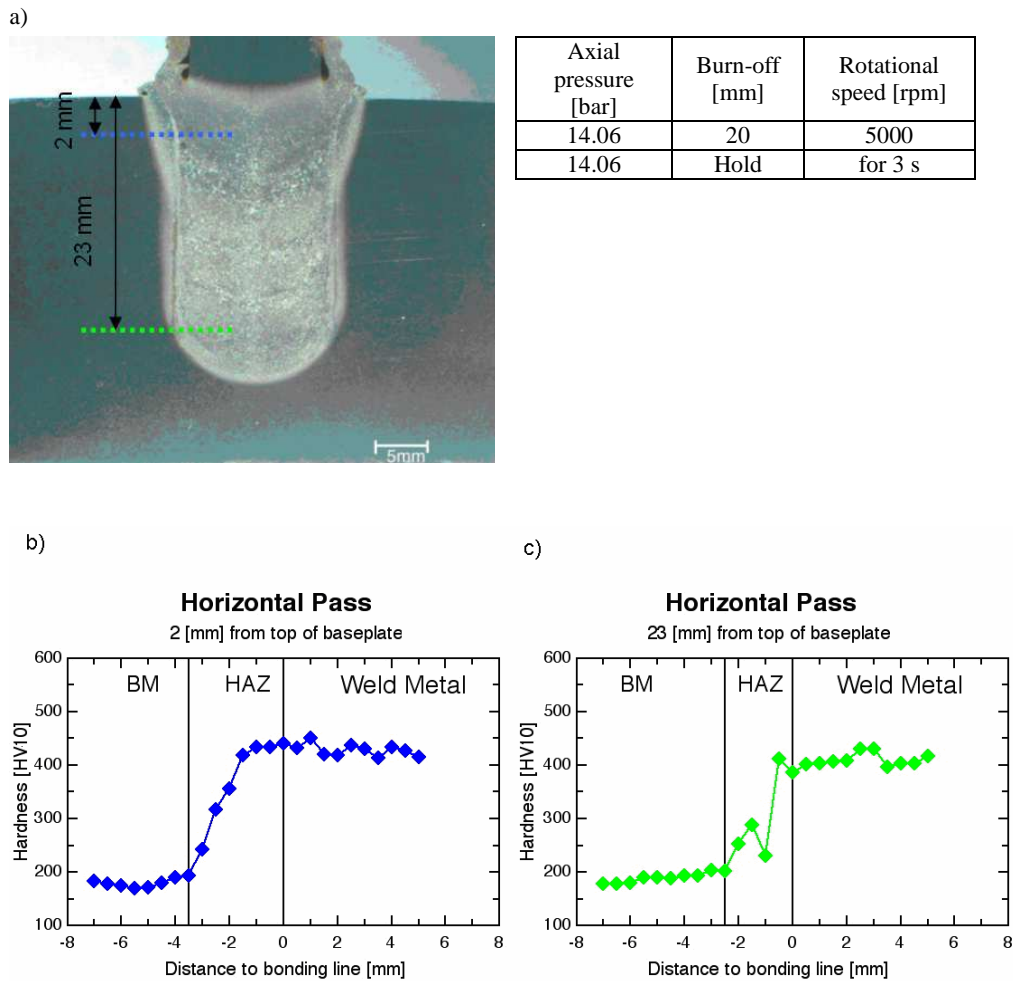
Fig. 5. Macrograph and hardness survey of single FHPP weld PT4-B10

Figure 6 shows parameter changes during the FHPP welding process. The graphs illustrate the three parameters which can be controlled in the welding process. The diagram shows normal parameter variation during the FHPP process. Axial pressure is

constant and burn-off steadily increases over welding time. Only rotational speed changes sharply due to welding system problems.
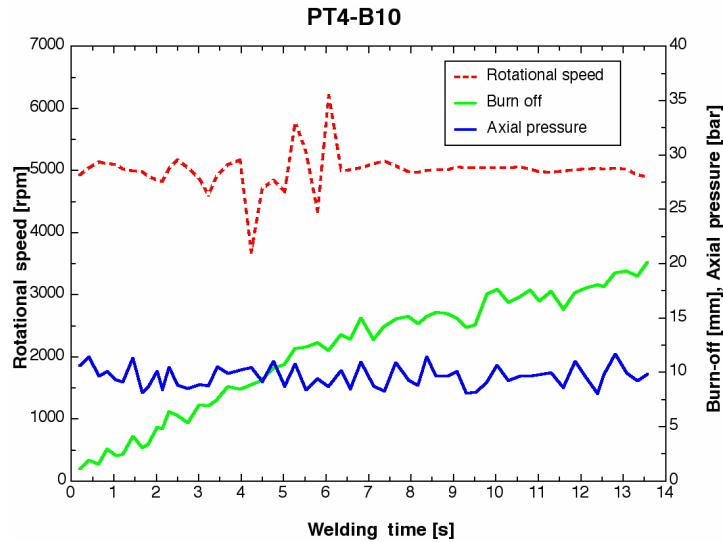
Fig. 6. Welding parameters diagram for weld PT4-B10

Table 3. Optimised welding parameter window for 10 mm stud diameter

Axial pressure [bar]	Rotational speed [rpm]	Burn-off [mm]
21.09	6000	20
21.09	hold for 3 s	

Axial pressure [bar]	Rotational speed [rpm]	Burn-off [mm]
21.09	5000	20
21.09	hold for 3 s	

Table 4. Optimised welding parameter window for 12 mm stud diameter

Axial pressure [bar]	Rotational speed [rpm]	Burn-off [mm]
14.06	6000	20
14.06	hold for 3 s	

Axial pressure [bar]	Rotational speed [rpm]	Burn-off [mm]
14.06	5000	20
14.06	hold for 3 s	

The results from this part of the research provide much information such as:

- All the experiments carried out within this project upgrade the knowledge of FHPP welding.

- So far sufficient weld quality can be produced only for stud diameters 10 and 12 mm for material S355 (hole depth – 25 mm). At the moment, other geometries are either not weldable or the weld quality is too poor. But in the future system modifications may allow one to obtain welds of satisfactory quality for other geometries.

- The systematic welding parameter investigations resulted in optimised parameter windows as shown in table 3 for a stud diameter of 10 mm and in table 4 for a stud diameter of 12 mm.

6. Conclusion

From the experiments presented in this paper one can draw the following conclusions.

Good quality of bonding has been demonstrated in FHPP trials only for 10 and 12 mm stud diameters. A welding parameter window, as presented above, was determined for the two stud diameters. Also the welded specimen's cross section and hardness diagrams attest to the good quality of the weld. For the larger stud sizes some defects occurred in the weld. The welding system needs some modifications in order to produce good quality welds for a stud diameter larger than 12 mm.

Because of the confines of this paper only a macrostructure and a hardness survey (no mechanical test results or more detailed microstructural analyses) have been presented. At first calibration system and crack problems were encountered but their solution contributed to better understanding of the process. Friction stitch welding trials for an underwater overlap joint configuration will be carried out in the future.

Microstructure examinations under a microscope revealed martensitic structure in the weld metal near the bonding line. The hardness of up to 430 HV10 measured in this area improves the martensitic structure. The results of this research provide a good basis for the next steps in the PipeTap Project and for future industrial applications. FHPP and sleeve welding are an attractive alternative to the traditional fusion welding processes.

References

[1] *Project funded by the European Community under the Energy Programme*, "PIPE TAP", 2002–2003.
[2] Dos Santos J.F., Mayer A., Blakemore G.R.: *Engineering applications of friction stitch welding*, 20th International Conference on Offshore Mechanics and Arctic Engineering, Rio de Janeiro, Brazil, 2001.
[3] AWS, *Welding Handbook*, 8th ed., R.L. O'Brien, Vol. 2, 1991, American Welding Society, p. 955.

[4] Spindler D.E.: *What industry needs to know about friction welding*, Welding Journal, March, 1994, p. 37–43.

[5] Grewe K.J.: *Friction welding takes on new applications*, Welding Journal, 1997, p. 39–40.

[6] Chandrasekaran M., Batchelor A.W., Jana S.: *Study of interfacial phenomena during friction surfacing of mild steel with tool steel and inconel*, Journal of Materials Science, 10, 1998, Vol. 33, p. 2709–2717.

[7] Vill V.I.: *Friction welding of metals*, New York, American Welding Society, 1962.

[8] Meyer A.: *Friction Hydro Pillar Processing – Bonding Mechanism and Properties*, PhD Thesis, GKSS-Forschungszentrum, 2003.

[9] Lucas W.: *Process parameters and friction welds*, Metal Construction and British Welding Journal, 1971, p. 293–297.

[10] Gul B.: *Initial investigations on underwater FHPP-overlap-welds in mild steel with different gap sizes*, Graduation Thesis, GKSS-Forschungszentrum, 2003.

Badania podwodnego zgrzewania tarciowego metodą FHPP stalowych złączy zakładkowych

Friction Hydro Pillar Processing (FHPP) jest jedną z najnowocześniejszych metod zgrzewania tarciowego opatentowaną przez TWI. Metoda ta służyć miała początkowo głównie do naprawy wad materiałowych, ale okazało się, że można z powodzeniem zastosować ją także do łączenia elementów o skomplikowanej konstrukcji. O zgrzewaniu metodą FHPP mówimy w przypadku, gdy mamy do wykonania spoinę otworową. Tak, więc proces ten zwykle jest poprzedzony wywierceniem otworu w wadliwym fragmencie materiału. Zgrzeina FHPP otrzymywana jest dzięki wprowadzeniu trzpienia w ruch obrotowy, a następnie przyłożeniu odpowiedniego docisku osiowego w celu wytworzenia mechanizmów tarcia pomiędzy powierzchniami. W artykule przedstawiono badania w ramach projektu PIPE TAP [1], nad doborem parametrów zgrzewania stalowych złączy zakładkowych (prędkość obrotowa, nacisk). Stwierdzono możliwość wykonywania złączy zakładkowych ze stali S355 w wodzie, przy średnicy trzpienia 10 i 12 mm.

Reciprocal theorem for the elastic-damage problem of mechanics and its application in the damage distribution estimation from displacement measurements

ZBIGNIEW PERKOWSKI

Opole University of Technology, Faculty of Civil Engineering, Katowicka 48, 45-061, Opole

The reciprocal theorem of mechanical problems for an elastic and brittle damaged medium is formulated under the assumption that the damage evolution may be described by the scalar parameter. Because of the physical non-linearity of problem the theorem is introduced in an incremental version. Next, a way of the damage detection in bar systems from displacement measurements is proposed on the basis of the theorem. Finally, possibilities of the approach presented are illustrated by the computational example and laboratory experiment.

Keywords: *reciprocity theorem, damage detection, elastic-brittle material*

1. Introduction

Continuum damage mechanics (CDM) and its stormy development during two last decades of the previous century made possible many solutions in the analysis of damage processes – especially in predicting of damage evolution in different kinds of engineering materials. The power of this scientific tool may be also used for the damage detection in engineering structures and the main aim of this article is a presentation of one of possibilities which may be offered by CDM in this matter. The damage detection in structures is a specific inverse problem where a location of damage is determined for instance from measurements of free vibration frequencies, mode shapes, displacements, temperature (for example see [1, 6, 7, 8, 10, 11]). However, damage is often considered in many approaches to its detection as a specific inclusion of different properties than the rest of homogeneous medium or, because of the numerical formulation, is treated as a discrete problem. In case when damage in the tested structures is not sharply formed like macro-cracks, voids, inclusions etc. the concepts of CDM are much more accurate and needed. Then we find not a specific distribution of inclusions simulating damage but a continuous function describing micro-damage in whole medium.

Building of such a task, among other things, is possible owing to the specific formulation of the reciprocal theorem for the problem of mechanics considered. That is why, first, one will present a general formulation of the reciprocity theorem for an elastic medium with brittle micro-damage [3, 4]. An example of particular application of the reciprocal theorem in the damage detection from displacement measurements

for a plane bar system will be presented in the second part of article. The approach shown in the work may be a complement for the existing damage detecting methods mentioned earlier.

Considerations in the work will be conducted under the following assumptions:

• Damage in a medium is assumed as a continuous field (adequately to the assumptions and methods of CDM, for example see [5, 9]) described by the dimensionless scalar damage parameter $\omega \in [0,1)$, which is equal to zero for material in the virgin state and tends to one at the moment of failure. It depends on variables of a thermodynamic process considered, for example: $\omega = \omega(\boldsymbol{\varepsilon},...)$, where $\boldsymbol{\varepsilon}$ is strain tensor.

• The medium in the virgin state is assumed to be an elastic one with a known initial stiffness described by the symmetric tensor of rank four $\mathbf{E}_0$.

• Stiffness of the damaged medium, described by the symmetric tensor of rank four $\mathbf{E}$, is reduced accordingly a value of the damage parameter up to the pattern $\mathbf{E} = (1-\omega)\mathbf{E}_0$.

In spite of the fact, that the assumptions specified above introduce the physical non-linearity in the relation between stresses and strains, the reciprocity theorem, which is formulated in mechanics formally only for linear problems owing to the symmetry of stiffness tensor $\mathbf{E}_0$, may be obtained for the presented problem on the grounds of the third assumption. Then the symmetry of tensor $\mathbf{E}$ can be analysed only for the sake of the initial stiffness tensor $\mathbf{E}_0$ separated from $\mathbf{E}$. It should be also mentioned that the first assumption – use of the scalar damage parameter – introduces a considerable simplification because it takes into account only the averaging isotropic influence of the damage on the medium stiffness (for example see [2]). It makes possible to neglect the anisotropic effects in the material stiffness change caused by the evolution of micro-cracks oriented perpendicularly to principal tensile stresses. To avoid the problems connected with the analysis of physical non-linearity appearing in questions of application, the problem of mechanics will be formulated in an incremental version.

2. Formulation of the reciprocal theorem for the problem

Let us consider the continuous deformable medium occupying an area V in the space R^3 restricted by a surface A and fixed on a surface $A_u \subset A$. The medium stiffness is described according to the assumptions specified in the introduction. The medium was subjected to a mechanical load and mass force which caused in it a state of displacements, strains and stresses described respectively by a vector $\mathbf{u}_0$ and tensors $\boldsymbol{\varepsilon}_0$ and $\boldsymbol{\sigma}_0$. Next, the medium was again subjected to a known load increment on a surface $A_\sigma = A \backslash A_u$ and to a known mass force increment in the area V described respectively by vectors $\Delta\mathbf{P}$ and $\Delta\mathbf{F}$. Then unknowns of the problem are increments of displacements, strains and stresses produced in such a way in the area V. They are described respectively by a vector $\Delta\mathbf{u}$, tensors $\Delta\boldsymbol{\varepsilon}$ and $\Delta\boldsymbol{\sigma}$, and may be determined, after the linearization of the problem, from the following system of equations (the equation of internal equilibrium, the geometrical equation and the physical equation in the incremental versions):

$$div\Delta\boldsymbol{\sigma} + \Delta\mathbf{F} = \mathbf{0} \,, \tag{1}$$

$$2\Delta\boldsymbol{\varepsilon} = grad\Delta\mathbf{u} + grad\Delta\mathbf{u}^T \,, \qquad 2\boldsymbol{\varepsilon}_0 = grad\mathbf{u}_0 + grad\Delta\mathbf{u}_0^T \,, \tag{2}$$

$$\Delta\boldsymbol{\sigma} = {}^t\mathbf{E}(\boldsymbol{\varepsilon} = \boldsymbol{\varepsilon}_0) : \Delta\boldsymbol{\varepsilon} \,, \quad {}^t\mathbf{E} = \left(1 - {}^t\omega(\boldsymbol{\varepsilon} = \boldsymbol{\varepsilon}_0)\right)\mathbf{E}_0 \,, \tag{3}$$

where ${}^t f\,(x = a)$ is tangent of a function f at a value of its argument $x = a$, $\mathbf{0}$ is a zero vector.
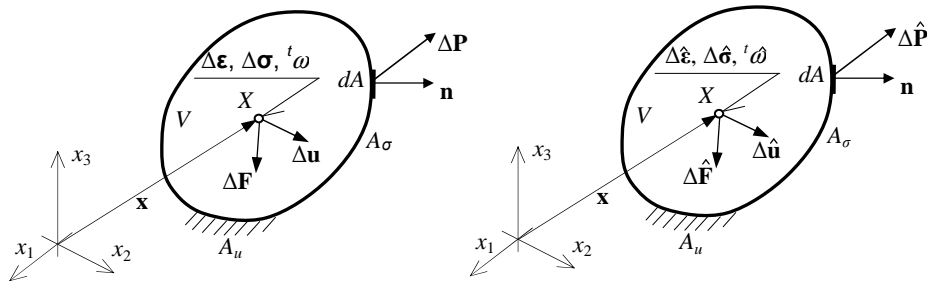
Fig. 1. Medium in two different states of load and damage

The tangent of damage parameter is graphically interpreted on the Figure 2 in the case of uniaxial compression. It should be mentioned that, the damage parameter tangent has different values at the same stress for loading and unloading process. That is why, to interpret properly the tangent of parameter ω as a damage measure, we should know the initial medium stiffness and if the loading or unloading process proceeds.

The damage measure is determined on the basis of damage evolution equation and, because of the thermodynamic limitations of the process [2, 9], if the self-regeneration of material structure does not proceed (for example during hydration in young concrete [12]), has to be not diminishing. For instance

$$\Delta\omega = \Delta\omega(\boldsymbol{\varepsilon},...) \,, \quad \Delta\omega \geq 0 \,. \tag{4}$$

The system of Equations (1–3) has to be completed by the following boundary conditions.

$$\Delta\boldsymbol{\sigma}(\mathbf{x})\,\mathbf{n}(\mathbf{x}) = \Delta\mathbf{P}(\mathbf{x}) \,, \quad \mathbf{x} \in A_\sigma \,, \tag{5}$$

$$\Delta\mathbf{u}(\mathbf{x}) = \tilde{\mathbf{u}}(\mathbf{x}) \,, \quad \mathbf{x} \in A_u \,, \tag{6}$$

where: $A_u \cup A_\sigma = A$, $A_u \cap A_\sigma = \varnothing$, $\tilde{\mathbf{u}}(\mathbf{x})$ is a known vector function.

Now, let us derive a formula of the reciprocal theorem for the problem stated [3, 4]. Let us consider two different states of the medium described by two sets of field increments which satisfy the Equations (1–4) and the boundary conditions (5–6):

Set 1: $\Delta\mathbf{u}, \Delta\boldsymbol{\varepsilon}, \Delta\boldsymbol{\sigma}, \Delta\mathbf{F}, \Delta\mathbf{P}$; $^{t}\mathbf{E} = \left(1-{}^{t}\omega\right)\mathbf{E}_0$,   (7)

Set 2: $\Delta\hat{\mathbf{u}}, \Delta\hat{\boldsymbol{\varepsilon}}, \Delta\hat{\boldsymbol{\sigma}}, \Delta\hat{\mathbf{F}}, \Delta\hat{\mathbf{P}}$; $^{t}\hat{\mathbf{E}} = \left(1-{}^{t}\hat{\omega}\right)\mathbf{E}_0$.   (8)

This situation causes that damage in the medium is given for each of the states by the different damage parameters – ω and $\hat{\omega}$.
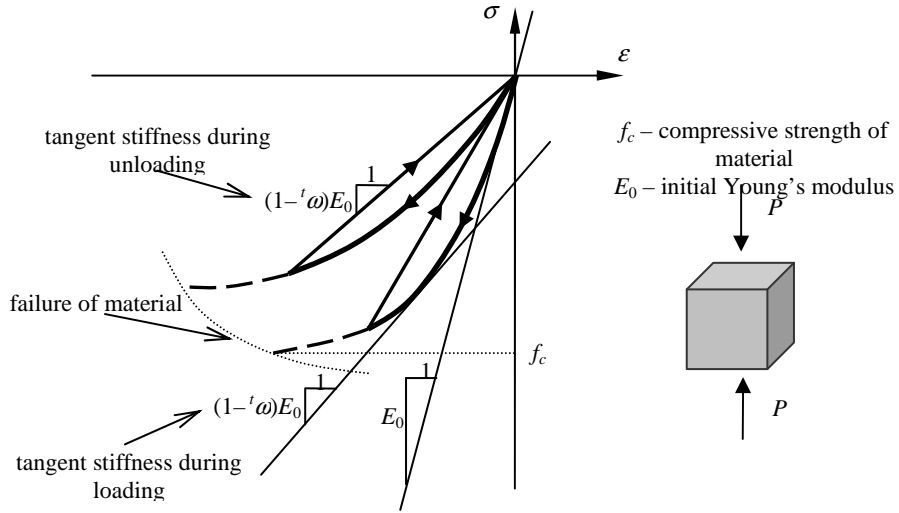
Fig. 2. Interpretation of the tangent of damage parameter $^{t}\omega$ for an elastic-brittle material
in the case of uniaxial compression during loading and unloading

Then, taking into account the symmetry of tensor $\mathbf{E}_0$ and the following identity $\mathbf{E}_0 : \Delta\boldsymbol{\varepsilon} : \Delta\hat{\boldsymbol{\varepsilon}} \equiv \mathbf{E}_0 : \Delta\hat{\boldsymbol{\varepsilon}} : \Delta\boldsymbol{\varepsilon}$ we can obtain on the basis of Equation (3) a local form of the reciprocal theorem

$$\Delta\boldsymbol{\sigma} : \Delta\hat{\boldsymbol{\varepsilon}} - \Delta\hat{\boldsymbol{\sigma}} : \Delta\boldsymbol{\varepsilon} + {}^{t}\omega\,\mathbf{E}_0 : \Delta\boldsymbol{\varepsilon} : \Delta\hat{\boldsymbol{\varepsilon}} - {}^{t}\hat{\omega}\,\mathbf{E}_0 : \Delta\hat{\boldsymbol{\varepsilon}} : \Delta\boldsymbol{\varepsilon} = 0 ,$$ (9)

and next in a global form as follows

$$\int_{A}\left(\Delta\mathbf{P}\cdot\Delta\hat{\mathbf{u}} - \Delta\hat{\mathbf{P}}\cdot\Delta\mathbf{u}\right)dA + \int_{V}\left(\Delta\mathbf{F}\cdot\Delta\hat{\mathbf{u}} - \Delta\hat{\mathbf{F}}\cdot\Delta\mathbf{u}\right)dV =$$
$$= -\int_{V}\left({}^{t}\omega\,\mathbf{E}_0 : \Delta\boldsymbol{\varepsilon} : \Delta\hat{\boldsymbol{\varepsilon}} - {}^{t}\hat{\omega}\,\mathbf{E}_0 : \Delta\hat{\boldsymbol{\varepsilon}} : \Delta\boldsymbol{\varepsilon}\right)dV .$$ (10)

It is worth to mention that the general identity (10) will be classical Betti`s recipro-cal theorem if the damage parameters $^t\omega$ and $^t\hat{\omega}$ are equal to zero. If they are not, the right side of the Relation (10) will express the reciprocal work change of forces ap-plied to the medium due to the damage evolution. Thus, for example assuming there is no damage in the first set of fields we can obtain information how much the reciprocal work differs in the damaged and not damaged medium. That is why, such a form of the theorem can be a basis of the damage estimation or detection for engineering struc-tures what will be shown in the example of statically determinate plane bar systems in the further part of elaboration.

3. Damage estimation in plane bar systems with a use of the theorem

The reciprocal theorem (10), in the case of plane bar systems which we assume for: $\Delta\mathbf{F} = \Delta\hat{\mathbf{F}} = \mathbf{0}$, $^t\hat{\omega} = 0$, $^t\omega\big|_F \approx const$, will have a form

$$\int_L \left(\Delta\mathbf{P} \cdot \Delta\hat{\mathbf{u}} - \Delta\hat{\mathbf{P}} \cdot \Delta\mathbf{u} \right) ds + \int_L \frac{^t\omega}{1 - ^t\omega} \left(\frac{\Delta M \, \Delta\hat{M}}{E_0 I} + k \frac{\Delta T \, \Delta\hat{T}}{G_0 F} + \frac{\Delta N \, \Delta\hat{N}}{E_0 F} \right) ds = 0 , \qquad (11)$$

where:
  L – variable describing centre lines of bars;
  ΔM, ΔT, ΔN – bending momentum, shear and axial force increments caused by $\Delta\mathbf{P}$ in the system damaged;
  $\Delta\hat{M}$, $\Delta\hat{T}$, $\Delta\hat{N}$ – bending momentum, shear force and axial force increments caused by $\Delta\hat{\mathbf{P}}$ in the system not damaged;
  E_0, G_0 – initial Young`s modulus and shear modulus;
  F, I – area and moment of inertia of bar cross-section;
  k – coefficient dependent on the shape of bar cross-section.
  Let us consider a use of the relation (11) for a determination of damage parameter distribution in a statically determinate example, where $L = \{ x : x \in [0,l] \}$. We will ap-proximate a function $z = {}^t\omega/(1 - {}^t\omega)$ by the first m summands of the Fourier series, ex-tended in the range $x \in [-l,l]$ as an uneven function

$$z = \frac{^t\omega}{1 - ^t\omega} \approx \sum_{i=1}^{m} b_i \sin\left(\frac{i\pi x}{l} \right). \qquad (12)$$

We will also assume that the function z will satisfy the Dirichlet conditions in the range considered. When we write the Relation (11) taking into consideration the series (12) for m different sets of loads, displacements and internal forces increments which

are known, we will obtain a linear system of equations where coefficients of the series $(b_1, b_2,..., b_m)$ are unknowns. That means

$$\mathbf{B} = \mathbf{A}^{-1}\mathbf{C}, \tag{13}$$

where:

$$B_i = b_i, \quad C_i = -\int_L \left(\Delta\mathbf{P}_{(i)} \cdot \Delta\hat{\mathbf{u}}_{(i)} - \Delta\hat{\mathbf{P}}_{(i)} \cdot \Delta\mathbf{u}_{(i)} \right) ds,$$

$$A_{ij} = \int_L \sin\left(\frac{j\pi x}{l} \right) \left(\frac{\Delta M_{(i)} \, \Delta\hat{M}_{(i)}}{E_0 I} + k \frac{\Delta T_{(i)} \, \Delta\hat{T}_{(i)}}{G_0 F} + \frac{\Delta N_{(i)} \, \Delta\hat{N}_{(i)}}{E_0 F} \right) ds = 0, \tag{14}$$

$$i, j = 1,2,...,m.$$

Solving such a system we determine the coefficients of series (12) and thus the approximation of damage distribution in the range L.

In the relation above the symbol $\Delta\mathbf{P}_{(i)}$ denotes a vector of functions describing i-load of the system damaged, which causes displacements and internal forces increments described respectively by the symbols: $\Delta\mathbf{u}_{(i)}, \Delta M_{(i)}, \Delta T_{(i)}, \Delta N_{(i)}$. On the other hand the symbol $\Delta\hat{\mathbf{P}}_{(i)}$ denotes a vector of functions describing i-load of the system not damaged, which causes displacements and internal forces increments described respectively by the symbols: $\Delta\hat{\mathbf{u}}_{(i)}, \Delta\hat{M}_{(i)}, \Delta\hat{T}_{(i)}, \Delta\hat{N}_{(i)}$.

It should be mentioned that the system of Equations (13) is determined in the case the pair of loads – $\Delta\mathbf{P}_{(i)}$ and $\Delta\hat{\mathbf{P}}_{(i)}$ – does not repeat itself for any i. It results from this that a use of the approach of damage detection presented can be simplified considerably in the range of experimental measurements. Because we can apply a load $\Delta\mathbf{P}$ and measure accompanying displacements $\Delta\mathbf{u}$ in the real damaged system and calculate internal forces increments $\Delta M, \Delta T, \Delta N$ only once. On the other hand, in the reference not-damaged system of material parameters E_0 and G_0 we can apply different $\Delta\hat{\mathbf{P}}$ and calculate $\Delta\hat{\mathbf{u}}_{(i)}, \Delta\hat{M}_{(i)}, \Delta\hat{T}_{(i)}, \Delta\hat{N}_{(i)}$ required amount of m times without any essential difficulties. Then

$$\Delta\mathbf{P}_{(i)} = \Delta\mathbf{P}, \ \Delta\mathbf{u}_{(i)} = \Delta\mathbf{u}, \ \Delta M_{(i)} = \Delta M, \ \Delta T_{(i)} = \Delta T, \ \Delta N_{(i)} = \Delta N \rightarrow$$

$$\rightarrow C_i = -\int_L \left(\Delta\mathbf{P} \cdot \Delta\hat{\mathbf{u}}_{(i)} - \Delta\hat{\mathbf{P}}_{(i)} \cdot \Delta\mathbf{u} \right) ds,$$

$$A_{ij} = \int_L \sin\left(\frac{j\pi x}{l} \right) \left(\frac{\Delta M \, \Delta\hat{M}_{(i)}}{E_0 I} + k \frac{\Delta T \, \Delta\hat{T}_{(i)}}{G_0 F} + \frac{\Delta N \, \Delta\hat{N}_{(i)}}{E_0 F} \right) ds = 0, \tag{15}$$

$$i, j = 1,2,...,m.$$

4. Analytical example

A beam four-point bent, as shown on the Figure 3a, was analysed as an illustrative example for the method proposed. The damage distribution was calculated for $x \in [0, l]$ in the middle bay of beam. In accordance with the number m – the amount of sum-mands of Fourier series (12) used in the analysis – in order to solve the system of Equations (13) one calculated displacements of the beam $y_{(i)}$ ($i = 1, 2,..., m$) in the points of coordinates

$$x_{(i)} = \frac{li}{m+1}, \quad i = 1, 2, ..., m .$$

(16)
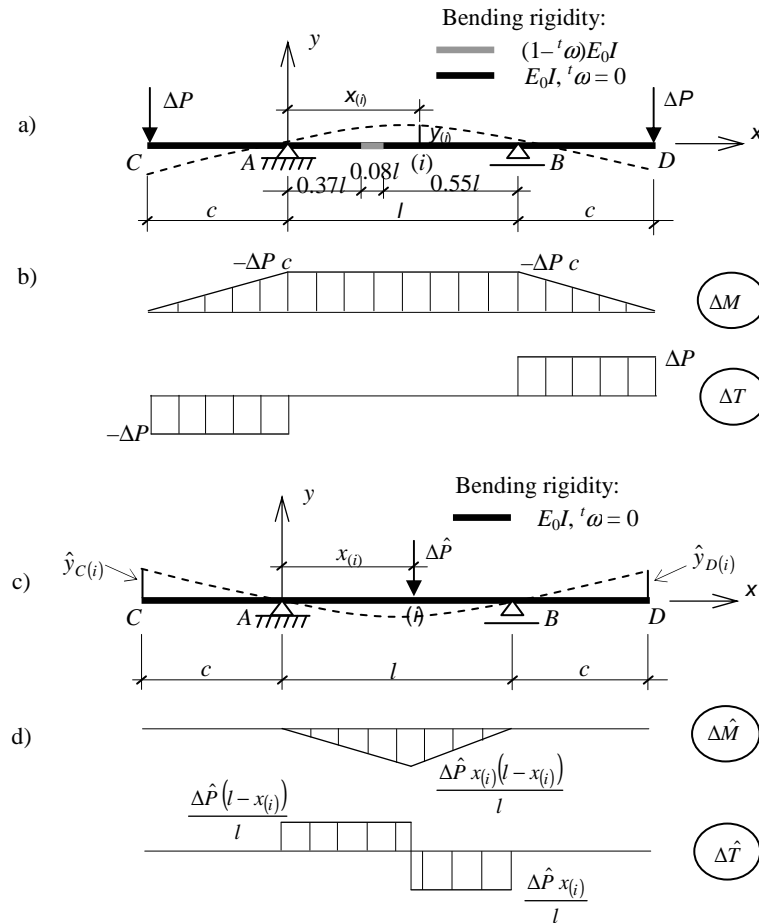
Fig. 3. Analytical example: a), b) scheme of the damaged beam with diagrams of internal forces; c),d) scheme of the not damaged beam with diagrams of internal forces

Next one applied a concentrated force to a not-damaged beam of the same sizes like the first one in the points as determined in the relation (16). One obtained this way m different schemes of load as shown on the Figure 3c. One determined simultaneously displacements of the free ends of beam in the points where the not-damaged beam is loaded – $\hat{y}_{C(i)}$ in the left end and $\hat{y}_{D(i)}$ in the right end. For so formulated schemes of loads, the components of system (13) had a form

$$B_i = b_i \, , \quad C_i = \Delta P \, \hat{y}_{C(i)} + \Delta P \, \hat{y}_{D(i)} - \Delta \hat{P} \, y_{(i)} \, ,$$

$$A_{ij} = \int_0^l \sin\left(\frac{j\pi x}{l} \right) \frac{\Delta M \, \Delta \hat{M}_{(i)}}{E_0 I} \, dx \, , \tag{17}$$

$$i, j = 1, 2, ..., m.$$
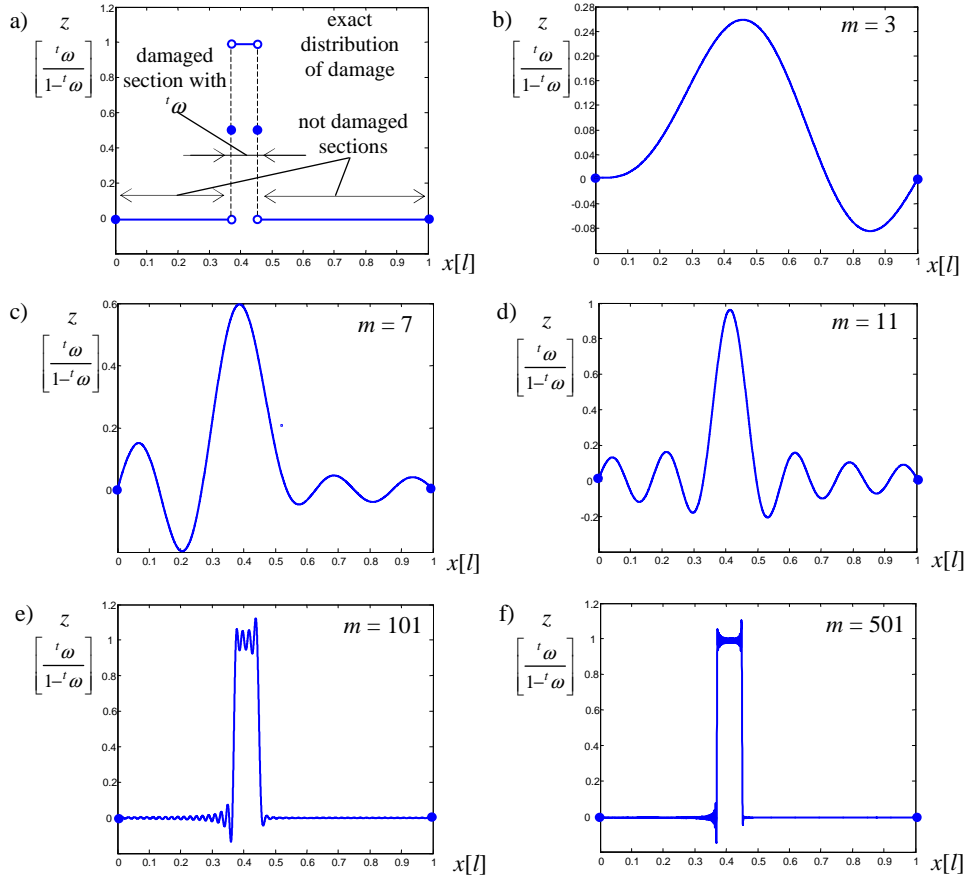
Fig. 4. Diagrams of the damage distribution in the middle bay of beam: a) the exact one
b), c), d), e), f) approximated with a help of the function $z = {}^t\omega/(1-{}^t\omega)$ respectively for $m = 3$,
$m = 7$, $m = 11$, $m = 101$ and $m = 501$

The matrix Equation (13) with components determined by the relations above was solved with a use of own program written in the Matlab environment. In the consequence of calculations for different numbers of summands in the Fourier series (12), that is $m = 3$, $m = 7$, $m = 11$, $m = 101$ and $m = 501$, one obtained different approximations of the damage distribution realised by the function z with accuracy increasing with a rise of the number m, what is shown by the diagrams on the Figure 4. Very accurate approximations for $m = 101$ and $m = 501$ are presented only to illustrate a sense of the method because related to this making of the same number of displacement measurements with required accuracy is practically impossible in real conditions. However satisfactory information about the damage distribution can be obtained already for 3 displacement measurements (for example see Figure 3b), what was tested also in own laboratory experiment discussed in the next point.

5. Experiment

Within a framework of the experiment one measured displacements of middle bays of three four-point bent aluminium laboratory-beams of the static scheme shown on the Figure 5a. Two of the rods had been ground off on the segments AB in order to reduce their bending rigidity respectively by 10% and 20%. That weakening in the segments AB simulated damage so as to the damage parameter $^{t}\omega$ was for them equal to 0.1 or 0.2. The displacements obtained were a basis of assessment for possibilities of a use of the Relations (13) and (17) in order to estimate a damage distribution for rods bent purely. The displacements were measured on the segment 0–4 and in order to estimate the damage on this segment, a substitute static scheme was used which was shortened by the segments A-0 and 4-B in comparison with the real rod (Figure 5b). That made possible to avoid an influence of the disturbance in the uniaxial state of stress in the segments at the supports on results of calculations, which were based on the Relations (17). Taking of these segments into account could undermine a correctness of the considerations formulated for rods bent purely. All the dimensions were fixed so as to the substitute static scheme corresponded with this shown on the Figure 2a in order to carry out a comparative analysis of the calculations based on the displacements of beams obtained theoretically and experimentally. The displacements of beam not damaged were also used for a determination of Young's modulus of aluminium alloy which the specimens had been made from.

The displacements of segments 0-1, 1-2, 2-3, 3-4 shown on the scheme were measured with a help of the digital photos taken before and after loading of the beams. Mutual displacements of the segments were examined each time in ten points chosen along the height at the ends of segments. Final results were calculated as an arithmetic mean of them. A resolution of photos used in the experiment made possible obtaining of the pictures with pixels which corresponded to size about 0.015×0.015 [*mm*]. Sizes and loads of three aluminium beams used in the experiment, which meaning is illustrated on the Figure 5, were matched as follows: l = 15.3 [*cm*], c = 12.5 [*cm*], b = 3.01

[cm], $h = 0.51$ [cm], $\Delta P = 29.27$ [N]. The particular rods differed from each other only in size b_d, which was equal respectively to: b, $0.9b$, $0.8b$. The displacement measurements of the rods for the points 1, 2, 3, that means $y_{(1)}$, $y_{(2)}$, $y_{(3)}$, are put together in the Table with those calculated theoretically. The displacement $y_{(2)}$ for the rod without the weakening was equal to 0.448 [mm], what enabled to calculate that the rods had been made from aluminium alloy of Young's modulus 71.83 [GPa]. Next basing on the Relations (13) and (17) one determined coefficients of the Fourier series approximating the damage distribution on the segment 0-4 of the rods damaged. Diagrams of these series are presented on the Figure 6.
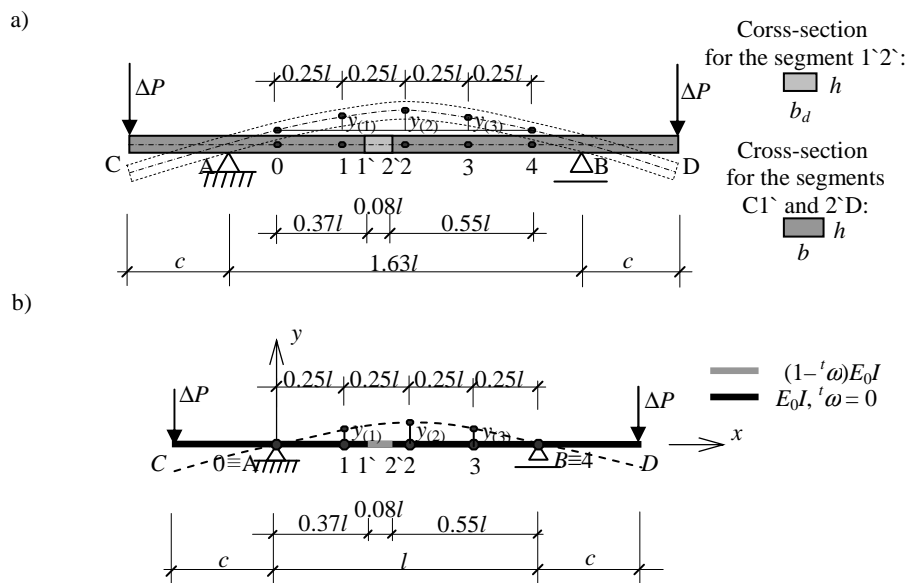
Fig. 5. a) Scheme of the beam used in the experiment. b) Equivalent scheme of the beam for calculations of damage distribution in the segment 0-4 of the beam used in the experiment

Damage distribution calculated on the basis of theoretical considerations
Damage distribution calculated on the basis of experimental measurements
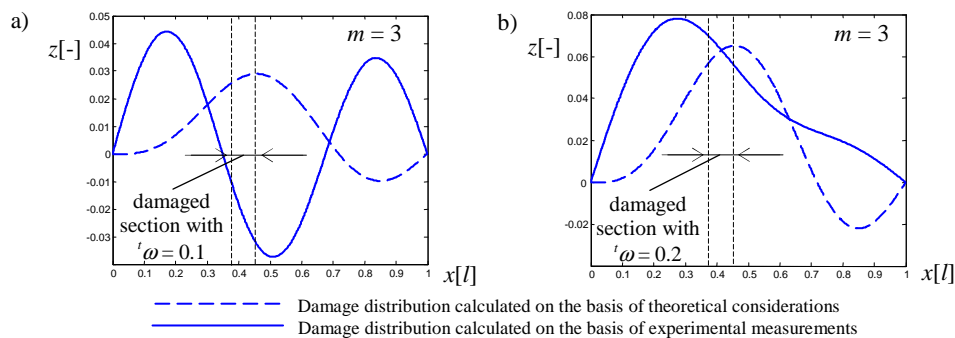
Fig. 6. Comparison of damage distribution approximations for beam section 0-4 (see Figure 5b) calculated on the basis of the theory and experimental measurements: a) $^{t}\omega = 0.1$, b) $^{t}\omega = 0.2$ for section 1`2`

Table. Displacements of the beams of scheme shown
on the Figure 5 determined experimentally and theoretically

Displacements [mm]		Measuring system		
		without notch	with notch = $0.1b$ ($b_d = 0.9b$)	with notch = $0.2b$ ($b_d = 0.8b$)
$y_{(1)}$	experimental	0.330	0.341	0.354
	theoretical	0.336	0.341	0.347
	difference in [%]	−1.8%	0%	2.0%
$y_{(2)}$	experimental	0.448	0.447	0.469
	theoretical	0.448	0.454	0.463
	difference in [%]	0%	−1.5%	1.3%
$y_{(3)}$	experimental	0.338	0.337	0.349
	theoretical	0.336	0.339	0.343
	difference in [%]	0.6%	−0.6%	1.7%

One could conclude on the basis of results obtained that measuring errors of the order of 1-2% in comparison with the theoretical calculations did not enable a determination of the damage distribution expected for the beam with segment 1`-2` damaged in 10% ($^t\omega = 0.1$) (Figure 6a). On the other hand, one obtained a satisfying result close to the theoretical one for the beam with segment 1`-2` damaged twice more ($^t\omega = 0.2$) (Figure 6b).

6. Conclusions

One presented a derivation of the reciprocal theorem for the CDM problem where the damage evolution was described by the scalar parameter for a considerable simplification of the task. The problem was introduced in an incremental version because of its physical non-linearity.

The theorem obtained enables a determination of damage distribution in the medium after suitable transformations, what was shown pictorially by the example of four-point bent and damaged beam. The approach presented can be a complement for the existing methods of the damage estimation in engineering structures. A certain advantage of the method presented in the work is a fact that the damage measure, according to the CDM assumptions, is a continuous function and can have a finite number of discontinuities in an area of a medium investigated and may describe this way any damage distribution. One used in the elaboration the approximation of the damage parameter by the Fourier series, where its coefficients were unknowns. A number of the coefficients corresponds to a number of displacement measurements made for a damaged system. Thus, limits in an applicability of the method are determined by possibilities of making of displacement measurements in the required number of points of the system with the satisfying accuracy.

References

[1] Cowley P., Adams R.D.: *The location of defects in structures from measurements of natural frequencies*, Journal of Strain Analysis 14, 1979, p. 49–57.

[2] Kubik J., Perkowski Z.: *Description of brittle damage to concrete*, Proceedings of Int. Symposium ABDM, Kraków-Przegorzały, 2002.

[3] Kubik J., Perkowski Z.: *Reciprocity theorem for a body with damage and distortion strains*, Proceedings of 2nd International Conference "New Trends in Statics and Dynamics of Buildings", Bratyslava, 2003, p. 177–182.

[4] Kubik J., Perkowski Z.: *Reciprocity theorem for mechanical problem in brittle damaged body with thermal distortion*, Mathematical Methods and Physicomechanical Fields, Vol. 49, No. 1, 2006, p. 182–187.

[5] Litewka A.: *Creep damage and creep rupture of metals*, Poznań University of Technology, Series: Dissertations, 250, Poznań, 1991 (in Polish).

[6] Liu G.R., Chen S.C.: *A novel technique for inverse identification of distributed stiffness factor in structures*, Journal of Sound and Vibration 254, 5, 2002, p. 823–835.

[7] Il-Yoon Choi, Jun S. Lee, Eunsoo Choi, Hyo-Nam Cho: *Development of elastic damage load theorem for damage detection in a statically determinate beam*, Computers and Structures, 82, 2004, p. 2483–2492.

[8] Mróz Z.: *Thermographic identification of defects in structures*, Proceedings of CISM-Advanced School on Parameter Identification of Materials and Structures, Udine, 2003.

[9] Murakami S., Kamiya K.: *Constitutive and damage evolution equations of elastic brittle materials based in irreversible thermodynamics*, Int. J. Solids Struct., 39, 1997, p. 437–486.

[10] Pandey A.K. Biwas M., Samman M.M.: *Damage detection from changes in curvature mode shapes*, Journal of Sound and Vibration 103, 1985, p. 301–310.

[11] Rucka M., Wilde K.: *Crack identification using wavelets on experimental static deflection profiles*, Engineering Structures, 28, 2006, p. 279–288.

[12] Schiessl P., Reuter C.: *Massgebende Einflussgrössen auf die Wasserdurchlässigkeit von gerissenen Stahlbetonbauteilen*, Annual Report, Institut für Bauforschung, Achen, 1992, p. 223–228.

Twierdzenie o wzajemności dla zagadnień mechaniki uszkodzenia i jego zastosowanie w szacowaniu rozkładu uszkodzeń na podstawie pomiarów przemieszczeń

W artykule przedstawiono ogólne sformułowanie twierdzenia o wzajemności dla ośrodka sprężystego z kruchymi mikro-uszkodzeniami. Zasada ta, po odpowiednich przekształceniach, może być wykorzystana do szacowania poziomu uszkodzeń w elementach konstrukcyjnych. Przykład szczególnego zastosowania twierdzenia przy detekcji uszkodzenia układów prętowych, na podstawie pomiarów przemieszczeń w wybranych punktach czysto zginanej belki, został przedstawiony w drugiej części artykułu. Przedstawione podejście szacowania uszkodzeń w konstrukcji może być uzupełnieniem dla istniejących już metod opartych na analizie zmian jej częstości drgań własnych, przewodnictwa cieplnego, czy przemieszczeń.

Rozważania w pracy prowadzone są w oparciu o następujące założenia:

• uszkodzenie w ośrodku rozważane jest jako ciągłe pole (adekwatnie do założeń i metod mechaniki uszkodzenia) opisane przez bezwymiarowy skalarny parametr uszkodzenia $\omega \in [0,1)$, który jest równy zero w materiale nieuszkodzonym i jeden w materiale w chwili zniszczenia; zależy on od zmiennych rozważanego procesu termodynamicznego np.: $\omega = \omega\,(\boldsymbol{\varepsilon},...)$, gdzie $\boldsymbol{\varepsilon}$ jest to tensor odkształceń,

• ośrodek nieuszkodzony traktowany będzie jako sprężysty o znanej początkowej sztywności opisanej symetrycznym tensorem czwartego rzędu $\mathbf{E}_0$,

• sztywność ośrodka uszkodzonego opisana symetrycznym tensorem czwartego rzędu $\mathbf{E}$ podlega redukcji stosownie do wartości parametru uszkodzenia, zgodnie z relacją $\mathbf{E} = (1-\omega)\mathbf{E}_0$.

Pomimo faktu, że założenia powyższe wprowadzają nieliniowość w równaniu fizycznym wiążącym odkształcenia i naprężenia, to zasada wzajemności, którą formalnie formułuje się tylko dla zagadnień liniowych w oparciu o analizę symetrii tensora $\mathbf{E}$, może być także wyprowadzona dla przedstawianego problemu dzięki założeniu trzeciemu. Wtedy symetria tensora $\mathbf{E}$ może być rozważana tylko względem wydzielonej z niego sztywności początkowej $\mathbf{E}_0$. Także, dla znacznego uproszczenia rozważań, uwzględniono uśredniony, izotropowy wpływ mikrouszkodzeń na zmiany sztywności ośrodka, stosując do ich opisu parametr skalarny, co pozwala pominąć efekty anizotropowe spowodowane ukierunkowanym powstawaniem mikrospękań w materiale prostopadle do naprężeń głównych rozciągających.

Letters to Editor

Scientific discussion

A. M. BRANDT
Discussion on the paper "The possibility of adjusting concrete mixtures' fluidity by means of superplasti-
cizer SNF", A. Kapelko, ACME, vol. VI, no. 3, 2006, p. 37–53

The paper does not satisfy elementary requirements that may be expected from re-
search articles published in a scientific magazine.

1. Superplasticizers, including SNF, have been used since over 60 years. Present
knowledge and instructions attached to such products are also known or easly avaiable
and the published paper does not contain any new and deeper knowledge - proposed
conclusions are trivial (1, 6 and 7), contain unverified suppositions that are not based
on any test (2), or are misleading (3, 4 and 5). In order to propose any conclusions
from the triple addition of a superplasticizerit is necessary to compare the results with
those from single addition of the same dosage of SNF. Reduction of the amount of
Portland cement is never a reason for application of superplasticizer: whether indi-
cated procentage concerns its water solution or dry mass addition.

2. The suggestion, that the majority of Portland cements are characterized by high
concent of C_3A is incorrect (page 39). The Author selected for his tests the Portland
cements with particulary high concent of C_3A – 9.8% – no competent manager in a
concrete plant would select such cements. Moreover, the Author has not determined
the setting time neither checked the compatibility between Portland cement and ad-
mixture.

3. Observaion that "the adsorbtion of cement granules on the superplasticizer sur-
face" (page 38) is entirely incorrect. Also the term "mineral and granite aggregate"
used several times, e.g. page 46, line 5 from top, has no sense. What kind of "SNF
particles" are mentioned on page 46, line 5 from the top?

4. Suggestion of a triple dosage of the superplasticizer is completely unacceptable
in practice because of additional cost. Also increasing the fluidity period of a concrete
mix up to 326 minutes (page 46) and even to 425 minutes (page 47) is useless. The
concretes with water/cement ratio equal to 0.7 are characterized by quite sufficient
workability and nobody will use a superplasticizer in either form.

5. Diagrams in Figures 5 and 6 show that the compressive strenght is increasing-
with decrease of w/c – this has been well known since middle of the past century. It is
also known since a long time that the brittlenes of concrete is increasing with its
strenght - that is presented by the Author in Figures 7 and 8 as results of research (!).
What does the "strenght of concrete mixtures" mean?

6. Comprehensive study of Chapter 2 of ref. [1] , or better its new edition of 1999, together with an analysis of numerous published papers on delayed dosage of superplasticizers, e.g. by Penttala, would certainly help the Author to avoid all basic mistakes or to restrain from carrying on these tests.

A. Kapelko

Response to the remarks of Professor Andrzej M. Brandt to my article "The possibility of adjusting concrete mixtures' fluidity by means of superplasticizer SNF", ACME, Vol. VI, No. 3, 2006, p. 37–53.

I have analyzed very thoroughly the remarks sent to the Editorial Offices of the Archives of Civil and Mechanical Engineering by Professor Andrzej M. Brandt concerning my article published in 3/2006 issue on pages 37–53.

Those remarks fall into two broad categories: (1) general remarks included in the first sentence and in point 6, and (2) remarks referring directly to the content of the article contained in points from 1 to 5. Below I discuss each of these respective remarks individually.

The first remark noted in the general category states that the paper does not satisfy elementary requirements that may be expected from research articles in a scientific journal. My response is that my article published in the Archives of Civil and Mechanical Engineering is my own and an original contribution. The work has been recommended to be published by two independent reviewers and after positive reviews has been accepted for a publication in ACME. Hence, the article fully satisfies the requirements established by the scientific journal.

1. In the first paragraph of the remarks it is pointed out that the author of the paper carried out the research of superplasticizer SNF, while the present knowledge and the content of its instruction manual was already sufficient. The conclusions and the discussion of the results and the purposefulness of Portland cement reduction in mixtures containing SNF are criticized as well. I respond that the opinion about the conclusions is unreliable and does not constitute scientific polemic. According to V.S. Ramachandran, R.F. Feldman, Y.Y. Beaudoin, Concrete Science. Treatise on Current Research, Heyden, London. Philadelphia. Rheine, 1981 superplasticizers were used for the first time in Japan in 1964, and in Europe – in Germany in 1972. As it is easy to calculate the European application of superplasticizers have only 35 years of history, but not over 60 years like it was pointed in the remarks. Two fundamental building materials – ceramics and concrete – were known much earlier than superplasticizers. Paraphrasing the statement of the author of the remarks we could also conclude that it is unnecessary to conduct a research of concrete, ceramics or superplasticizers. Based on the literature review one can see that it is those materials that are very often the subject

of research. Many technological facts are being researched which later on can be used for an optimal application of this in building practice.

The present knowledge concerning superplasticizer usage, including SNF, is fragmented [M. Collepardi, Chemical Admixtures Today. Proceedings of Second International Symposium on Concrete Technology for Sustainable Development with Emphasis on Infrastructure, Hyderabad, India, 2005, p. 527–541]. In my opinion it is unacceptable to rely on the content of instructions and it is necessary to conduct a broadened research verifying the SNF performance in the specific conditions of materials and technology. The triple dosage of the superplasticizer allows for a comparison between the first dosage and the second one, the first dosage to the third one, and the second dosage to the third one.

A careful reader of my paper can compare without any effort the effects of multiple SNF dosage as it is presented and explained on Figures 1 to 4, on pages 42 and 43. In the paper I introduced a new and original parameter S_m – an average slump-as the estimation of a multiple SNF dosage's effectiveness with respect to the high level of concrete mixtures' fluidity in the function of time. This parameter allows for the possibility of an estimation of the concrete mixture's modification using SNF with respect to their fluidization in the specific material conditions. In my view the reduction of cement amount is one of the aims of superplasticizer SNF addition. It is known that decreasing an amount of cement causes the reduction of shrinkage and thermic strain of concrete. According to the work of V.S. Ramachandran et al. cited before, and for example, R. Rixom and N. Mailvaganam, Chemical Admixtures for Concrete, London, UK: Spon Press, 1999, one of the aims of SNF addition is an economical usage of cement. Below I present the scheme from page 2 of R.Rixom and N. Mailvaganam referring to economical usage of water-reducing admixtures, including SNF as well.
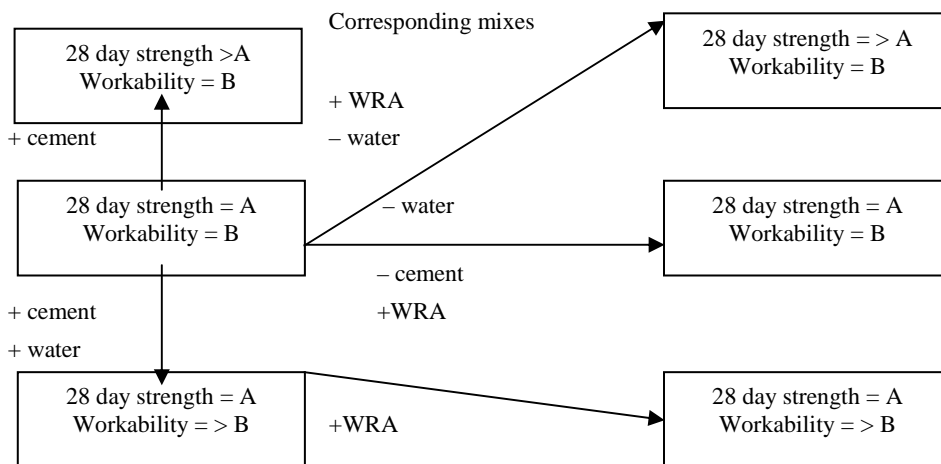

Fig. 1.1 The concept of corresponding mixes

The content of dry substance in the water solution was 34% and the superplasticizer density in $+20^{\circ}C$ was 1,165 g/ml.

2. I disagree with the criticism included in the second point of the remarks, that it was a mistake to use a cement with the C_3A content equal to 9,8%. It has nothing to do with a competent concrete manufacturer. A competent or an incompetent concrete manufacturer has to take into account that the majority of cements produced in Poland has a particularly high content of C_3A. The concrete manufacturers working in existing conditions in Poland have a minimal influence on the choice in the make up content of the cement. Very often the main factor influencing this choice is the cost of the cement and admixture usage. Superplasticizer SNF intended to be used mainly in ready-mixed concrete and it is and will still be used for a long time to modify concretes because of its low cost compared to other superplasticizers, for example those of a new generation. The determination of compatibility between Portland cement and admixture was not the objective of my research. The scientific literature provides a sufficient number of investigations on this subject. A competent researcher will find the necessary information in many articles and monographs, for example J. Szwabowski, Rheology of Mixes on Cement Binders, Gliwice, 1999 or J. Gołaszewski, Modelling of Fresh Concrete Workability Using Superplasticizers, Gliwice, 2003. The influence of SNF on the setting time of cement was a subject of my investigations. This issue is presented in another work of mine. Figure 1.2 shows the setting time of concrete with superplasticizer SNF.
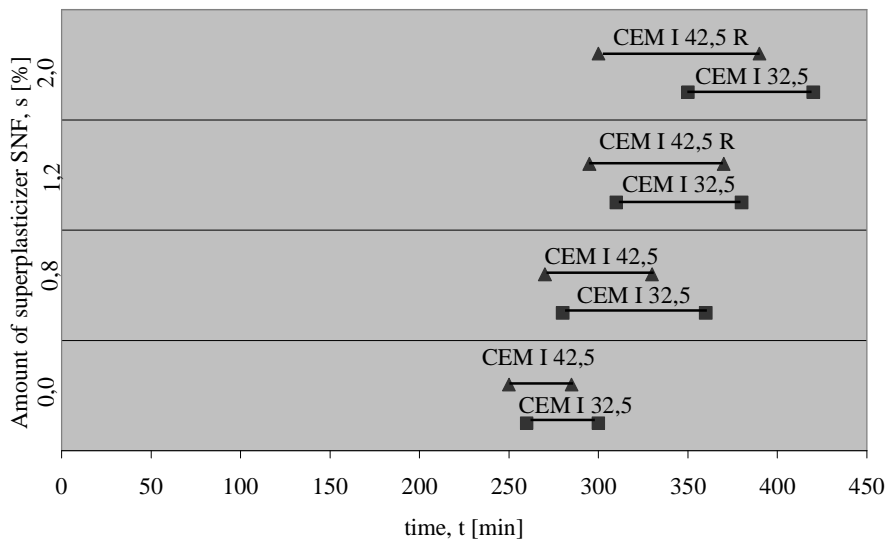

Fig. 1.2. The setting time of standard grouts with SNF

When superplasticizer is added only once together with mixing water, in the amount of 0.8–2.0% by weight of cement, the initial setting time of standard grouts is ex-

tended by 20 to 90 minutes, while the final setting time by 60 to 120 minutes. At the same time the setting time of cements with SNF is lengthened by 25 to 55 minutes. A bigger admixture influence was observed in grouts prepared with CEMI 32.5R. It is associated with the smaller fineness of this binder in comparison to CEM I 42.5 R. Both cements that were analyzed are produced from the same clinker and are characterized by the specific surface, according to Blaine'a of 306 and 315 m^2/kg, respectively.

In addition, the author conducted a research of concretes with superplasticizer SNF concerning the material durability in the water environment. The test of its resistance to water penetration was made using 3 cube specimens with a 30 cm diameter and a 15 cm altitude – these kinds of cubes allow for a better estimation of water penetration in comparison to cubes with a 15 cm side. The pressure was being risen by 0.2 MPa every 24 hours until it reached the level of 0,8 MPa. Graph 1.3 shows these results of its resistance to water penetration of concretes.
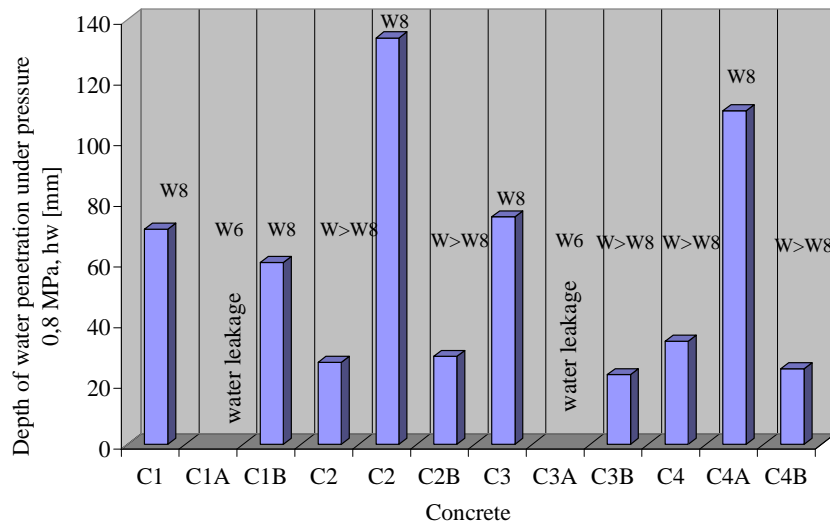

Fig. 1.3. Resistance to water penetration of concretes with SNF

The concrete mixtures' modification made with admixtures in order to reduce the amount of mixing water, while keeping the initial consistency (decrease in W/C), reduces significantly the depth of water penetration under the pressure and increases the degree of resistance to water penetration W>W8. The resistance to water penetration of concrete made from concrete mixtures fluidized with superplasticizer and containing smaller amounts of cement < 320 kg/m^3, decreases by one degree W6 in comparison is resistant to water penetration of control concretes W8.

3. The remarks included in the third point arise partially from the translation of the text from Polish to English. It is composed of some small language mistakes by the author.

4. I disagree with the remark included in the first sentence of the fourth point. In practice the triple dosage of the superplasticizer SNF is acceptable and has been applied. As a part of cooperation with the industry I was elaborating some variants of triple dosage of this admixture under specific transportation conditions: high environment temperature, considerable distance of transportation through built-up areas, which worked out in practice. I also used a combination of superplasticizer SNF with set-retarding admixture in order to modify mixtures. Under conditions of market economy the additional amounts of the admixture does not increase the cost of production significantly with respect to, for instance, manufacturing $1m^3$ of concrete mixture. These are measurable costs. It would be advisable to analyze unmeasurable costs caused by an increasing SNF content and associated with, for example, usage of a smaller amount of energy to thicken mixtures, faster completion of structural element, faster advance of works, shortening construction time and the like.

The author of the article does not impose lengthening fluidity of mixtures up to 325 or 425 minutes. The author's original research implies that triple SNF dosage allows for maintaining the fluidity up to 325 minutes at the S3 consistency level while at the S2 consistency level up to 425 minutes. The competent concrete manufacturer can use my figures 1 to 4 on pages 42–43, find the time needed to transport mixture with SNF and correlate this time with the amount of admixture dosages.

The workability of concrete mixtures does not depend only on w/c ratio. The workability can be modified by: the consistency, the amount of grout, the amount of mortal, the shape of coarse aggregate grains, the total of cement amount and other components with grains up to 0,125 mm, the admixtures' application [Z. Jamroży, Concrete and Its Technologies, PWN Warszawa-Kraków, 2000].

5. The statements contained in the fifth point of the remarks and referring to figures 5, 6, 7 and 8 contained in my paper could not be known since the fifties of the past century, because superplasticizer SNF was unknown. It is my paper which gives the relevant information that in the given material conditions adding SNF does not change any known tendencies resulting from the ordinary concrete research arranged in f_c – w/c and $C.../...$(compressive strength class) – k (brittleness).

6. The general statements formulated in the sixth point of the remarks together with my review of many monographs and articles made me convinced about the purposefulness of the carried out research, which findings of were published in 2/2006 issue of ACME.

It is obvious that discovering new technological initiatives broadens the knowledge in the field of technology and concrete research.

Information about PhD thesis at the Civil Engineering Faculty and the Mechanical Engineering Faculty of Wrocław University of Technology

Title: *The influence of degeneration of synovial joints on his tribological properties* (**in Polish**)
Wpływ zmian zwyrodnieniowych stawów synowialnych na ich właściwości tribologiczne

Author: Tomasz Trzaskacz
Supervisor: Professor Czesław Koziarski, Wrocław University of Technology
**Promoting Council: Scientific Council of Institute of Machines Design and Operation
Reviewers:**
   Professor Prof. dr hab.inż. Jan Burcan,
   Professor Prof. dr hab. inż. Romuald Będziński, Wrocław University of Technology
Date of PhD thesis presentation: July 11th, 2006
PhD is available in Main Library of Wrocław University of Technology
The monograph contains: 113 pages, 100 figs, bibliography: 68 items
Keywords: *biotribology, articular cartilage, degeneration of cartilage*

Abstract: In dissertation was show influence of degeneration of articular cartilage on tribological properties of modeled synovial joint. In this dissertation acchieved classification of damaged articular cartilage, on the base of investigation: macroscopic and microscopic observations, measurement of surfaces roughnest, measurement of shape and area of contact surface. Next, testing machine was build. The swinging, rolling-sliding motion with liquid lubricant occurs between samples on this testing machine. Next, measurement of frictions moment acchieved, and coefficient of friction and mean value of shearing stress on the contact surface was obtain. In the last part of dissertation was show results of investigations. Results was show as changes of value of friction coefficient and value of shearing stress in function of phase of human walk.

Title: *Analysis of the possibilities of numeric simulating of processes based on development of deformation localization* **(in Polish)**
Analiza możliwości numerycznego symulowania procesów bazujących na rozwoju lokalizacji odkształceń

Author: Sebastian Ławrusewicz
Supervisor: Doctor Edward Stanisław Dzidowski, Wrocław University of Technology
Promoting Council: Scientific Council of Institute of Production Engineering of Wrocław University of Technology
Reviewers:
  Professor Józef Zasadziński, Professor of AGH University of Science and Technology
  Professor Jerzy Gronostajski, Professor of Wrocław University of Technology
Date of PhD thesis presentation: November 10th, 2004
PhD is available in Main Library of Wrocław University of Technology
The monograph contains: 174 pages, 133 figs, 19 tables, bibliography: 311 items
Keywords: *shearing process, metal working, FEM simulations*

Abstract: In the analysis of the processes based on deformation localization and fracture of sheared material numeric method are used more and more frequently. So far, the processes based on shearing such as blanking, haven't fully included real course of shearing process, the deformation characteristic in shearing zone was skipped. This simplifying doesn't reflect the core of shearing process. The way of result compliance verification of such simulation with the experimental is additional reason of objection. Usually only one criteria is taken into account in conducting such verification. The criterion is depth of roll-over in the beginning of fracture. Therefore the aim of this thesis is the attempt to verify the attitude mentioned above and simulation processes based on deformation localization. This is why the numeric simulation and experimental research of copper flat bar shearing process has been conducted. The influence of finite elements quantity, coefficient of friction and different methods of simulations were taken into account into these simulations. The obtained results were verified by the criteria based on meso- and macroscopic conception and shear fracture model developed by Dzidowski. Thanks to these criteria it has been shown that compatibility to date simulation results with experiment has signs of randomness. It has been established that another defect of Abaqus/Standard method is discrepancy in influence of finite elements quantity on sheared material geometry and non-dilatational strain value. This discrepancy precludes unequivocal establishment of optimum finite elements quantity.

The above limitations were the reason for searching other way to simulate shearing process and Abaqus/Explicit method allows to eliminate finite elements penetration with knives and makes non-dilatational strain simulated distribution gets similar to experimental. But using that method should be more investigated.

All the facts mentioned above justify usability of proposed verification criteria of numeric simulations results and confirm the thesis of work.

Title: *Evaluation method of chosen safety systems usage in vehicles*
   (in Polish)
   Metoda oceny stosowania układów bezpieczeństwa w pojazdach
   samochodowych

Author: Grzegorz Andrzej Feliczak
Supervisor: Professor Piotr Wrzecioniarz
Promoting Council: Scientific Council of the Institute of Machines Design and Operation
Reviewers:
   Professor Jerzy Merkisz,
   Doctor Tomasz Nowakowski, Wrocław University of Technology
Date of PhD thesis presentation: July 14th, 2006
PhD thesis is available in Main Library of Wrocław University of Technology
The monograph contains: 169 pages, 39 figs, bibliography: 106 items
Keywords: *vehicles, safety systems, evaluation method*

Abstract: In the paper basic problems connected with car safety are presented. Fundamental data about technical defects, traffic safety and modern car equipment are discussed. Influence of chosen safety systems usage on vehicles users is analyzed. A new method of vehicles safety evaluation have been proposed. By analysis of chosen popular passenger cars the proposed new method and equation describing level of vehicle is explained. Conclusions about new direction of research works are formulated.

Information about habilitations at the Civil Engineering Faculty and the Mechanical Engineering Faculty of Wrocław University of Technology

Title: *Analysis of the variation of strength and deformability of gypsum in various states of stress and humidity* **(in Polish)**
Analiza zmienności wytrzymałości i odkształcalności gipsu w różnych stanach naprężeń i wilgotności

Author: Stanisław Klin
Promoting Council: Council of Faculty of Civil Engineering
Wrocław University of Technology
Reviewers:
 Professor Mieczysław Król, Lublin University of Technology
 Professor Wiesław Kurdowski, Kraków AGH University of Science and Technology
 Professor Leonard Runkiewicz, Warsaw Building Research Institute
 Professor Edward Szymański, Warsaw University of Technology

Information for Authors

Archives of Civil and Mechanical Engineering (ACME) publishes both theoretical and experimental papers which explore or exploit new ideas and techniques in the following areas: structural engineering (structures, machines and mechanical systems), mechanics of materials (elasticity, plasticity, rheology, fatigue, fracture mechanics), materials science (metals, composites, ceramics, plastics, wood, concrete, etc., their structures and properties, methods of evaluation), manufacturing engineering (process design, simulation, diagnostics, maintenance, durability, reliability). In addition to research papers, the Editorial Board welcome: state-of-the-art reviews of specialized topics, letters to the Editor for quick publication, brief work-in-progress reports, brief accounts of completed doctoral thesis (one page is maximum), and bibliographical note on habilitation theses (maximum 250 words). All papers are subject to a referee procedure, except for letters, work-in-progress reports and doctoral and habilitation theses, which are briefly reviewed by the Editorial Board.

The papers submitted have to be unpublished works and should not be considered for publication elsewhere.

The Editorial Board would be grateful for all comments on the idea of the journal.